Non-stationary multivariate extreme events in mangrove environments

A global impact assessment

MSc Thesis – Civil Engineering, Delft University of Technology

W. J. Bellinga

TU Delft

Witteveen Bos

Non-stationary multivariate extreme events in mangrove environments

A global impact assessment

by

W.J. Bellinga

Chair Committee:	Dr. ir. J.A.A. Antolínez
Committee member:	Dr. B.K. van Wesenbeeck
Committee member:	Dr. M.F.S. Tissier
Company mentor:	Ir. C.W.T. van Bemmelen
Institution:	Delft University of Technology
Place:	Faculty of Civil Engineering, Delft
Company:	Witteveen+Bos
Project Duration:	September, 2021 - June, 2022

Cover Image: Kanenori (2021)

TU Delft

Witteveen+Bos

Preface

This document is the report of my MSc thesis research, which is the final product of my master of Hydraulic Engineering at the Delft University of Technology. I carried out this research together with the help of my supervisors at the Delft University of Technology and the assistance of Witteveen+Bos.

I would like to thank my committee members for advising and supporting me during the complete duration of the project. Many thanks to Cas van Bemmelen, for your genuine interest during all our meetings and your support in prioritization till the end. Special thanks to José Álvarez Antolínez, for introducing me to the applications of Machine Learning in Coastal Engineering and for your endless enthusiasm for the project. I am grateful for the time you took to explain the ideas you had for the project and provide constructive feedback during all steps taken. Thanks to Marion Tissier, for your enthusiasm and interest in the progress of the study and the support you provided with the hydrodynamic model. Last buth not least, I want to thank Bregje van Wesenbeeck for the constructive meetings and the valuable feedback you provided.

The opportunity of Witteveen+Bos to perform my graduation project at their offices and with their assistance brought this research to the next level. I am very grateful for the possibility to work in an environment full of expertise in the world of Hydraulic Engineering.

This study indicated the increased impact of extreme events. Therefore, I hope that these results may contribute to the appropriate measures to secure coastal safety under these changing conditions. I focused on a Nature-Based solution to protect against the expected increased impact, while I believe that these solutions should be applied on a broader scale to prepare the coastlines worldwide against the predicted sea-level rise.

My gratitude goes to all my family and friends, who gave feedback on the intermediate and final products of this research project. Their constructive feedback brought the final result to the next level and provided suggestions leading to new discussions.

Finally, I want to thank my family and friends who were supporting me during the entire duration of my study at the Delft University of Technology. I also want to thank the group of fellow graduate students for making the final phase of my project a great period and all my friends for making my study time one great experience. I want to thank Jessica, for supporting me in the different phases of the project and listening with patience and good suggestions to all my stories about waves, extreme events and mangrove trees. Special thanks go to my family, for their genuine interest and support through the complete project. A final word of appreciation goes towards my parents, who supported me during my complete Bachelor and Master at the Delft University of Technology.

W.J. Bellinga
Delft, June 2022

Summary

Mangrove is a coastal vegetation type primarily located in the tropical regions between 5° North and 5° South. This coastal vegetation is capable of reducing the force of incoming waves. This is a result of the obstruction created by the roots, stems and canopies against waves to propagate through. Because of this capability, mangrove vegetation offers coastal protection against extreme annual flood events for 15 million people. Recent studies identified that in 2050, the present-day 100-year extreme sea level will occur annually in a large part of the tropical region. The increase of these extreme events is primarily driven by the projected sea level rise. The hypothesis is that before this chronic flooding is observed, storm-induced flooding might already be observed. The expected increase in the probability of these extreme events is defined as non-stationarity of extreme events. The hypothesis therefore is that the non-stationarity of extreme events could already be observed in historical data.

This study examined non-stationary extreme events between 1987 and 2018 for a total of 5809 hydrodynamic environments distributed around the global mangrove coastline. These mangrove environments defined the hydrodynamic wave characteristics and water levels. The results showed that 87.5% of the mangrove environments have a positive trend in the location parameter of the Generalized Pareto Distribution for the extreme events. The shift of the location parameter indicates an increase of the impact of the extreme events. These extreme events were defined as multivariate extreme events consisting of the significant wave height, the mean wave period and the skew-storm surge, respectively the parameters H_s, T_m and S. This combination is based on the fact that the coastal protection offered by mangroves is depending on the water level and the energy within the long-period waves.

The methodology proposed is capable to perform a non-stationary multivariate extreme value analysis and observe the evolution of the extreme events in these three dimensions between 1987 and 2018. The study showed that the average of the extreme events has been increasing at 70.6%, 72.6% and 64.6% of the mangrove environments in the discussed three dimensions. The average multivariate extreme event in mangrove environments increased by 0.06 m, 0.16 s, and 0.7 cm in three dimensions respectively H_s, T_m, and S. Furthermore, the number of extreme events increased, on average, between the first and second half of the time period, from 4.16 to 4.32 extreme events per year.

The global impact assessment of the non-stationarity of these multivariate extreme events was translated to the 27440 mangrove locations along the global coastlines. Statistical upscaling methods allowed the application of a numerical expensive hydrodynamic model to propagate the offshore conditions to onshore. The impact of the non-stationarity of extreme events was applied to a theoretical framework, introducing the possibility of defining the vegetation width as an optimization parameter. To meet the same safety standard for the 1/40 year design condition in 2018 concerning 1987, the vegetation width of the theoretical framework had to increase on average by 16.8 m. After post-processing the hydrodynamic runs, the results showed that the coastal safety offered by mangrove vegetation is depending on the combined impact of these three parameters, emphasizing the importance of expanding the mangrove vegetation to withstand the non-stationary multivariate extreme event.

The main recommendations from this study are based on the results. First, the study showed that the required vegetation width to ensure coastal safety has increased. It is therefore highly questionable if a stationary extreme value analysis is still valid in these environments, especially when the currently neglecting sea level rise is taken into account. Second, the observed increase in multivariate extreme events and the number of extreme events may reduce the persistence of mangroves and therewith their ability as coastal protection. It is therefore recommended to monitor the condition of the global mangrove forests more closely and to take action when mangrove vegetation is decreasing.

Contents

1 Introduction

1.1. Background

Around 600 million people live in the coastal areas that are more than 10 meters below sea level and therefore they are vulnerable to flooding (McGranahan et al., 2007). Despite the fact that these areas only cover 2% of the world's land area, it attracts around 10% of the human population (McGranahan et al., 2007).

The globally projected extreme sea level rise will increase the risk of flooding in these populated regions. Between the year 200 and 2100 the extreme sea-level invent is expected to increase with 34 to 76 cm based on a moderate-emission-mitigation-policy scenario. The defined business as usual emission scenario results in an increase of 58 to 172 cm of these extreme events (Vousdoukas et al., 2018).

It is expected that in 2100 0.2 - 4.6 % of the human population is annually exposed to flooding. Thus results in an annual loss of the global gross domestic product by 0.3 - 9.3% (Hinkel et al., 2014). The traditional solution to prevent flooding based on climate change scenario's are estimated to have an annual cost of US$ 12-71 billion in 2100 (Hinkel et al., 2014).

Nature-based Solution for coastal protection are often proposed as a more cost-effective and sustainable approach (Spalding et al., 2014). Examples of Nature-based Solutions are vegetated foreshores with mangroves or salt marshes and reefs, which are capable of attenuating waves and reducing the risk of flooding (Gedan et al., 2011). These Nature-based Solutions have the capability to adapt to the sea level rise (Marijnissen et al., 2020; Winterwerp et al., 2005).

Previous research identified that especially in the tropical region flood risks are increased by the year 2050. It is stated that a large part of this region will be annually exposed to a present-day 100-year extreme sea level by the year 2050 (Vousdoukas et al., 2018). Based on the expectation that these regions will already be exposed to storm-induced, high tide or nuisance flooding, before chronic inundation occurs introduces the expectation of an increase in the probability of these extreme events (Shadmehri Toosi et al., 2020).

Mangrove can be found in this tropical region, primarily located between 5 North and 5 South. It covers 137.760 km^2 of the earth surface with often considerable co-benefits (Spalding et al., 2014; Giri et al., 2011). This coastal vegetation can effectively reduce wave heights between 0.14% to 1.1% per meter vegetation (Mcivor et al., 2012).

Previous research has shown that this wave attenuation capacity differs over the vertical, due to the vertical density differences between the roots, stem, and canopy (Quartel et al., 2007). Furthermore, studies have shown that mangroves have a reduced wave attenuation capacity of long-period waves (Horstman et al., 2014; Phan et al., 2015; Gijsman et al., 2021). Still, the coastal protection offered by this Nature-based Solution are worth over $ US 65 billion per year and protection 15 million people against annual extreme flood events (Menéndez et al., 2020). Therefore, efforts are being made to enhance nature-based solutions in coastal protection and to propose design guidelines for them (Sutton-Grier et al., 2015)

The identification of the extreme events against which mangrove protects and their probability of occurrence is commonly based on a stationary assumption. When the stationary assumption is applied in an extreme value analysis, the probability of a design event is equal over time $p_0 = p_t$ (Salas and Obeysekera, 2014). This probability statement is visualized in figure 2.5a

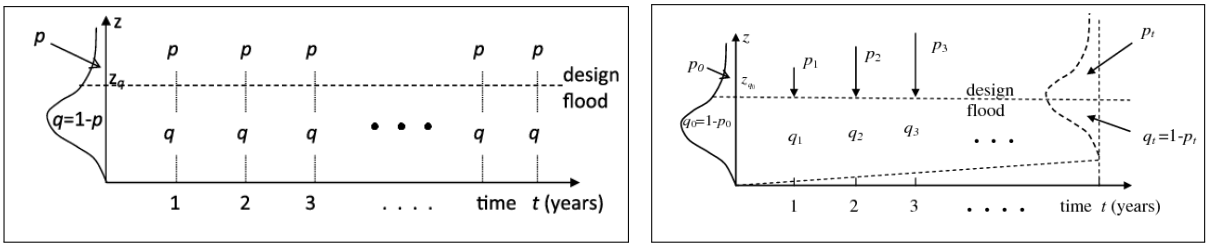

***(a)** Stationary by Salas and Obeysekera (2014)* ***(b)** Non-stationary by Salas and Obeysekera (2014)*

***Figure 1.1:** The impact of non-stationarity vs. stationarity assumption on the probability of a design flood.*

However, the expected increase of extreme events in the tropical region could mean that this stationary assumption no longer holds. This would mean that the probability for an extreme event changes over time, $p_0 \neq p_t$. The implication of the non-stationarity of the extreme value distribution over time is an increase in probability of these extreme events. This increase of the probability is displayed in figure 2.5b.

Methodologies to take into account this non-stationarity of extreme events in the determination of the probability of occurance of these events are available (Mentaschi et al., 2016; Ragno et al., 2019; De Leo et al., 2021). However, these are commonly defined on a extreme events driven by one paramter. The coastal protection offered by mangrove is also depending on the waterlevel and the energy within the long-period waves. Therefore a multivariate extreme value analysis should be defined and applied, to assess the impact of the non-stationarity of these multivariate extreme events on the coastal protection offered by mangroves.

1.2. Problem definition

The expected increase of extreme flood events for the year 2050 in the tropical region described in Vousdoukas et al. (2018), could already be observed as storm-induced flooding (Shadmehri Toosi et al., 2020). Mangroves are primarily located in these tropical regions between 5 degrees North and South (Giri et al., 2011). Therefore the coastal protection offered towards 15 million people against annual flooding could be affected (Menéndez et al., 2020).

Therefore, this study will extend the knowledge of extreme value analysis under the assumption of non-stationarity for multivariate extreme events in mangrove regions. These multivariate extreme events are applied while the coastal protection offered by mangroves is depending on the water level and long-period waves, besides the incoming wave height. This will give insight in the vulnerability against the non-stationarity of these extreme events in mangrove regions.

Based on the statements of Shadmehri Toosi et al. (2020), it is expected that the extreme events in mangrove areas have already been increased. This should imply that more coastal vegetation is needed to ensure the identified coastal protection for the regions where in total 15 million people are protected against annual flooding.

1.3. Research objective and questions

The research objective for this master thesis is to examine the impact of the non-stationarity of multivariate extreme events on the coastal protection offered by mangroves. This results in the main research question, which is stated as:

Main question	•	*What is the impact of the non-stationarity of multivariate extreme events with respect to the coastal safety in mangrove areas?*

Several sub-questions are introduced to answer this main research question and create further insight into the processes involved. These sub-questions are:

Sub-question 1	•	*How to identify an extreme event in respect to coastal safety offered by mangroves?*
Sub-question 2	•	*How to identify and incorporate non-stationarity of a multivariate extreme event in the assessment of the coastal protection offered by mangrove on a global scale?*
Sub-question 3	•	*How did the extreme events transform in the considered period using a multivariate extreme value analysis?*
Sub-question 4	•	*Which sensitivities of the coastal protection offered by mangroves can be identified from the results and what is the influence of this sensitivities?*

1.4. Research approach

The research objective will be fulfilled by using an approach that is split in three sections. First, the non-stationarity of the multivariate extreme events is identified in the extreme value analysis, where global data will lead towards time-dependent hydrodynamic conditions. Second, the extrem events are used as input for the hydrodynamic model to identify the transformation from offshore towards onshore of these different extreme events. Third and final, the impact of the non-stationarity on the coastal safety will be identified. The approach of this studie is schematized in figure 1.2.

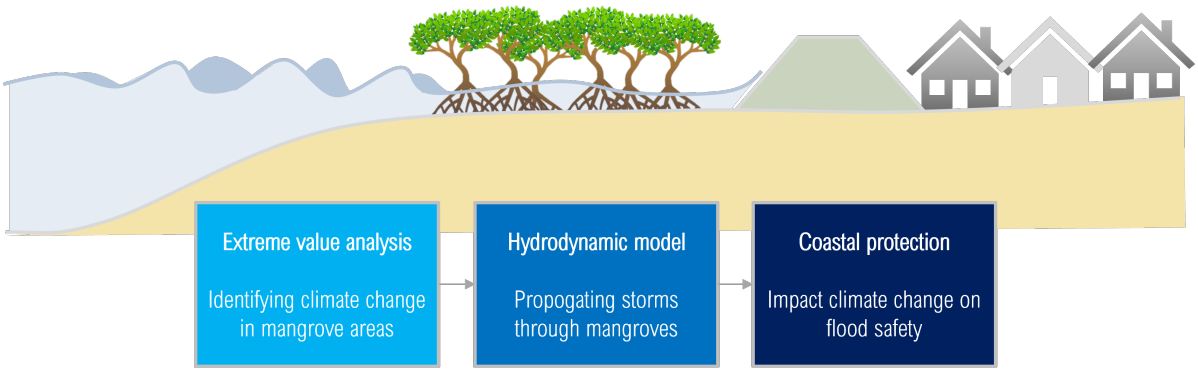

Figure 1.2: *Schematized overview of the three steps performed in this study to work towards the research objective.*

2

Literature background

This study uses different methods that need an introduction to make the application more clear. This chapter will therefore elaborate on the literature background, the different techniques and researches leading to the applied methodology.

2.1. Coastal mangrove vegetation

Mangrove is a coastal vegetation type which grows partly in water. The vegetation can mainly be found in tropical areas between 5° North and South and are covering 137,760 km^2 of the world's surface, as shown in figure 2.1a (Giri et al., 2011). Mangrove define a group of currently approximated 77 halophytic tree and shrub species (Duke et al., 1998), examples are shown in figure 2.1b and 2.1c. This vegetation grows in areas between the mean sea level and the highest astronomical tide (Wilms et al., 2020).

***(a)** Distribution of mangrove on a global scale (U.S. Geological Survey, 2010)*

***(b)** Mangrove tree (Chen, 2013)*

***(c)** Mangrove tree (Wilkins, 2008)*

***Figure 2.1:** Overview mangrove vegetation*

Characteristics
Mangrove trees can be divided into Red, Black and White mangrove. In this study the focus is on Black (Avicennia germinans) and the Red (Rhizophare mangle) mangrove, because White mangrove trees are located more inland. The Red mangroves have a prop rootsystem to lift itself from the ground, figure 2.2a (Kazemi et al., 2018). Black mangroves have a large extending rootsystem of pneumatophores to breath, figure 2.2b (of Environment and Natural Resources, 2021; Geißler et al., 2002). Both root systems are complex structures and influence the attenuation of the waves.

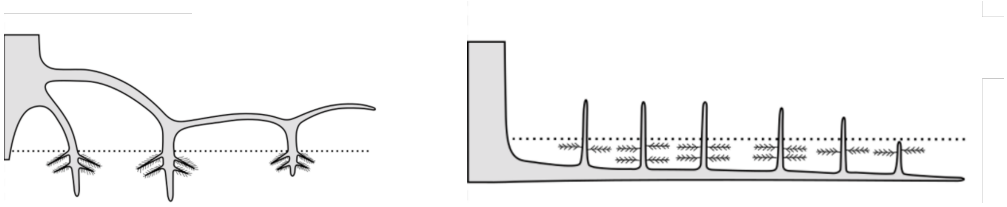

***(a)** Rootsystem Red mangrove (Stabrin, 2018)* ***(b)** Rootsystem of Black and White mangrove (Stabrin, 2018)*

***Figure 2.2:** Mangrove root-system schematization*

The rootsystem of mangrove is a dense obstruction for the waves. This density is not equal over the whole vertical of a mangrove tree. The dense root structure, spare structure of the stems in the middle and the again dense structure of the canopies, the attenuation of wave energy differs over the vertical. This is visualized in figure 2.3. This results in a water level depending wave attenuation capacity of the mangrove vegetation (Spalding et al., 2014).

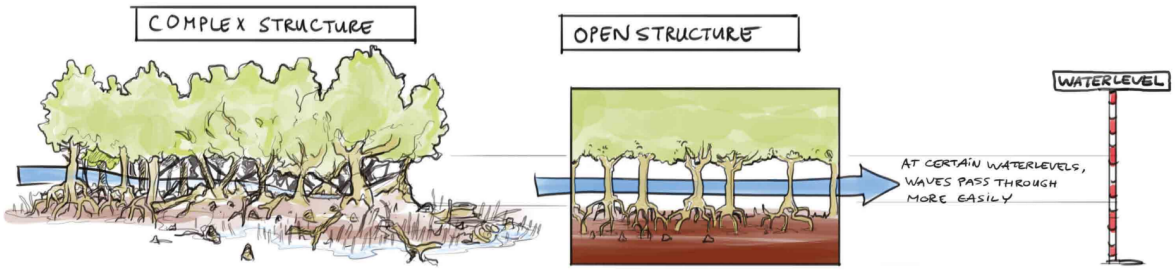

***Figure 2.3:** Vertical layerization of mangrove trees resulting in a water level dependent wave-attenuation (Spalding et al., 2014)*

Wave-attenuation capacity
The dissipation of wave energy due to coastal vegetation has been concluded from several field studies. In the research of Vo-Luong and Massel (2008) the wave height reduction due to mangrove vegetation is measured in the Can Gio Mangrove Biosphere Reserve, Southern Vietnam. This resulted in a set of datapoints along a close to uniform bed for three different wave heights, offering the opportunity to create more insight in the added value of vegetation on the dissipation of wave energy. The study suggest that most of the waves are dissipated within the mangrove forest even at relatively small vegetation widths. In the study of Mcivor et al. (2012), different studies were combined to define the wave height reduction of mangrove trees. The conclusion was that this coastal vegetation has the capability to reduce the wave height between 0.14% to 1.1% per meter vegetation.

However, in the study of Gijsman et al. (2021), it is argued that the functionality of mangroves is decreasing by an increase of the storm intensity. This due to the lower attenuation capacity for longer period waves. The studies of Horstman et al. (2014) and Phan et al. (2015) can emphasize this vulnerability of mangrove vegetation for long period waves.

The observations shared in Horstman et al. (2014), measured in two transects in the southern Andaman region of Thailand, show that the mean wave periods along a mangrove transect were slightly increasing. From 2.9 - 6.4s to 4.1 - 5.7s and from 2.8 - 4.1s to 4.8 - 5.0s. This increase in mean wave period is explained by the fact that shorter waves lose more energy while propagating through mangrove vegetation than longer waves.

In the study of Phan et al. (2015) a numerical experiment was performed with the goal to define a minimum width for a healthy mangrove forest along the Vietnam coastline. To better understand the hydrodynamics within the mangrove forest the short and long-period waves were modelled with XBeach. The wave energy of the short waves was significantly reduced in the first 100 m of vegetation. However, the long waves were able to penetrate much further into the mangrove forests, even in the order of 1000 m, but mention-able is that after 300 to 400 m the long-wave energy is only 10% of the initial energy at the seaward-edge of the mangrove forest.

2.2. Extreme value analysis

Mangroves offering coastal protection against annual flooding for 15 million people (Menéndez et al., 2020). They are even protecting against the extreme conditions of tropical cyclones with their presence in areas known for tropical cyclones, indicated in figure 2.4. However, the extreme events are becoming more extreme in the tropical region (Vousdoukas et al., 2018). Therefore this section introduces the methods applied in this study to identify the extreme events in these coastal regions.

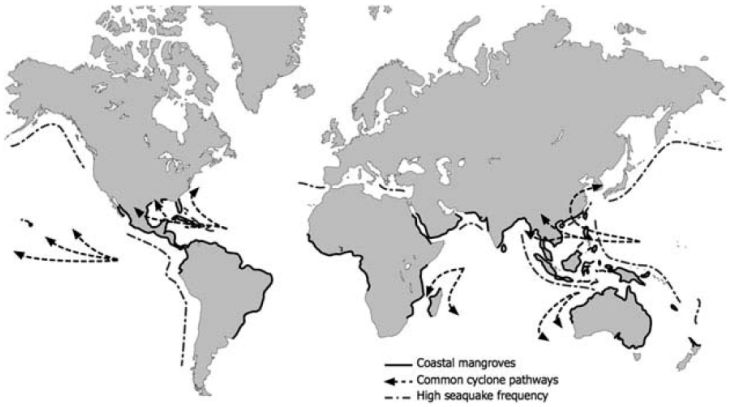

Figure 2.4: *Global distribution of mangrove areas known for their presence of cyclones or seaquake (Marois and Mitsch, 2015)*

Peak over Threshold analysis

Identifying the extreme events is commonly performed by the easily implemented Block-Maxima approach, where the focus is on the extreme value of a particular time window (Jenkinson, 1955). However, the main weakness of this method is that only one feature of a certain period is stored, neglecting the information regarding the remaining extremes. The Peak Over Threshold (POT) method is an extreme value analysis method, which can include these features (Méndez et al., 2006). This approach is collecting extremes which are above a certain threshold, u. This may result in multiple exceedances over the threshold, based on the chosen threshold. Based on this remaining data the tail of the extreme events can be determined fitting it to the Generalized Pareto distribution, as shown in equation 2.1 Méndez et al. (2006).

$$F(x,\mu;\sigma,\xi) = \begin{cases} 1-(1+\frac{\xi(x-\mu)}{\sigma})^{-1/\xi} & \xi \neq 0 \\ 1-\exp(-\frac{x-\mu}{\sigma}) & \xi = 0 \end{cases} \tag{2.1}$$

Where $F(\mu;\sigma;\xi)$ is the cumulative distribution function, μ the location parameter, σ the scale parameter and ξ the shape parameter. The cumulative distribution function show the distribution X, by evaluating the probability of X at level x being smaller or equal to x.

Stationary vs. Non-stationary

The threshold for the peak over threshold analysis is time-independent. This means that the extremes defining the GPD over the whole time-series have to be above the same threshold value, which will be the stationary assumption in this study. When the stationary assumption is applied to the Generalized Pareto distribution of the extreme events, the change of occurrence of a design event is equal over time $p_0 = p_t$. However, if the tropical regions are already exposed to storm-induced flooding, this assumption does not hold (Shadmehri Toosi et al., 2020). This makes the extremes non-stationary and as a result, the probability of the value of an extreme event changes over time, $p_0 \neq p_t$. The figures of the study of Salas and Obeysekera (2014), figure 2.5a and 2.5b, explains the implication of the non-stationarity of the distribution of extreme events.

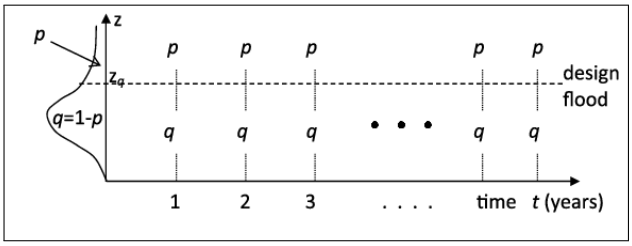

(a) *Stationary by Salas and Obeysekera (2014)*

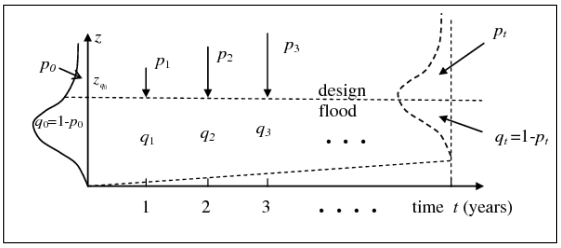

(b) *Non-stationary by Salas and Obeysekera (2014)*

Figure 2.5: *The impact of non-stationarity vs. stationarity assumption on the probability of a design flood.*

There are two methods discussed in this study to implement the non-stationary assumption in the definition of the GPD deistirbution. The first approach is by defining the trend in the extremes and translate this towards time-dependent relations (Ragno et al., 2019; De Leo et al., 2021). The second approach takes into account the non-stationarity of the complete initial time-series and is therefore less sensitive for outliers (Mentaschi et al., 2016). Therefore the second approach is applied in this study for addressing the expected non-stationary.

This analysis is performed with a stationary time series $x(t)$ based on the non-stationary time series $y(t)$. The first step in this approach is shown in equation 3.3 in which the data is normalized by re-scaling it with the standard deviation $S_{0y}(t)$ of time window W_C and the mean, $T_{0y}(t)$, of a time window W_T. The $T_{0y}(t)$ is calculated by the centralized mean of the time series as shown in equation 3.4. To decrease the sensitivity of the $S_{0y}(t)$ for outliers, the $S_{0y}(t)|_{ROUGH}$, from equation 3.5 is smoothed with a moving average based on the time window $W/2$ resulting in equation 3.6. The extreme value analysis can be performed on the stationary time series to eventually be transformed back to the real non-stationary situation. By applying this method only to the resulting values of P_{xy} the dependency between the different variables is equal to the real-time series. When the approach of Mentaschi et al. (2016) would be applied to the wave parameters (H_s, T_m, θ_m) the resulting P_{xy} would be based on variables of which the dependency has changed due to different standard deviations and trends.

$$x(t) = f(y,t) = \frac{y(t) - T_{0y}(t)}{S_{0y}(t)} \tag{2.2}$$

$$T_{0y}(t) = \sum_{tt=t-W/2}^{tt=t+W/2} y(tt)/N_t \tag{2.3}$$

$$S_{0y}(t)|_{\text{ROUGH}} = \sum_{tt=t-W/2}^{tt=t+W/2} \sqrt{[y(tt) - \bar{y}(tt \in [t-W/2, t+W/2])]^2/N_{\text{Wsn}}} \tag{2.4}$$

$$S_{0y}(t) = \sum_{tt=t-W/4}^{tt=t+W/4} 2S_{0y}(tt)\Big|_{\text{ROUGH}} /N_t \tag{2.5}$$

In which $x(t)$ is the stationary time series, $y(t)$ the non-stationary time series, $T_{0y}(t)$ is the long-term trend in the time series, $S_{0y}(t)$ equals the long-term varying standard deviation, W is the time window and N_t is the number of observations available during the time window W.

The found distribution of the GPD resulting from the POT analysis based on the stationary time-series is transformed to the original non-stationary time-series (Mentaschi et al., 2016). This results in a time-dependent threshold $u_y(t)$. With the same approach the found distribution of GPD are transformed to the original non-stationary scale. This is performed for the location parameter μ with equation 3.8, the shape parameter ϵ stays constant, shown in equation 3.9, and the scale parameter σ is calculated with equation 3.10. The subscripts $_y$ and $_x$ show respectively the stationary and the non-stationary parameters.

$$u_y(t) = S_y(t) \cdot u_x + T_y(t) \tag{2.6}$$

$$\mu_y(t) = S_y(t) \cdot \mu_x + T_y(t) \tag{2.7}$$

$$\varepsilon_y = \varepsilon_x = \text{ const.} \tag{2.8}$$

$$\sigma_{\text{GPD}y}(t) = \sigma_y(t) + \varepsilon_y \left[u_y(t) - \mu_y(t)\right] = S_y(t) \cdot \sigma_{\text{GPD}x} \tag{2.9}$$

Design conditions
With the mean number of exceedances per year and the GPD distribution, the probability of exceedances can be defined. By identifying the impact can be translated towards design conditions. The mean number of exceedances per year N_s, indicates the average number of extreme events per year. Using this parameter, the return period of a extreme event with a minimum impact can be calculated. The return period is the expected time between two extreme events that are at least of a certain level of impact. The return period of a POT analysis follows from the fitted Generalized Pareto Distribution on the observed extreme events, equation 2.1. This cumulative equation expresses the non-exceedence probability, meaning the probability of a certain extreme event being smaller than the examined extreme event. This is transformed towards the exceedance values, Q, with equation 2.10 (Van Den Bos and Verhagen, 2018). Eventually the obtained equation can be transformed towards equation 2.11, the expected return period of a extreme values R (Van Den Bos and Verhagen, 2018).

$$Q = 1 - F(\mu; \sigma; \xi) \tag{2.10}$$

$$R = \frac{1}{Q \cdot N_s} \tag{2.11}$$

Multivariate dependency model
In this study the focus is on multivariate extreme events, introducing a multivariate dependency between the different parameters. With taking into account these dependency extreme events that have not been recorded yet can be created based on the observed probability distributions of the extreme value analysis. The extreme event for a particular return period can be substracted from this multivariate dependency model. By sampling a total of the return period of interest times the N_s, the extreme event with the largest impact is the design condition for the particular return period (Gräler et al., 2013).

A method to represent the multivariate dependence structure is by applying the vine method, where the dependence structure is based on the bivariate dependence between the variables (Bedford and Cooke, 2002). In which the vine, V, is a nested set of trees, T, where the edges of T_j are the the nodes of the T_{j+1} Kurowicka and Joe (2010). This dependence structure is shown in figure 2.6, representing a regular vine with 5 variables. This means that this method gives the ability to represent a multivariate dependence structure.

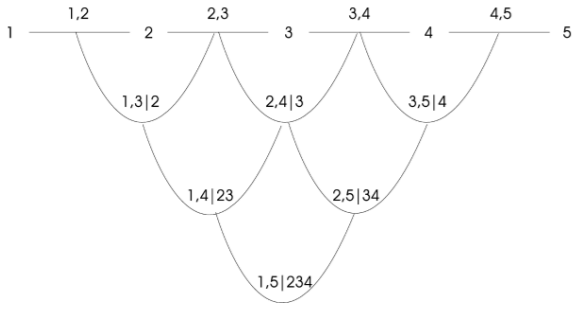

Figure 2.6: *A regular vine (Bedford and Cooke, 2002)*

The edges represent the dependency between two parameters based on the copula theory. Copulas, C, are flexible joint distributions for modelling the dependence structure between two or more random variables (Bender et al., 2014). These are based on uniform marginal distributions. These copula functions can be written as shown in equation 2.12. In this study, Archimedean copulas are applied to capture the dependencies within the Vine-D model. Based on previous research, the assumption is made that the Archimedean copulas are capable of representing the dependency between these variables (Corbella and Stretch, 2013; Li et al., 2018; Lira-Loarca et al., 2020).

$$C\left(u_1, \ldots, u_n\right) = F\left(F_1^{-1}\left(u_1\right), \ldots, F_n^{-1}\left(u_n\right)\right) \tag{2.12}$$

In which F is the multivariate distribution with margins $F_i(u_i), i = 1, ..., n$, being n the number of variables, F_i^{-1} are the inverse distribution functions of the marginals.

2.3. Statistical upscaling

This study will define the impact of non-stationary of extreme events in a global analysis with a computational demanding hydrodynamic model. Other studies left this out of the scope, due to the computational demand (Van Zelst, 2018). However, the application of statistical upscaling will reduce the computational demand of this approach.

In the study of Camus et al. (2011) clustering and selection algorithms are analyzed to give insight in the differences between the different algorithms. In this analysis, it was concluded that the K-means algorithm, KMA, is capable of giving the best representation of the average wave conditions in comparison to the Self-organizing maps, SOM, and the maximum dissimilarity algorithm, MDA.

The K-means clustering method divides the multi-dimensional data space into a number of clusters, each defined by a prototype and formed by the data the nearest to this prototype (Camus et al., 2011). The data of the different points is converted to a n-dimensional vector $X = (x_1, ..., x_N)$, where N is the total amount of data locations. Then the K-means algorithm is searching for M groups with a prototype $v_k = (x_{1k}, ..., x_{nk})$, in which $k = 1, .., M$. The location of these prototypes in the data starts with a random initialization of the prototypes. Then by an iterative process a set of centroids is searched for which the overall within-cluster distance, variance, converges and the designation of data of data points to clusters converges (Camus et al., 2011). In this iterative search, two steps are continuously performed after the sum-of-squares criterion, also called inertia, shown in equation 2.13 converge. The first step is assigning the different samples to the closest centroid. The second step is determine the mean of the samples assigned to a single centroid to determine a new centroid within the data set.

To prevent that the algorithm searches to a local minimum within equation 2.13, the method *k-mean++* can be applied. This means that the initial centroids are not randomly selected but to be distant from each other. By applying weights to certain variables within the vector X, the importance of these variables in finding the centroids differs.

$$\sum_{i=0}^{n} \min_{\mu_j \in C} \left(\|x_i - \mu_j\|^2 \right) \tag{2.13}$$

The number of centroids are validated with the Silhouette coefficient and the Sum Squared Error (SSE). The Silhouette coefficient is a way to describe how well the different clusters can be distinguished within the dataset. This value ranges from -1 to 1, where 1 means that the centroids of the clusters are well apart from each other. A value 0 means that the distance between the centroids is not significant, and -1 represents that the centroids are not assigned properly. The SSE represents the sum of the squared differences between the centroids and the observation allocated to this group. The larger the number, the more difference between the different vectors and the centroids.

2.4. Vegetation implementation in hydrodynamic model

The propagation of the offshore extreme wave conditions is transformed towards the mangrove vegetation belt with the use of a hydrodynamic model. Hydrodynamic models which could be applied are for example SWAN, XBeach and SWASH. In this study SWASH is selected, because it is capable of solving the transformation of waves towards onshore with a non-hydrostatic approach.

SWASH is a non-hydrostatic wave-flow model and is developed to predict the transformation of dispersive surface waves (The SWASH team, 2020). It can be applied to model unsteady, non-hydrostatic, free-surface, rotational flow and transport phenomena. Due to the non-hydrostatic application the model is expensive in the sense of computational time. The nonlinear shallow water equations with the non-hydrostatic pressure term are used in SWASH to model the propagation of offshore waves into the coastal waters.

SWASH is capable to model the additional momentum loss of the waves caused by vegetation, allowing to model the coastal protection of mangrove vegetation (Suzuki et al., 2019; Reis et al., 2020). The vegetation is defined with separate layers for the roots, stem and canopy, following the methodology of Suzuki et al. (2012) and visualized in figure 2.3. This offers the opportunity to apply the vertical differences in wave attenuation capacity of mangrove vegetation. The characterizations of the different layers is performed by applying a layer specific height of the vegetation $h_{v,i}$, thickness of the cylinders of vegetation $b_{v,i}$ and the number of roots N_i. The eventually wave energy dissipation of the mangrove vegetation is depending on the drag coefficient $C_{D,i}$, which is separately defined for the three layers in SWASH. The formulation of this drag coefficient contains a lot of uncertainty (Sumer and Fredsøe, 1998; Van Wesenbeeck et al., 2021). The drag coefficient for rigid cylinders is usually set to 1.0 (Narayan et al., 2011; Reis et al., 2020). However, due to the swaying of vegetation under extreme storm conditions this value could be smaller. The study Van Wesenbeeck et al. (2021), indicates that a C_D of 0.7 could be more representative for the wave attenuation of the canopy of a tree.

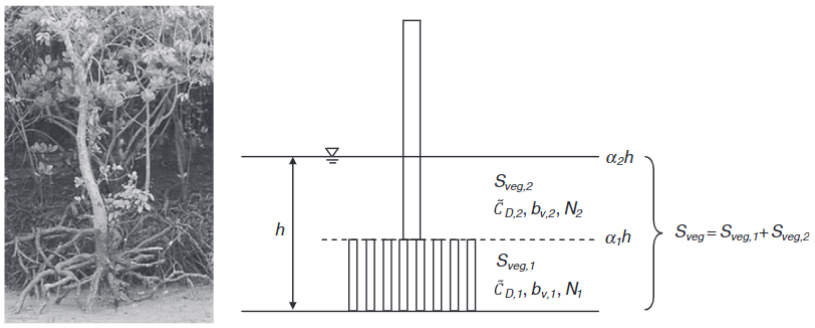

Figure 2.7: *Layer schematization of a mangrove tree in the applied hydrodynamic model (Suzuki et al., 2012)*

2.5. Coastal safety assessment

The eventual impact of the non-stationary of the extreme events on the coastal safety is calculated based on two flood hazard mechanisms. The first is wave run-up and the second is wave-overtopping. Wave run-up is the phenomena when waves run-up against the slope of a dike. Overtopping is the amount of water flowing over a dike due to the breaking and non-breaking waves. These two failure mechanisms of the coastal safety determine the eventually needed height of the protection against the waves to protect the hinterland. The required dike height, also called crest height R_c, is calculated with two empirical relation of Van der Meer et al. (2018).

Run-up is the maximum water level is the maximum water level at a slope during a wave period. For irregular waves the calculation is based on the a run up level that is only exceeded by two percent of the waves, $R_{u2\%}$, calculated with equation 2.14. Based on the design guide lines of the EurOtop Manual (Van der Meer et al., 2018), it is advised that the crest height of the dike should be at least one standard deviation above the calculated maximum run up, to be design a safe protection. Based on results of field experiments the deviation between the found results and the proposed equation follows a normal distribution with a standard deviation of 7%. This results in a safe crest height for run-up given in equation 2.15. The failure mechanism overtopping requires a dike height that can be calculated with equation 2.16, with an upper limit based on equation 2.17.

$$\frac{R_{u2\%}}{H_{m0}} = min\left[1.65 \cdot \gamma_b \cdot \gamma_f \cdot \gamma_\beta \cdot \xi_{m-1,0}, \gamma_f \cdot \gamma_\beta \left(4 - \frac{1.5}{\sqrt{\gamma_b \cdot \xi_{m-1,0}}}\right)\right] \tag{2.14}$$

$$R_c = 1.07 \cdot R_{u2\%} \tag{2.15}$$

$$\frac{q}{\sqrt{g \cdot H_{m0}^3}} = \frac{0.023}{\sqrt{\tan\alpha}} \gamma_b \cdot \xi_{m-1,0} \cdot \exp\left[-\left(2.7 \frac{R_c}{\xi_{m-1,0} \cdot H_{m0} \cdot \gamma_b \cdot \gamma_f \cdot \gamma_\beta \cdot \gamma_v}\right)^{1.3}\right] \tag{2.16}$$

$$\frac{q}{\sqrt{g \cdot H_{m0}^3}} = 0.09 \cdot \exp\left[-\left(1.5 \frac{R_c}{H_{m0} \cdot \gamma_f \cdot \gamma_\beta \cdot \gamma_v}\right)^{1.3}\right] \tag{2.17}$$

In these equations $R_{u2\%}$ is the 2% run-up level, q the overtopping $[l/s/m]$, g the gravitational acceleration $[m/s^2]$, H_{m0} the significant wave height $[m]$, α the slope of the foreshore of the dike or levee $[\circ]$, $\xi_{m-1,0}$ the Iribarren number $[-]$, R_c the free board of the crest $[m]$, γ_b the reduction factor for the berm $[-]$, γ_f the reduction factor of the slope roughness $[-]$, γ_β the reduction factor for the incoming angle of the wave $[-]$ and γ_v the reduction factor for walls $[-]$.

The height of the dike to prevent the failure mechanism is depending on the type of breaking of the waves. This is defined in the equations with the Iribarren number, which can be calculated with equation 2.18. The equation is dependent on the steepness of the wave and the slope of the dike where the waves might break on.

$$\xi_{m-1,0} = \frac{\tan\alpha}{\sqrt{H_{m0}/L_{m-1,0}}} \tag{2.18}$$

3

Material & Methods

This chapter elaborates on the material and methods applied in defining the answer to the research questions. The methodology is introduced by defining the data sources and parameters for the study. The next section describes the non-stationary extreme value analysis. Based on the results of these two phases a statistical upscaling method is applied to reduce the computational demand, which is explained in the next section. The last section will elaborate on the global impact assessment. This impact assessment defines the impact of the non-stationarity of the multivariate extreme events.

3.1. Data collection and parameter definition

This section describes the different data collection of the study. The study requires a theoretical framework to identify the impact of the non-stationary extreme events. The framework is visualized in figure 3.1. The parameters in this theoretical framework are:

- $width_{ns}$
- $width_{fs}$
- h_{fs}
- $z_{0,veg}$
- h_{veg}

These parameters represent respectively the width of the nearshore in m, the width of the foreshore in m, the height of the foreshore in m, the vertical starting point of the vegetation in m with respect to mean sea level and the height of the vegetation in m.

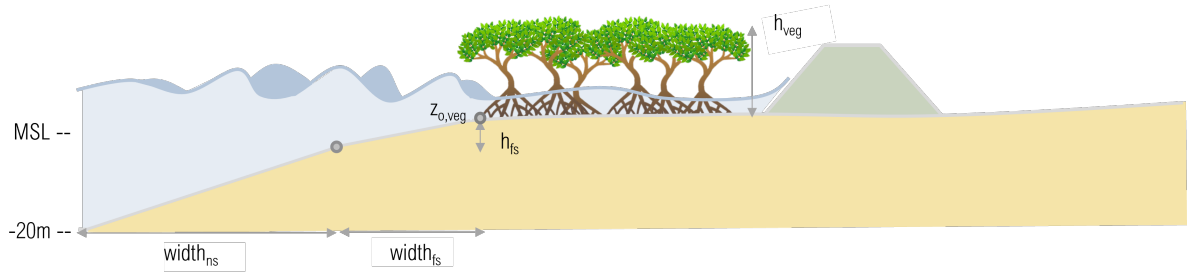

Figure 3.1: *Theoretical frame work applied in the study, identifying the 5 parameters $width_{ns}$, $width_{fs}$, h_{fs}, $z_{0,veg}$ and the h_{veg}, used to represent the mangrove transects.*

The data needed for the analysis can be split in three sections. The first set of data is required to identify where mangrove is present in front of the coastline. The second source are the hydrodynamic conditions at these mangrove locations over time to identify the non-stationary. The third part are the natural conditions at these locations and how these parameters are represented in the hydrodynamic model.

3.1.1. Coastal mangrove locations

The study performs a global assessment of the impact of non-stationary multivariate events by implementing 27440 coastal mangrove locations collected from the study of Van Zelst (2018). These coastal mangrove locations are based on a methodology in which along the global coastlines the presence and type of vegetation is determined. This resulted in a minimum spatial distribution of 1 km along the coastline. The spatial distirbution of the 27440 coastal mangrove locations is given in figure A.1. Further elaboration on the filtering of the data of the study of Van Zelst (2018) and the methodology applied in that study can be found in appendix A.1.

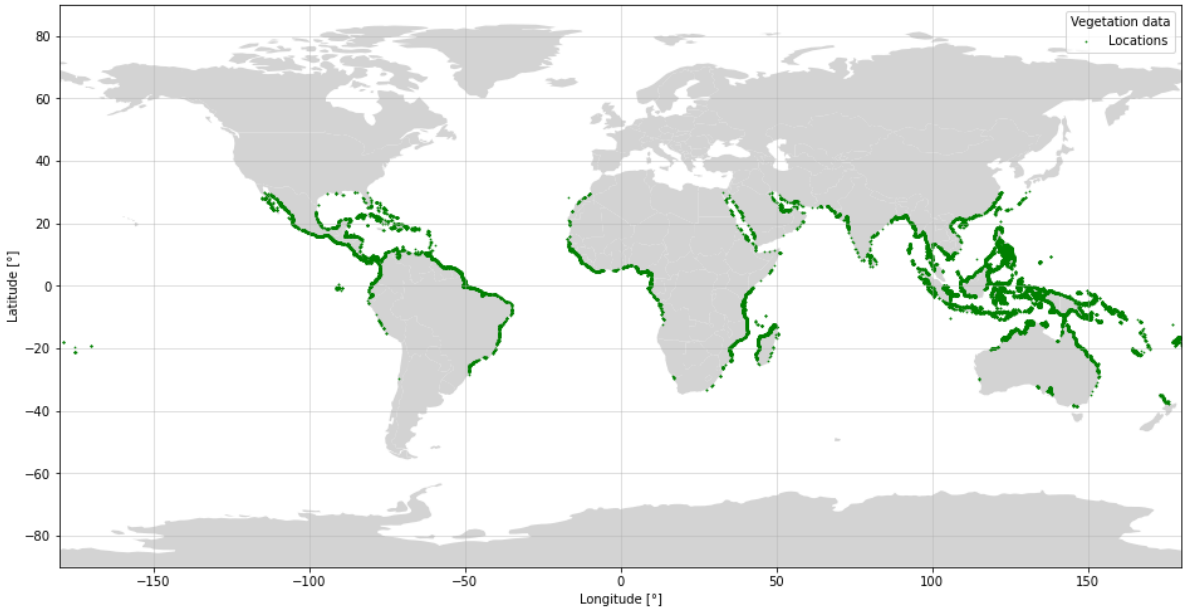

Figure 3.2: *The 27440 locations where mangrove is present at the coastline, based on the study of Van Zelst (2018)*

3.1.2. Environmental data sources

For these 27440 locations the non-stationarity of the multivariate extreme events is identified by using the data source of a period of 32 years of two data-sources. The first time-series is the ERA5 model of the European Centre for Medium-Range Weather Forecasts, ECMWF, which describes atmospheric, land, and oceanic climate variables in a 30 km global grid (ECMWF, 2021). This model will be used to define the wave-characteristics at the mangrove locations. Appendix A.2 will elaborate further on the characteristics of the dataset and the data extraction from these data sets based on the mangrove locations used in this study.

The second data source is the water level characteristics driven by extreme events extracted from the Global Tide and Surges Model, called GTSM (Verlaan et al., 2015; Muis et al., 2016). The GTSM applied in this study is updated with ERA5 data, instead of ERA-I. The time-series of the GTSM is the sum of the tidal signal, the storm surge, and the observed increase in water levels in the past years. By extracting the calculated tidal signal and sea-level rise from the calculated time-series of the model, the result is the so-called skew-surge, which will be the definition of storm surge used in this study (Batstone et al., 2013). The GTSM model is furthermore used to define the highest astronomical tide at the different mangrove locations. The sea-level rise in the GTSM model is added with a constant height per year, appendix A.2. This makes it possible to calculate a stationary time series representing the tidal signal, from which the HAT is extracted. With the use of a nearest neighbor method, called KD-tree, the environmental locations of interest are selected (Maneewongvatana and Mount, 1999) . These locations are based on the coastal mangrove locations. This resulted in 2200 locations of the ERA5 model and 4708 locations of the GTSM model, which are of interest for the environmental conditions in the specified mangrove locations.

The two data sources have a different grid from which the data is extracted, resulting in 5809 different combinations of these two data sources. An example of this is given in appendix A.2. The minimum number of mangrove locations represented by one of these unique combinations is 1 and the maximum is 68. The time-series starts at 1987-01-01 and ends on 2018-12-31. The start of this time frame of 32 years is based on the limiting accuracy of the ERA5 model at the beginning of the 80s. The end of the time frame is a result of the fact that the time-series of the Global Tide and Surges model end at 2018-12-31.

3.1.3. Natural protection data sources and parameter definition

The parameters $width_{ns}$, $width_{fs}$, h_{fs}, $z_{0,veg}$ and the h_{veg} for the 27440 mangrove locations are extracted from three different data-sources. The parameter $width_{ns}$ is extracted from the work of Athanasiou et al. (2019). The dataset from that study has a resolution of 1 km along the global coastline. It contains the coastal slopes defined between the depth of closure and the mean sea level. Further explanation of the method used in this study can be found in appendix A.3. By applying the KD-tree the dataset is combined with the original dataset. While all the slopes are determined on the shoreline, some show the slope within a delta, which is not representative of the transformation of offshore conditions towards onshore conditions. For that reason literature was used to provide a filter on the data set, resulting in an upper limit of 0.02 [m/m] and a lower limit of 0.0005 [m/m] before the nearest neighbor within the dataset was searched (Tas, 2016; Bakker, 2017). When the calculated $width_{ns}$ is above 10000 m, it is replaced with 10000 m. This step is introduced to prevent a computational expensive hydrodynamic domain.

The parameters $width_{fs}$, h_{fs} and $z_{0,veg}$ are extracted from the dataset of Van Zelst (2018). The slope of the foreshore, height of the starting point of the foreshore and the starting point of the vegetation are calculated. Appendix A.3 elaborates on the methodology applied in the study of Van Zelst (2018). The starting point of the foreshore, is at some locations higher then $z_{0,veg}$. Based on the method applied in the study of Van Zelst (2018), this should not be feasible. For that reason at these location $z_{0,veg}$ is set equal to the $z_{0,fs}$. When the calculated $width_{fs}$ is above 10000 m, it is replaced with 10000 m. This step is introduced to prevent a computational expensive hydrodynamic domain.

The height of the mangrove trees are extracted from the study of Simard et al. (2019). Along the transects at the 27440 mangrove locations the average height of the maximum basal weighted height is collected. The creation of the transects is explained in further detail in appendix A.1. For 74.1% (20333) of the locations, an average vegetation height was found. For the other locations, the height of the nearest neighbor was used. The result of this data extraction is visualized in figure 3.3.

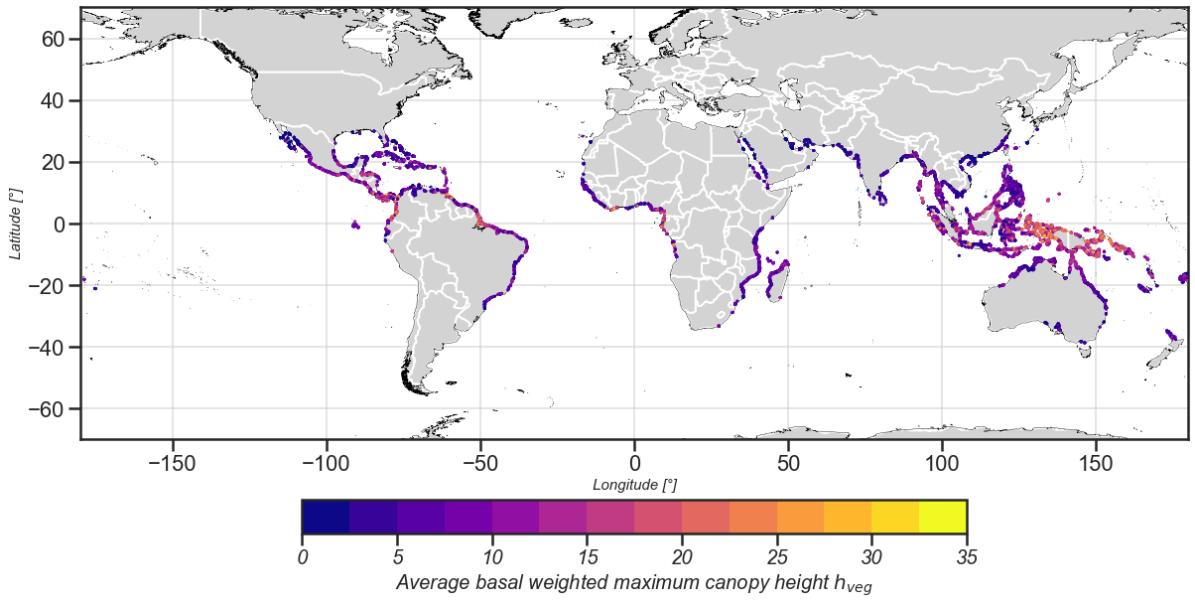

Figure 3.3: *Maximum canopy basal weighted height in meters of the coastal mangrove tree defined with the data set of Simard et al. (2019)*

The transects resulting in the vegetation height have to contain at least 5 grid cells of data along the transect before the h_{veg} can be calculated, otherwise the h_{veg} of the nearest location is applied. When the vegetation height was below 1.37 m, it was replaced with a minimum vegetation height of 1.37 m.

The vegetation height is used as input to define the different parameters for the coastal vegetation. The three layers to define are the roots, stem and canopy. With the use of the extensive literature study of Janssen (2016) on parameterization of vegetation and the representation of a pioneering tree in van Zelst et al. (2021), 7 different trees have been defined in this study. These trees represent Red mangroves trees. Appendix A.3 discusses the results of the differences of Black and Red mangrove trees based on the results of the hydrodynamic model. The conclusion was made that Red trees are less effective in attenuating waves, and therefore leads to a more conservative approach. The first tree, representing a young pioneering tree, has a height of 1.37 meter based on the representation in the forest model of Chen and Twilley (1998). The other trees increase in height from 5 until 30 meters, to cover the distribution of found heights. The definition of parameters is defined on two assumptions.

The first assumption is that with an increasing height the density and the dimensions of the cylinders within a layer are increasing. This results in an increase of the parameters $b_{v,i}$ and $N_{v,i}$ when the height of the tree is increasing. This assumption is based on the fact that a higher tree needs more and thicker roots to stabilize itself. This is in line with the parameterization made in Janssen (2016).

The second assumption is that the maximum $BM_{fac,3}$ for the canopy is 100, based on the study of Narayan et al. (2011). This results in a decrease of density of the canopy for the largest trees, observed in the parameters $N_{v,3}$ and $b_{v,3}$. This is in line with the maximum $BM_{fac,3}$ of 100, being a representation of the biomass in the third layer of the tree known as the canopy. This parameter is calculated with equation 3.1.

$$BM_{fac,i} = N_i \cdot b_{v,i} \cdot h_{v,i} \tag{3.1}$$

The parameters of the 7 trees are listed in table A.1. SWASH requries a minimal number of stems per squared meter of 1, therefore the lowest N_i value present in the vegetation is set to 1. The parameters of the tree with the closest height to the one of the transect are applied in the hydrodynamic model.

	Roots			*Stem*			*Canopy*			*Height*
	$N(r/m^2)$	$b(cm)$	$h(m)$	$N(r/m^2)$	$b(cm)$	$h(m)$	$N(r/m^2)$	$b(cm)$	$h(m)$	h_{tot}
Tree 1	1	0	0	1	0	0	30	3.5	1.37	1.37
Tree 2	15	1	0.15	1	5	2	33	3.5	2.9	5
Tree 3	25	1.5	0.275	1	13	4	36	3.5	5.7	10
Tree 4	35	2.0	0.40	1	20	6	40	2.9	8.6	15
Tree 5	47	2.3	0.53	1	28	8	43	2.0	11.5	20
Tree 6	58	2.6	0.66	1	38	10	46	1.5	14.3	25
Tree 7	70	3.0	0.80	1	50	12	50	1.2	17.2	30

Table 3.1: *Vegetation parameters for the hydrodynamic model of the three different layers, namely roots, stem and canopy, of a representative Red mangrove tree, selected for 7 different heights.*

The last parameter to represent the vegetation in the hydrodynamic model is the bulk drag coefficient, C_D. This parameter is set to the commonly used 1.0, representing mangrove as rigid cylinders (Narayan et al., 2011; van Zelst et al., 2021).

3.2. Non-stationary extreme value analysis

In literature, methods are available to perform multivariate extreme value analyses with the use of a Proxy value. However, these methods are based on a stationary assumption (Gouldby et al., 2014; Lira-Loarca et al., 2020). In this study, the non-stationarity of extreme events is implemented in a multivariate extreme value analysis. The hypothesis is that storm-induced flooding will already occur before chronic flooding is expected in the tropical region in 2050 (Vousdoukas et al., 2018; Shadmehri Toosi et al., 2020).

3.2.1. Proxy

The application of a Proxy is already introduced in previous studies and offers the capability to define combinations of parameters leading towards extreme multivariate events (Gouldby et al., 2017; Lira-Loarca et al., 2020). The Proxy is used to define the region of multivariate extreme events based on two vulnerabilities of the coastal protection offered by mangrove trees.

The first vulnerability of mangrove forests as coastal protection is the lower wave-energy attenuation capacity for long-period waves (Horstman et al., 2014; Phan et al., 2015; Gijsman et al., 2021). This means that the wave period of the waves during an extreme event is of importance in the determination of the added value of mangrove vegetation in coastal protection. For that reason, a proxy with the mean wave period is favored above a proxy with a peak wave period, resulting in taking into account the long-period waves of the spectrum.

The second vulnerability is the difference in wave attenuation capacity over the vertical of a mangrove tree. This is a result of the more dense roots and canopies of a tree with respect to the stems (Mcivor et al., 2012; Van Wesenbeeck et al., 2021). This means that the proxy should incorporate the storm driven water level, called the skew surge (Batstone et al., 2013).

These two vulnerabilities resulted in the selection of the multivariate extreme event definition used in the study of Gouldby et al. (2014). The multivariate event applied in that study is the notional flooding level, l, shown in equation 3.2. This equation is originally defined by Stockdon et al. (2006), to represent the 2% run-up level for at dissipative beach. It was extended with the addition of the surge in the study of Gouldby et al. (2014).

$$l = S + 0.043 \left[\frac{H_s g T_m^2}{2\pi} \right]^{1/2} \tag{3.2}$$

In which is the l is the flood level in $[m]$, S the storm surge in $[m]$, H_s the significant wave height in m, g the gravitational acceleration in $\frac{m}{s^2}$ and T_m the mean wave period in s.

This multivariate event definition includes the the storm driven water level and the characteristics of the wave spectrum. With the inclusion of the T_m and S, it takes into account the vulnerabilities of the wave attenuation capacity of the mangrove tree and therefore indicate the region of multivariate events of interest. This results in the proxy, P_{xy} of equal to equation 3.2.

With the use of this Proxy, the extreme multivariate events can be identified. In this study an event has to meet the following three requirements to make sure that the event is indeed an extreme event:

- *The sampling should only identify one peak during an extreme event. This leads to a minimal inter-arrival time, δ, is defined as 48 hours between extreme events, following the study of Caires and Sterl (2005).*
- *To prevent that two short crested peaks may result in the classification of a storm, the duration of a storm is based on the total duration of a group of peaks above the threshold. This is visualized in figure C.4, where the time between the different peaks determines if it is classified as a single storm with multi peaks or a storm with a single peak. The minimal duration of a group of peaks above the threshold before it is identified as a storm is set to 12 hours (Van Den Bos and Verhagen, 2018).*
- *The number of extreme events has to be between 2.5 and 10 per year, to secure enough data points for the following analysis.*

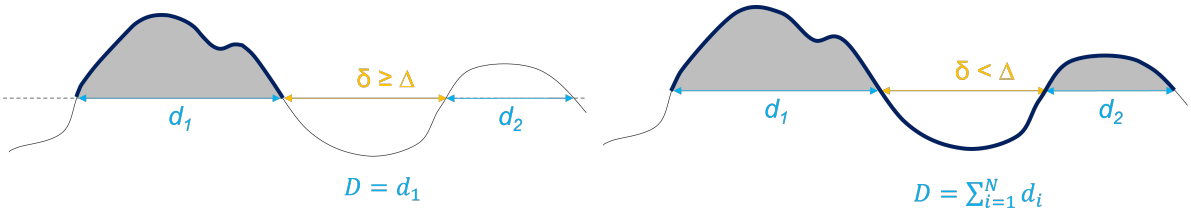

(a) *Single peak storm* **(b)** *Multi peak storm*

Figure 3.4: *Visualization how the requirement for the minimal duration of a storm is defined*

The duration requirement mentioned above differs from the study of Lira-Loarca et al. (2020) Where the duration of a storm was the time between the first upward crossing of the threshold and the last downward crossing of the last peak of a group of peaks above a threshold. That approach may result in two short peaks above the threshold with an interarrival time just below the maximum interarrival time. In the study of Corbella and Stretch (2013) the duration of a storm is only based on a single peak and the time of it above the threshold. This means that neighboring peaks around this peak are not considered in the analysis. Due to this consideration, the requirement is set on the total duration above the threshold. Summarized, the assumptions used for identifying the extreme compound events are listed in table 3.2.

Parameter	**Relation**	**Value**
Duration, D	$\geq$	12 hours
Interarrival time, Δ	$\geq$	48 hours
Number of extreme events, N_s	$\geq$ $\leq$	2.5 per year 10 per year

Table 3.2: *Overview of the the selection procedure of extreme events as input for the multivariate extreme value analysis performed with the Proxy.*

The next step is to define the threshold applied in the Peak over Threshold analysis, POT, which is applied as extreme value analysis in this study. This optimization process for the 5809 environmental locations is performed with a statistical test, to identify when the threshold is indeed selecting the extreme events. The classification of the Proxy is identified as an extreme is based on the assumption that the found extreme events follow a Generalized Pareto distribution, equation 2.1 (Méndez et al., 2006). This classification is selected after investigating different approaches (Caires and Sterl, 2005; Gouldby et al., 2017; Lira-Loarca et al., 2020).

The statistical test to define the goodness of fit of to a statistical hypothesis is the Kolomogorov-Smirnov test, following part of the methodology of Lira-Loarca et al. (2020). The statistical hypothesis in this case is the GPD distribution of the extreme values of the Proxy. The Kolmogorov-Smirnov test searches for the largest vertical distance between the expected distribution and the obtained distribution. To test if the assumption of an exponential distribution for P_{xy} is met with a certain threshold for P_{xy} called $P_{xy,u}$, a Generalized Pareto distribution is fitted through the data as shown in figure 3.5. The level of significance of the null hypothesis from the Kolmogorov-Smirnov test is given by p, defining the level of significance of the null hypothesis. This reflects the probability of rejecting the null hypothesis when it is true. When p is larger than α, the null hypothesis holds with a significance level of α. The level of significance for which the null hypothesis is met should be at least $\alpha = 0.05$. This level of significance is in line with previous studies (Caires and Sterl, 2005; Gouldby et al., 2014; Solari et al., 2017; Lira-Loarca et al., 2020).

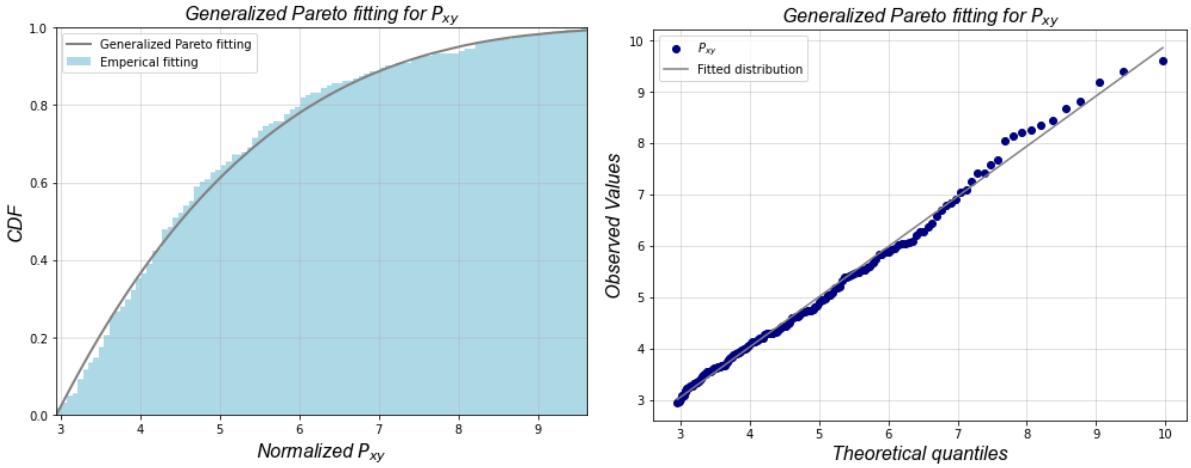

(a) *CDF of Generalized Pareto distribution of $P_{xy,u}$*

(b) *QQ of Generalized Pareto distribution of $P_{xy,u}$*

Figure 3.5: *Visualization of the goodness of fit approach of the extreme events following the required GPD for $P_{xy,u}$.*

For this study, an optimization script is used to search for the lowest percentile of the Proxy data to meet this requirement. It will select the lowest percentile based on the values presented in table 3.3, which meets the statistical test. This will result in the largest amount of data for further analysis, which is advised by Caires and Sterl (2005). A decrease in stepsize is applied for the percentile above 98.5%, because this increased the capability of the approach to find a percentile for which the requirements were met.

If the number of defined extreme events does no longer meet the requirement of N_s, the previous lower percentile is chosen. This approach is applied to be as close as possible to the required level of significance. When the level of significance is met, but the N_s is to large, the script will continue to search for a larger percentile meeting the statistical test.

$P_{xy,u}$	percentile	0.950, 0.955, 0.960, 0.965, 0.970, 0.975, 0.980, 0.985, 0.986. 0.987, 0.988, 0.989, 0.990, 0.991, 0.992, 0.993, 0.994, 0.995, 0.996, 0.997, 0.998, 0.999

Table 3.3: *Percentiles of the Proxy time-series to test the statistical assumption of the Generalized Pareto distribution on.*

3.2.2. Non-stationary extreme value analysis

In appendix B.1, implications are explained when a stationary approach is applied in a non-stationary climate. Based on the hypothesis of this study, that non-stationarity can already be observed in the tropical regions, a non-stationary extreme value analysis will be performed on the Proxy. This approach is based on the following two assumptions:

- *The transformation of N_s over time is left out of the scope of this analysis, because only 32 N_s values are available, resulting in a large sensitivity to outliers.*
- *The non-stationarity is defined by fitting the trend in the mean and standard deviation of the complete dataset, to prevent sensitivities to outliers.*

The first assumption is based on the limited length of the time-series. These time-series would only resultin in 32 N_s values. For that reason, a trend analysis on this parameter would be too sensitive for outliers and is therefore left out of the scope. This introduces the application of a stationary N_s

The second assumption is applied with the technique proposed in this study of Mentaschi et al. (2016). In that study the extreme value analysis is performed with a stationary time series $x(t)$ based on the non-stationary time series $y(t)$. The first step in this approach is shown in equation 3.3 in which the data is normalized by re-scaling it with the standard deviation $S_{0y}(t)$ of the time window W and the mean $T_{0y}(t)$ of a time window W. The $T_{0y}(t)$ is calculated by the centralized mean of the time series as shown in equation 3.4. To decrease the sensitivity of the $S_{0y}(t)$ for outliers, the $S_{0y}(t)|_{ROUGH}$, from equation 3.5 is smoothed with a moving average based on the time window $W/2$ resulting in equation 3.6. Seasonality within a year is left out of the analysis, as only the extreme events during the storm season are of interest. The time window W of 6 years is applied, advised for shorter time series like the 32 years in this analysis (Mentaschi et al., 2016).

$$x(t) = f(y,t) = \frac{y(t) - T_{0y}(t)}{S_{0y}(t)} \tag{3.3}$$

$$T_{0y}(t) = \sum_{tt=t-W/2}^{tt=t+W/2} y(tt)/N_t \tag{3.4}$$

$$S_{0y}(t)|_{\text{ROUGH}} = \sum_{tt=t-W/2}^{tt=t+W/2} \sqrt{[y(tt) - \bar{y}(tt \in [t-W/2, t+W/2])]^2/N_{\text{Wsn}}} \tag{3.5}$$

$$S_{0y}(t) = \sum_{tt=t-W/4}^{tt=t+W/4} 2S_{0y}(tt)\Big|_{\text{ROUGH}} /N_t \tag{3.6}$$

In which $x(t)$ is the stationary time series, $y(t)$ the non-stationary time series, $T_{0y}(t)$ is the long-term trend in the time series, $S_{0y}(t)$ equals the long-term varying standard deviation, W is the time window and N_t is the number of observations available during the time window W.

The obtained distribution of the GPD resulting from the POT analysis based on the stationary P_{xy}, is transformed to the original non-stationary P_{xy} to result in useful parameters for the clustering phase following the approach of Mentaschi et al. (2016). The threshold $P_{xy,u}$ and the location parameter μ are transformed in the same way as shown in equations 3.7 3.8, the shape parameter ϵ stays constant as shown in equation 3.9 and the scale parameter σ is calculated with equation 3.10. The subscripts $_y$ and $_x$ show respectively the stationary and the non-stationary parameters. By assuming a linear trend over the time series of $T_{0,y}(t)$ a line is fitted through the obtained $P_{xy,u}$, resulting in a linear trend over time. Examples of this complete analysis can be found in appendix B.4 for 4 of the 5809 environmental locations.

$$P_{xy,uy}(t) = S_y(t) \cdot P_{xy,ux} + T_y(t) \tag{3.7}$$

$$\mu_y(t) = S_y(t) \cdot \mu_x + T_y(t) \tag{3.8}$$

$$\varepsilon_y = \varepsilon_x = \text{ const.} \tag{3.9}$$

$$\sigma_{\text{GPD}y}(t) = \sigma_y(t) + \varepsilon_y \left[u_y(t) - \mu_y(t)\right] = S_y(t) \cdot \sigma_{\text{GPD}x} \tag{3.10}$$

3.2.3. Non-stationary multivariate extreme value analysis

The extreme compound events identified represent a combination of the parameters H_s, T_m and S. This means that the non-stationarity could be in three dimensions with respect to time. This transformation of the multivariate extreme events is visualized in figure 3.6 for a two-dimensional multivariate extreme event. On the horizontal and vertical axis, the transformation of the mean over time is given with, $\Delta\mu_X$ and $\Delta\mu_Y$. The non-stationary scale parameter, results in a different extend of the cloud of extreme events at $t = 1$ in comparison to $t = 0$. This is a result of the fact that the scale parameter influences the spread of extreme events.

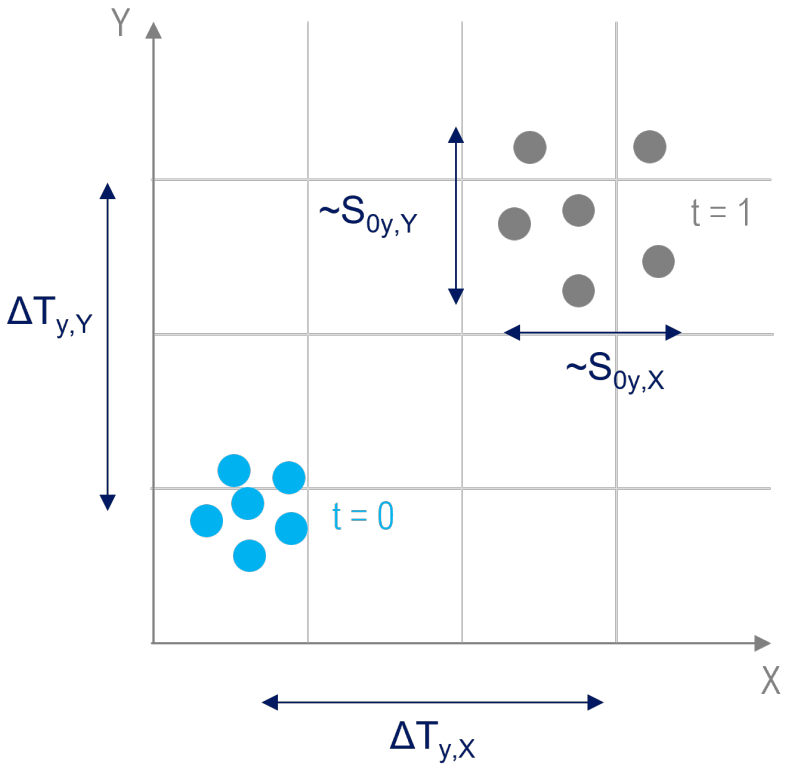

Figure 3.6: *Assumptions of non-stationary location and scale parameter of the multivariate extreme value analysis*

The time-dependent mean, $T_y(t)$, and standard deviation $S_y(t)$, are introduced to track the discussed degrees of freedom in the three directions of the parameters. With the assumption of a linear trend over time for both parameters, equations 3.11 and 3.12 are introduced.

$$T_{0y}(t) = T_y(0) + T_T * t \tag{3.11}$$

$$S_{0y}(t) = S_y(0) + T_S * t \tag{3.12}$$

where $T_{0y}(t)$ is the time-dependent mean, $T_y(0)$ the stationary part of the mean, T_T the linear trend over time, t the moment in time, $S_{0y}(t)$ is the time-dependent standard deviation, $S_y(0)$ the stationary part of the standard deviation and T_S the linear trend over time.

The first step in this approach is transforming the non-stationary univariates towards a stationary time series, applying the methodology of Mentaschi et al. (2016) on the identified cloud of compound events. For the three different parameters the mean, $T_{0y}(t)$, and the standard deviation, $S_{0y}(t)$, are determined using the equations 3.3 to 3.6.

The time dependent procedure of the parameters results in a transformation procedure to transform the non-stationary H_s, T_m and S over time towards the stationary H_s^*, T_m^* and S^*. The linear assumptions used are applied in equation 3.3 resulting in equation 3.13:

$$U^* = \frac{U - (T_{0y} + T_T \cdot t)}{(S_{0y} + T_S \cdot t)} \tag{3.13}$$

where U is the non-stationary univariate and U^* the detrended stationary univariate. T_{0y} and S_{0y} are the stationary part of the mean and standard deviation of the univariate. T_T and T_S represent the non-stationary part of these detrending parameters. Parameter t is the time in days with respect to the begin of the time series at 1987-01-01. The fitting procedure is visualized in figure 3.7. For the three parameters the linear fitted slope T_S is indicated with light and dark blue and the slope T_T is indicated in orange.

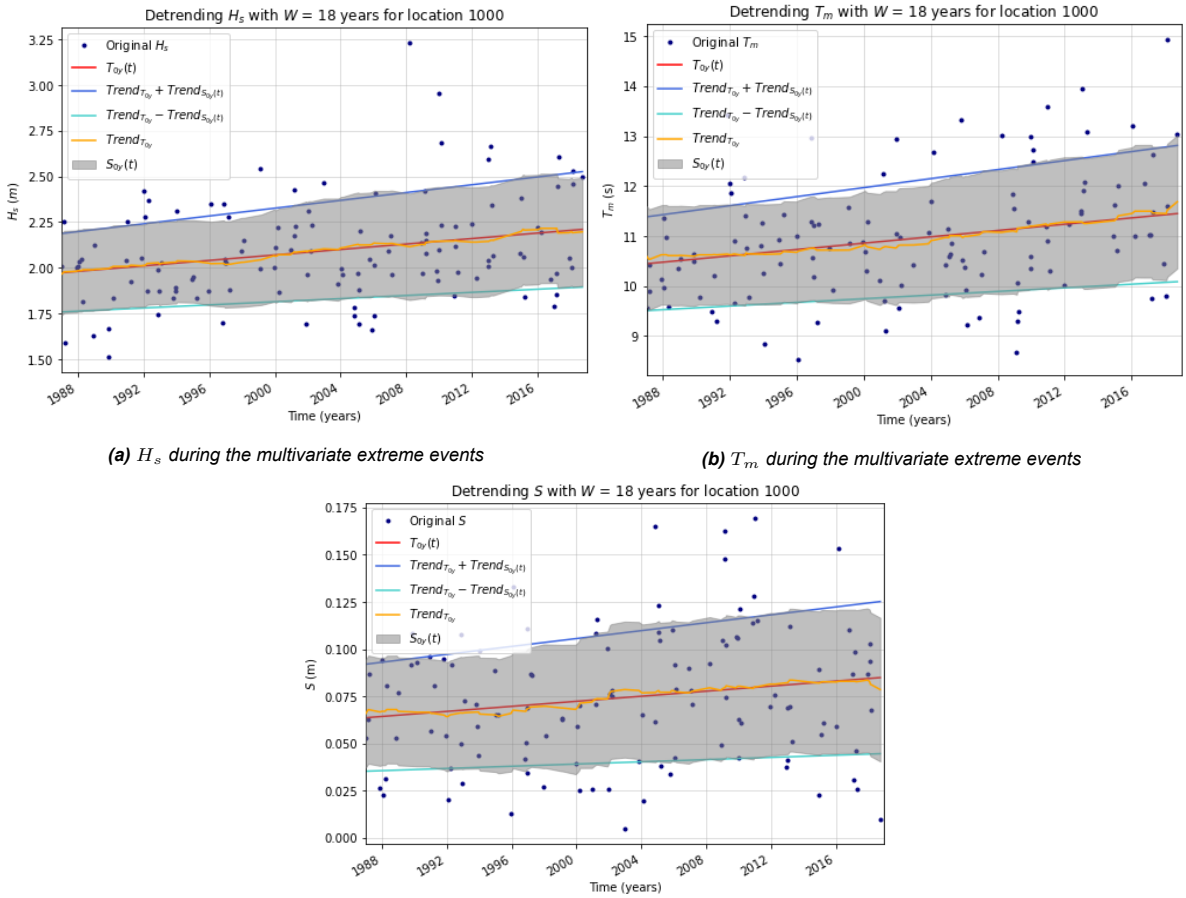

(a) *H_s during the multivariate extreme events*

(b) *T_m during the multivariate extreme events*

(c) *S during the multivariate extreme events*

Figure 3.7: *Mentaschi et al. (2016) method applied to univariates of extreme compound events with time window of 18 years for location 1000.*

These linear fittings result in the time dependent $T_{0y}(t)$ and $S_{0y}(t)$ applied in equation 3.13. Detrending of the univariates from the extreme value analysis is presented in figure 3.8. The blue dots indicate the univariates at the original scale, the light blue points indicate the stationary result of the univariates.

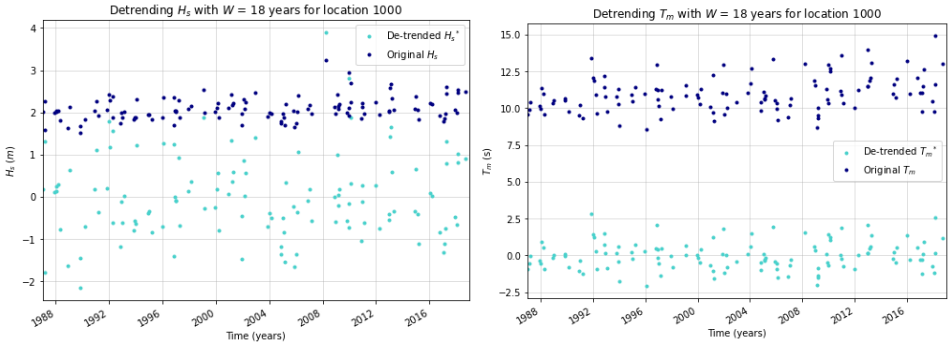

(a) H_s and H_s^* during the multivariate extreme events **(b)** T_m and T_m^* during the multivariate extreme events

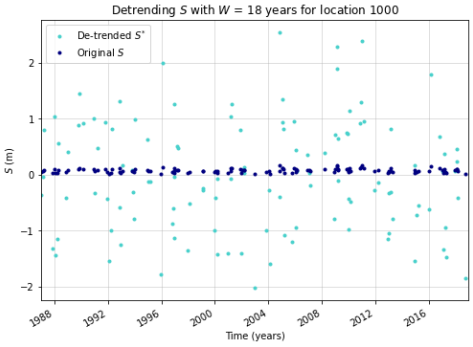

(c) S and S^* during the multivariate extreme events

Figure 3.8: *Transformation of non-stationary univariates to stationary univariates with equation 3.13*

The next step is to represent these stationary univariates with a statistical distribution. With the comparison and a focus on the fitting of the upper and lower tail of the distributions, different distributions found in literature to fit the extreme values of a compound event are tested in appendix C (De Michele et al., 2007; Lira-Loarca et al., 2020). A Log-Normal distribution was found to best represent the compound extreme events examined in this study. The Log-Normal distribution shown in equation 3.14, contains the parameters ε, μ and σ, which are the shape, location and scale parameter. In figure 3.9, this procedure step is visualized. The relation of the observed and expected values are given based on the fitted distribution. The outliers of H_s could be a result of an event that is extremely wave-driven.

$$f(x, \varepsilon, \mu, \sigma) = \frac{1}{\frac{x-\mu}{\sigma}\varepsilon\sqrt{2\pi}} \exp\left(-\frac{(\log^2(\frac{x-\mu}{\sigma})}{2\varepsilon^2}\right) \tag{3.14}$$

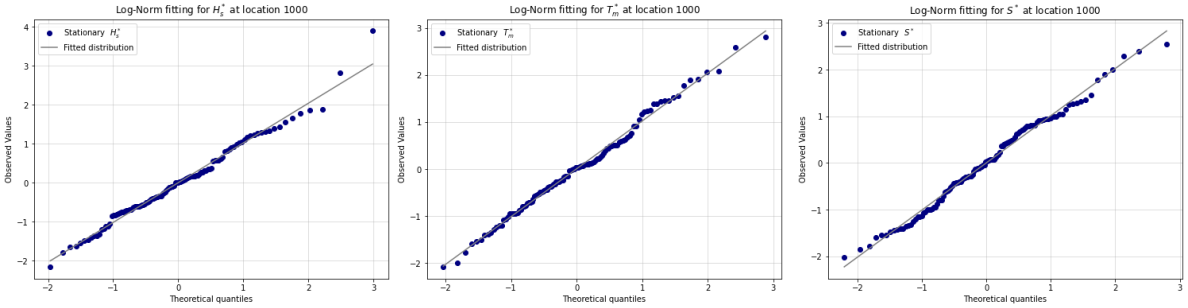

(a) QQ-plot fitting for H_s^* **(b)** QQ-plot fitting for T_m^* **(c)** QQ-plot fitting for S^*

Figure 3.9: *Cumulative distribution functions for the detrended variables*

The dependency between the different variables is defined by applying a Vine model, based on H_s^*, T_m^*, and S^*. The Archimedean copulas are applied to capture the dependencies within the Vine-D model. Based on previous research, the assumption is made that the Archimedean copulas are capable of representing the dependency between these variables (Corbella and Stretch, 2013; Li et al., 2018; Lira-Loarca et al., 2020). This results in three bivariate copulas applied on the set (H_s^*, T_m^*), (T_m^*, S^*) and $(C_{H_s^* T_m^*}, C_{T_m^* S^*})$, where $C_{H_s^* T_m^*}$ and $C_{T_m^* S^*}$ are the determined copula's of the first level of the Vine tree. The construction of the Vine-D model is performed with the python Copula package written by the MIT Data To AI LAB (SDV - MIT Data to AI Lab, 2018). The selection of the best fitting copula is based on the sum of the error of the upper and lower tail between the empirical cumulative distribution function and the candidates. The candidates are the three Archimedean copulas with their fitted parameters to the data set. A visual inspection is a commonly used approach, as there is no clear procedure for selecting (Lira-Loarca et al., 2020; De Michele et al., 2007). A visualization of this procedure step is shown in figure 3.10. In this figure the relation between the marginal of two stationary parameters is shown, yellow indicates the original distribution of the marginals, and grey the points generated with the Vine-D structure.

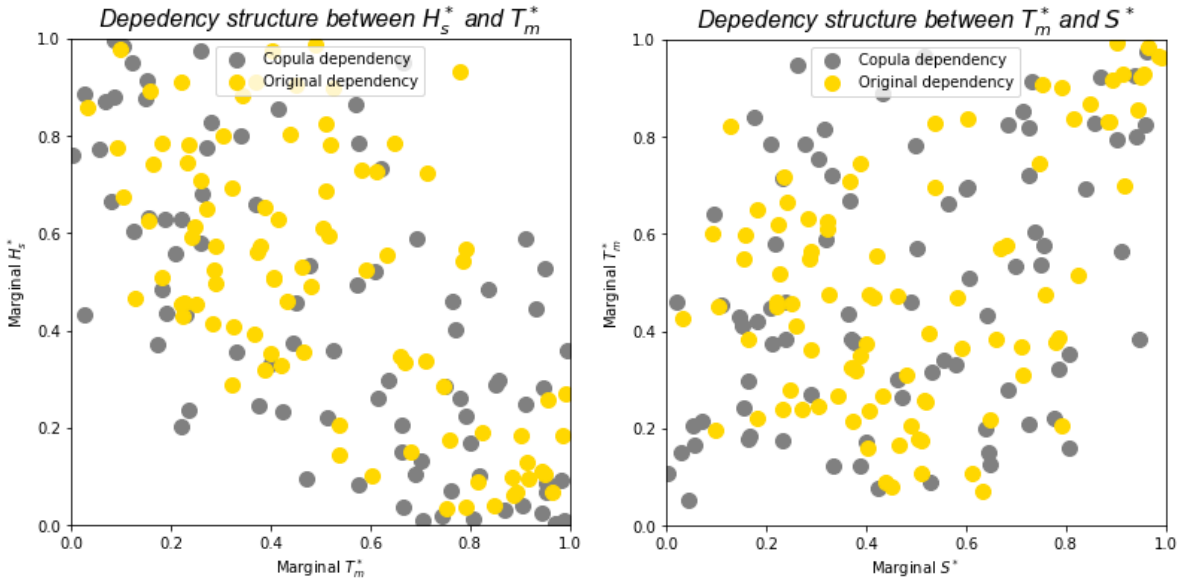

(a) *Copula dependency between H_s^* and T_m^**

(b) *Copula dependency between T_m^* and S^**

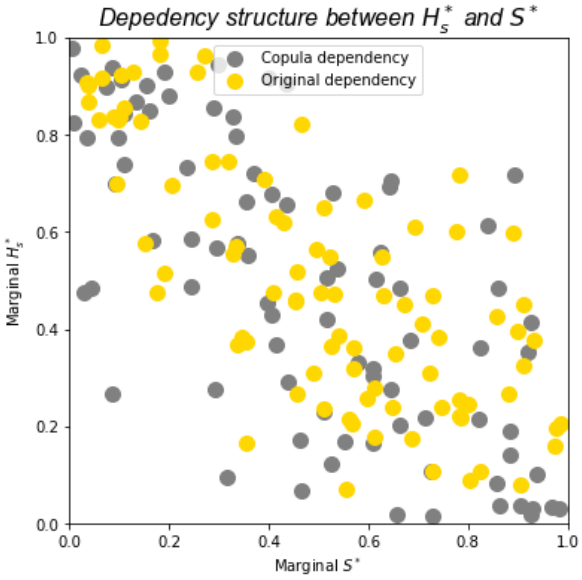

(c) *Copula dependency between H_s^* and S^**

Figure 3.10: *Vine-D dependency structure of compound events*

From this multivariate dependency model, the stationary design conditions can be extracted. The choice is made to sample the 1/40 year design condition, to keep the range of 32 year of the original data set in mind. The dependency structure between the univariates defines the probability of the combinations of the three parameters during the extreme events and the univariate probability function defines the probability of occurrence of these parameters. With these constraints extreme events can be sampled from the dependency model in the stationary domain. The 1/40year design conditions, means that 40 times N_s samples are extracted, as explained by equation 2.11. With the use of the inverse of equation 3.13, these design conditions can be transformed to the moment of time of interest. In this study, the interest lies within the transformation of these design conditions between the beginning and the end of the time period. For that reason, the design conditions are transformed towards 1987-01-01 and 2018-12-31.

Based on the probability functions, samples can be created which are beyond physical bounds. For that reason, two restrictions are applied to the sampled parameter combinations. These two restrictions will be applied to the trended data of the two time periods. When one of the restrictions is not met at one of the time periods, this parameter combination is replaced with a newly generated sample from the Vine-D model.

The first restriction is to validate that the sampled H_s and T_m are positive values, while negative values for these parameters have no physical sense. The parameter S on the contrary can be a negative value, representing a negative surge.

The second restriction on the data generation is checking the shape of the wave input, based on the maximum wave steepness that can occur. Waves that are too steep can not hold and will break. For this validation, the first step is transforming the mean wave period T_m to the peak wave period T_p by applying equation 3.15 (Schiereck, 2017). The second step is based on the equation of Miche (1944), where it is argued that the maximum steepness for H/L is equal to 0.142. By transforming wavelength L towards the peak wave period T_p, the equation of 3.16 is the result, assuming deep water.

$$T_m = 0.9 \cdot T_p \tag{3.15}$$

$$\frac{H}{L} = \frac{2H_s\pi^2}{gT_p^2} \leq 0.142 \tag{3.16}$$

3.3. Statistically upscaling

The computational demand of the non-hydrostatic hydrodynamic model would be too large for this study to apply to all the different climates and transects as indicated in a previous study (Van Zelst, 2018). For that reason, a statistical upscaling technique is introduced on the original 5809 mangrove environments and the 27440 mangrove locations. The statistical upscaling method applied is a clustering technique called K-means. The K-means algorithm searches for groups of data that can be represented with one single scalar. Based on searching the locations with the smallest error to the complete dataset as defined in equation 2.13. Figure 3.11 depicts a simplified visualization of this procedure, where grouped points represent the clusters and the gray points represent the selected scalar value.

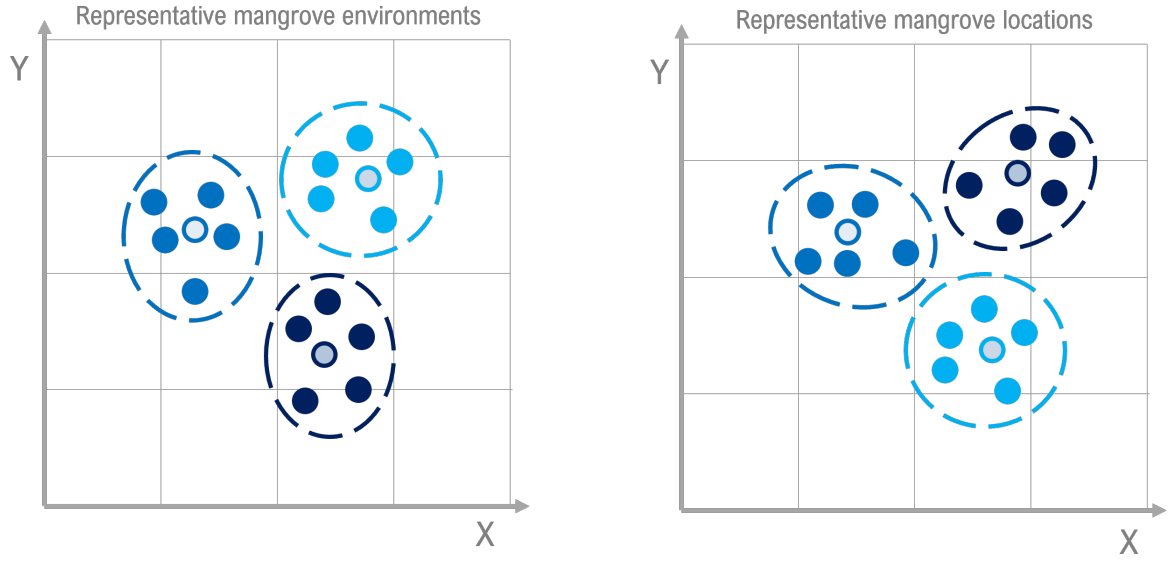

Figure 3.11: *Visualization of statistically upscaling approaches applied. Defined by representative mangrove environments and representative mangrove locations.*

The first step is to reduce the number of mangrove environments with clustering within the 31-dimensional mangrove environments. This will result in a reduced number of representative mangrove environments. To make sure that the optimization does not work towards a local minimum, the distributions of the data are evened out by applying the maximum dissimilarity approach, resulting in 1000 mangrove environments. This approach selects a reduced number of the original environments resulting in largest intermediate distance between the different environments. The different mangrove environments are represented by 31 parameters, resulting from the non-stationary extreme value analysis of the Proxy, the analysis on the detrended H_s^*, T_m^* and S^*, the Copula model Vine-D representing the dependency and the fitted univariate distribution of H_s^*, T_m^* and S^*. The different parameters of the different statistical analyses are listed in table 3.4.

Analysis	*Resulting parameters*
Non-stationary extreme value analysis	N_s
Non-stationary univariate transformation	T_{0y,H_s}, $T_{T_{H_s}}$, S_{0y,H_s}, $T_{S_{H_s}}$ T_{0y,T_m}, $T_{T_{T_m}}$, S_{0y,T_m}, $T_{S_{T_m}}$ $T_{0y,S}$, T_{T_S}, $S_{0y,S}$, T_{S_S}
Time-independent univariate distribution	$\mu_{H_s^*}$, $\sigma_{H_s^*}$, $\epsilon_{H_s^*}$ $\mu_{T_m^*}$, $\sigma_{T_m^*}$, $\epsilon_{T_m^*}$ μ_{S^*}, σ_{S^*}, ϵ_{S^*}
Multivariate dependency model	$C_{H_s^*,T_m^*}$, θ_{C_1}, τ_{C_1} $C_{T_m^*,S^*}$, θ_{C_2}, τ_{C_1} C_{C_1,C_2}, θ_{C_3}, τ_{C_3}

Table 3.4: *The 31 parameters on which the statistical representation of the 5809 mangrove environments is based for the statistically upscaling. Where the dots indicate the raw data points, the dashed line encircles the cluster and the grey colored dot represents the centroid of the cluster.*

For this first step, weight factors are introduced, to give more attention to parameters important for this study of the 31 dimensions. The importance of each of these parameters is included in the optimization process of the K-means cluster. The consideration of the weight of the different parameters is based on expert judgement of how the clusters will be applied in the further analysis. The goal is to generate design conditions that are representing the combined environmental locations. This resulted in the eventual distribution of the weight factors as listed in table 3.5.

Analysis	*Weight*	*Parameters with double weight*
Non-stationary extreme value analysis	**5%**	-
Non-stationary univariate transformation	**45%**	T_{0y,H_s}, $T_{T_{H_s}}$, T_{0y,T_m}, $T_{T_{T_m}}$, $T_{0y,S}$, T_{T_S}
Time-independent univariate distribution	**20%**	μ_{H_s}, σ_{H_s} μ_{T_m}, σ_{T_m}, ϵ_{T_m} μ_S, σ_S
Multivariate dependency model	**30%**	C_{H_s,T_m}, $C_{T_m,S}$, C_{C_1,C_2}

Table 3.5: *The distribution of the weight over the 4 analysis resulting in the 31 parameters for the statistically upscaling, with in the last column the parameters that have obatined a double weight.*

The second step is to cluster the 6-dimensional mangrove locations, to reduce the number of locations that are used as input for the hydrodynamic model. In table 3.6 these different parameters are listed. Literature emphasizes a relation between the water level and the cross shore location where mangroves occur. Mangroves are namely expected to grow below the HAT and above the MSL (Wilms et al., 2020). This implies that there is a relation between the starting point of vegetation along the foreshore and the tide. For that reason, HAT, is defined as location specific in this study. In this 6-dimensional domain, the first step is applying the maximum disssimilariy algorithm on the original dataset. This will prevent that the K-means algorithm works towards a local optimum. The number of maximum dissimilarity points within the cloud selected are 5000, which is 18.2% of the original 27440 mangrove locations. After this pre-processing step of the data, the second step is to apply the K-means clustering method to the resulting 5000 datasets.

Part	*Parameters*
Nearshore	$width_{ns}$
Foreshore	$width_{fs}$, h_{fs}, $z_{0,veg}$
Vegetation	h_{veg}
Tidal signal	HAT

Table 3.6: *The 6 parameters on which the statistical representation of the 27440 mangrove locations is based for the statistically upscaling.*

3.4. Hydrodynamic model & safety assessment

The impact of the non-stationary conditions is assessed in the two step methodology with the hydrodynamic model and the empirical coastal safety equations. These steps are introduced in this chapter and visualized in figure 3.12. The output locations of the hydrodynamic model are indicated with red arrows. The in- and output parameters of the different parts of the analysis are indicated in the blocks.

Step 1 is to identify the multivariate extreme event requiring the largest crest height at the beginning of the horizontal plane. For this analysis the offshore design conditions of 1987-01-01 and 2018-12-31 are propagated towards onshore conditions with the use of the hydrodynamic model SWASH. Based on the time-series of the water level from SWASH, H_s and T_m are calculated at the beginning of the horizontal plane. These two parameters are combined with the inital S and used as input of the safety assessment. The empirical equations 2.14 to 2.17 are used to transform this input to a required crest height to meet the coastal safety standards. The event with the highest R_c is defined as the expected event with the most impact, defined as the 1/40 year design condition.

Step 2 calculates the required vegetation width of the 1/40 year design condition. The first part of this analysis is to propogate the offshore conditions towards onshore and through the mangrove vegetation with the use of SWASH. SWASH delivers the transformation of H_s and T_m over the horizontal plane with mangrove vegetation for every 10 meter. The same empirical flood safety equations of Pullen et al. (2018) are used to define the location of the dike along the horizontal plane to meet the required crest height, $R_{c,lim}$. This results in a required width of vegetation, $width_{veg}$.

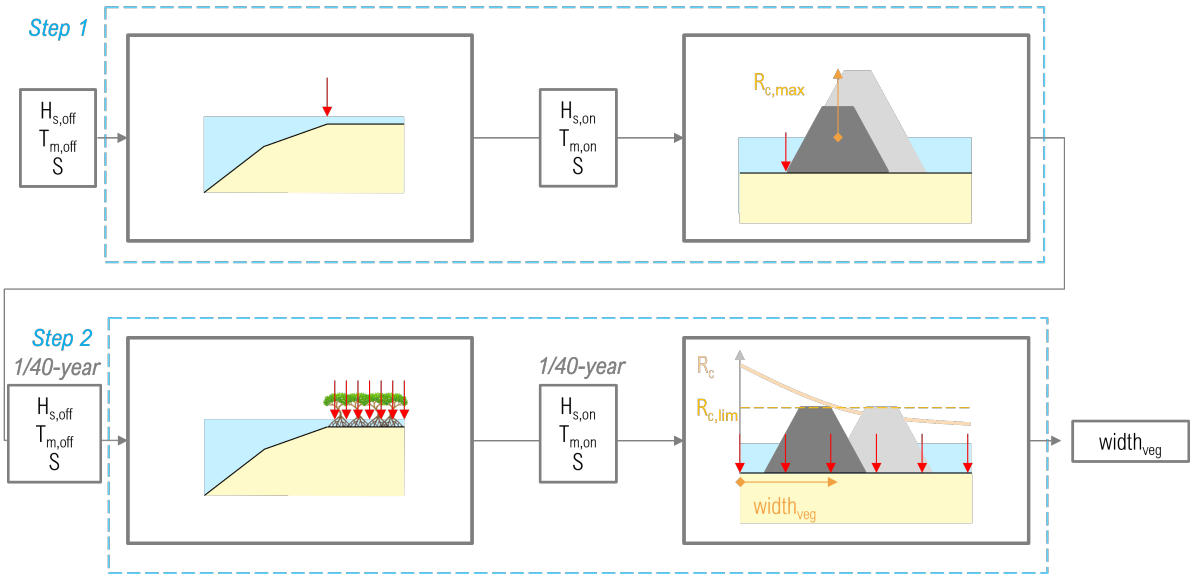

Figure 3.12: *The first step is used to identify the 1/40-year design condition. The second step identifies the required vegetation width. The red arrows indicate where the output of the hydrodynamic model is obtained and which location it represents in the empirical relations of Pullen et al. (2018).*

3.4.1. Hydrodynamic model set-up

First the set-up of the hydrodynamic model in SWASH is introduced. Step specific set-up conditions are indicated in the steps of this chapter. SWASH uses three grids to set up the numerical wave model.

Bathymetry grid

The first grid is the bathymetry grid. This grid defines the location of the bottom of the domain. The grid will start at -20 meter water depth and will use the parameters $z_{0,veg}$, h_{fs}, $width_{ns}$ and $width_{fs}$ to construct the bathymetery at the other locations in the domain. At every 5 meter the location of the bottom is defined, this is sufficient for the linear slopes of the theoretical framework.

An overview of the construction of the bathymetery of the different test cases is displayed in figure 3.13. $z_{0,veg}$ is the reference point for the construction of the bathymetery. Based on this reference point, h_{fs} is used to calculate until which height the nearshore has to be constructed over a width of $width_{ns}$. At the end of the nearshore the foreshore starts. This part of the bathymetry has width $width_{fs}$ and a height of h_{fs}. The last part of the bathymetry starts at $z_{0,veg}$, continuing with a horizontal plane for the vegetation. The bottom friction of the bathymetry is set to the default of SWASH, which is a Manning coefficient of $0.019 m^{-1/3}/s$ (The SWASH team, 2020).

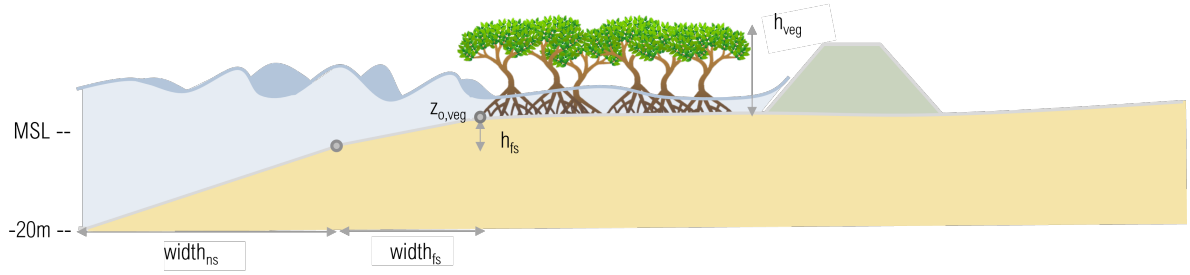

Figure 3.13: *Schematic representation of the hybrid coastal structure introduced in the coastal safety assessment with the horizontal vegetation plane and the dike located behind.*

Vegetation grid
The second grid defines the characteristics of the vegetation. The step size of this grid is equal to the step size of the bottom grid and defines the location of the vegetation. SWASH is only capable to apply an uniform vegetation grid at the specified locations, this results that only one mangrove tree can be applied at a single SWASH run. This is limiting the spatial differences in vegetation observed at mangrove locations (Verhagen and Loi, 2012). SWASH uses the vertical layerization of the vegetation, making it possible to represent the roots, stems and canopy separately as introduced in Suzuki et al. (2012). The parameters for these layers is given in chapter 3.1.3 and is depending on the vegetation height.

Computational grid
The third grid is the computational grid. This grid defines at which locations the non-linear shallow water equations are solved in SWASH. The discretization of the computational grid in time and space is depending on the courant number, indicating the stability of the system based on the traveling speed of information. For waves the courant number is defined with equation 3.21 (The SWASH team, 2020).

$$\sigma_{waves} = \frac{\sqrt{g \cdot h} \cdot \Delta t}{\Delta x} \tag{3.17}$$

where σ_{waves} is the courant number for waves, g the gravitational acceleration in m/s^2, h the water depth in m, Δt the step size for the time-discretization and Δx the step size for the space discretization.

With the implementation of an explicit time scheme an upper and lower limit for the courant number is introduced. SWASH will then search during the integration for the time-step resulting in a courant number between the upper and lower limit. Default SWASH implies an minimum courant number of 0.4 and an upper limit of 0.8. This study examines high waves with wave breaking involved, which results in a lower limit for the courant number. The lower limit is 0.2 and the upper limit is 0.6 for the determination of the most extreme event. For the runs where the width of the vegetation is calculated the advised upper limit of 0.5 is applied to solve the non-linearities correctly (The SWASH team, 2020).

In contrast with the time-discretization step, the space-discretization has to be selected beforehand. In principle the step size in space should be able to resolve the most energetic wave components accurately. This means that a sufficient number of grid cells should be applied per wave length. The rule of thumb is 50 grid cells for the peak wave length (The SWASH team, 2020).

In contrast with the time-discretization step, the space-discretization has to be selected beforehand. In principle the step size in space should be able to resolve the most energetic wave components accurately. This means that a sufficient number of grid cells should be applied per wave length. The extreme events considered in this study have a T_m value ranging from 2.5 till 17 seconds. Using the assumption of $1.1 \cdot T_m$ is equal to T_p, the wave length can be calculated with equation 3.18 (Holthuijsen, 2007).

$$L = \frac{gT^2}{2\pi} * tanh(\frac{2\pi d}{L}) \tag{3.18}$$

The rule of thumb is 50 grid cells for the peak wave length (The SWASH team, 2020). This results in a range of the space-discretization step of 0.12 till 2.5 meter. In this study, large numerical domains are applied, with in some cases a domain up to 20 kilometer. For that reason, the space-discretization will be discussed separately in the different chapters of Step 1 and Step 2.

To track the wave transformation more precisely the number of vertical layers in the computational grid is determined and is depending on the linear frequency dispersion (The SWASH team, 2020). This will indicate the accuracy in the phase velocity of the different wave components and thus the transformation of wave energy. The product of k and d, being the dimensionless water depth, is of special interest in this determination indicating the

relative error in the normalized wave celerity of at most 1%. Where k is the wave number calculated with equation 3.19 (Holthuijsen, 2007).

$$k = \frac{2\pi}{L} \tag{3.19}$$

The wave lengths ranging between approximately 11.8 and 251.8 meter, based on the T_m of 2.5 and 17 seconds at the offshore boundary result in a relative water depth between the 10.6 and 0.5. This would mean accordingly to the manual that three vertical layers should be applied to meet the relative error for the extreme events with a T_m below 2.9 seconds. However, 98.8% of the input for the determination of the most extreme event has a larger T_m then this limit. Taken into account the computational demand of applying 3 vertical layers instead of 2 vertical layers and the small percentage of events that will have a larger error, the choice is made to only apply two vertical layers.

Sponge layer
While a horizontal plane with a certain water depth is considered in the theoretical framework, a sponge layer is applied at the end of the domain to absorb the outgoing waves. The thumb of rule of determine the width of the sponge layer is at least 3 times the typical wave length. While the wave lengths used as input for the determination of the most extreme multivariate event range approximately between 11 and 250 meter. The choice is made to introduce a sponge layer of 1000 meter at the end of the domain.

Water level
The waterlevel in the domain is calculated with equation 3.20. The mean sea level, MSL, is located at 0 m. The eventual waterlevel in the domain WTL is calculated with the increasing the waterlevel with highest astronomical tide, HAT, and the storm surge, S, both in meters.

$$WTL = MSL + HAT + S \tag{3.20}$$

Wave spectrum
The other boundary condition implemented in the model is on the offshore location. At this location a wave spectrum is constructed, based on the H_s and T_m of the specific extreme condition. The wave spectrum used in this study is the JONSWAP spectrum (Hasselmann et al., 1973).

By imposing a spectrum in SWASH, evanescent modes may occur in the computations. These modes are decaying exponentially in the beginning of the domain and are therefore not modelled in SWASH (The SWASH team, 2020). The frequency where above these frequencies may occur can be calculated by equation 3.21, where ω_{cf} is the so called cut off frequency, K the number of layers in the computational domain and g the gravitational acceleration.

$$\omega_{cf} = 2K\sqrt{\frac{g}{d}} \tag{3.21}$$

The water depth is approximately ranging between 20 tot 25 meter. While SWASH runs with two vertical layers the cut-off frequency is between 0.40 and 0.45 Hz. This means that waves with a larger frequency will not be modeled in SWASH, resulting in a reduction of the significant wave height H_s. This decrease in H_s is solved with increasing the input of the system. The increase is often defined in an iterative process. However, due to the large number of computations in this study, another approach is designed. The solution applied in this study is based on the defined relation between the steepness and the drop in H_s. An further explanation of the process is described in appendix D.1. The result of this analysis is visualized in figure 3.14. The color of the dots indicate the drop in H_s observed in the results from SWASH, ranging between 0 m and 0.38 m. The contourlines behind indicate the applied increase of H_s, to reduce the mismatch between input and the H_s at the start of the domain in SWASH.

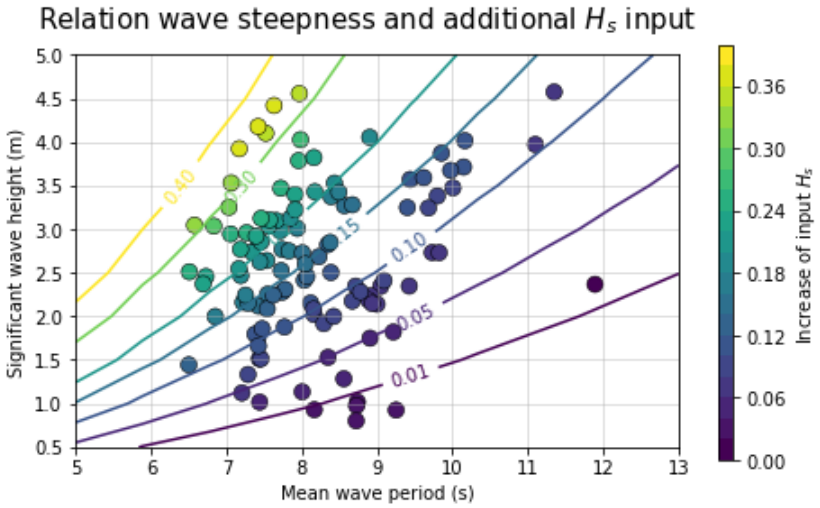

Figure 3.14: *Observed drop in signficant wave height and the applied relation between the wave steepness and the increase of the significant wave height at the boundary of the domain.*

Post-processing

The time-series of the water level produced by SWASH are transformed into a variance density spectrum. With this spectrum the parameters, H_s and T_m can be calculated. The spectrum is defined with equation 3.22 (Holthuijsen, 2007). where a is the amplitude of the oscillation and Δf the chosen frequency band for the analysis. With the use of these variance density spectra the spectral moments of the signal can be calculated, indicating the energy stored within the system. The equation for the nth-order of moment of $E(f)$ is equation 3.23. These spectral moments define with the use of equation 3.24 the parameters H_s and T_m (Holthuijsen, 2007).

$$E(f) = \lim_{\Delta f \to 0} \frac{1}{\Delta f} E\left\{\frac{1}{2}\underline{a}^2\right\} \tag{3.22}$$

$$m_n = \int_0^\infty f^n E(f) df, \quad for \quad n = ... -3, -2, -1, 0, 1, 2, 3, ... \tag{3.23}$$

$$T_{m-1,0} = \frac{m_{-1}}{m_0} \quad H_s = 4\sqrt{m_0} \tag{3.24}$$

3.4.2. Step 1: Identifying the extreme event

The first step in the analysis is to identify the 1/40 year design condition of a specific mangrove environment. This step is performed to use the multivariate extreme events that have a H_s above the 75% percentile. This pre-processing step is introduced based on the positive correlation between H_s and S, and reduces the computational demand. The result of this step is the input of the hydrodynamic SWASH model of this step.

SWASH

The hydrodynamic model of Step 1 is introduced to propagate the offshore conditions towards onshore. Besides the previous explained set-up of the hydrodynamic model, some set-up parameters are step-specific. These parameters are listed in table 3.7.The space discretization step for this domain is 1 meter. This is based on a sensitivity analysis for different step sizes, given in appendix D.5.

Set-up parameter	*Value*	*Unit*
Modelled time	2	$hours$
Space-discretization step	1	m
Spin-up time	40	$minutes$
Frequency band	0.0076	Hz
$WTL_{MSL+HAT}$ *above* $z_{0,veg}$	1	m

Table 3.7: *The 6 parameters on which the statistical representation of the 27440 mangrove locations is based for the statistically upscaling.*

With tracking the transformation of a set of extreme events on three different transects, the methodology is introduced to run the different extreme events on one specific transect. The three different transects differed in length and slopes, to identify the influence of the nearshore and foreshore bathymetry. The influence was limited resulting in the proposed methodology. A further elaboration on the validation of this assumption can be found in appendix E.1.

This domain applied in SWASH for step 1, is visualized in figure 3.15. In this figure the red lines indicate the locations where the output of SWASH is generated. The first location is used to validate the increased $H_{s,off}$, needed to solve the underestimation of the evanescent modes. The second red line indicate the location where the $H_{s,on}$ and $T_{m,on}$ are obtained for the safety assessment.

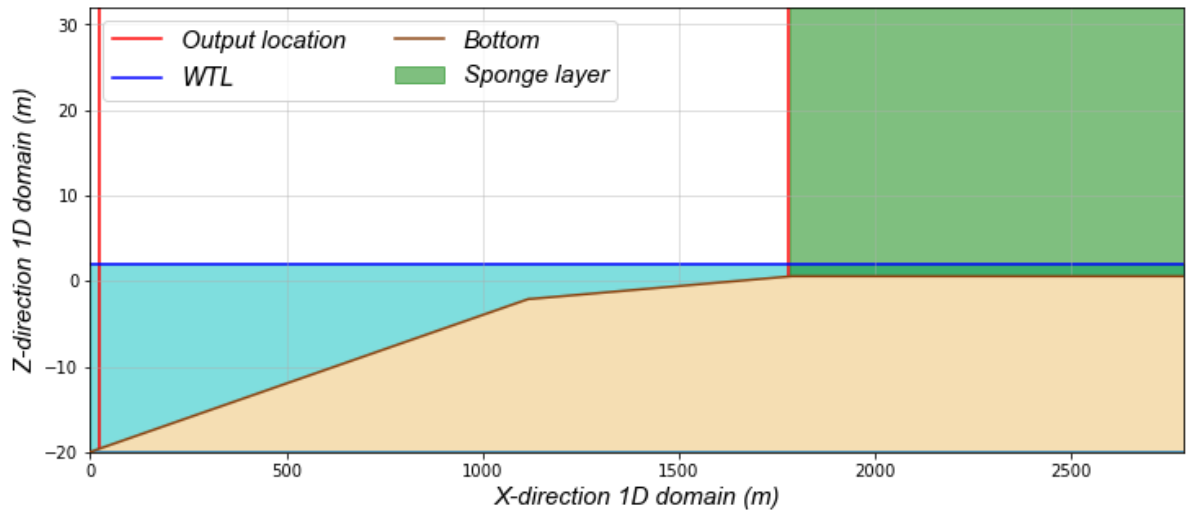

Figure 3.15: *Domain of the hydrodynamic model, SWASH, for step 1. The second red line indicates the locations where the output for the safety assessment is obtained.*

Coastal safety assessment

The $H_{s,on}$ and $T_{m,on}$ based on the output of SWASH are combined with the S of the multivariate extreme event. With the use of the empirical relation of Pullen et al. (2018), a R_c is calculated. The dike in this study has slopes of $tan(\alpha) = \frac{1}{3}$ and a maximum allowable overtopping volume of 1 l/m/s, assuming a normal quality slope (Schiereck, 2017). With the addition of the S on top of the calculated R_c, the R_c of the multivariate extreme event is defined. The 1/40 year design condition is then the multivariate extreme event requiring the largest dike height. The initial offshore conditions of this event are then used as the 1/40 year design condition for the next step in the analysis.

3.4.3. Step 2: Identifying the required mangrove width

For every mangrove environment, step 1 results in a 1/40 year design condition for the 1987-01-01 and 2018-12-31. These design conditions are the input for the analysis in step 2. With the use of the hydrodynamic model the required vegetation width is calculated for the different representative mangrove locations.

SWASH

The set-up specific parameters for the hydrodynamic model of step 2 differs from step 1, given in table 3.8. The most important change is the applied spac=discretization step of 2 m. With domains reaching up to a length of 21600 meter, a space-discretization step of 1 m turned out to be to computational expensive. The implication with this is that SWASH will reach its limitations to solve the short-period waves correctly. This will be discussed in more detail in the discussion.

Another adjusted parameter is the spin-up time. As a result of the large computational domains, the conclusion was made that the spin-up time had to be increased towards 50 minutes. This while the numerical domain can reach a length up to 21500 meter in this step. The increase of the spin-up time, resulted in an increase of the frequency band to 0.0086 Hz.

The water level during the extreme conditions is not reaching the horizontal in 6.9% of the 9864 SWASH runs. To solve this problem, a minimal water depth of 0.5 m is introduced at the horizontal plane where vegetation is present. This increase of the water level is eventually applied at 26.7% of the runs.

Set-up parameter	***Value***	***Unit***
Modelled time	2	$hours$
Space-discretization step	2	m
Spin-up time	50	$minutes$
Frequency band	0.0086	Hz
Minimal WTL *above* $z_{0,veg}$	0.5	m

Table 3.8: *The 6 parameters on which the statistical representation of the 27440 mangrove locations is based for the statistically upscaling.*

The set-up of this hydrodynamic model is used to transform the offshore $H_{s,off}$ and $T_{m,off}$ towards the onshore $H_{s,on}$ and $T_{m,on}$ within the mangrove vegetation. The characteristics of the mangrove forest are based on the height of the mangrove location, h_veg, which defines the parameters for the three layers of the mangrove tree. These parameters are provided in chapter 3.1.3. SWASH only has the capability to model a single type of vegetation.

The numerical domain applied in this step is depending on the parameters of the different representative mangrove location. One example is visualized in figure 3.16. The coastal mangrove vegetation is located at the start of the horizontal plane and has a width of 500 m.

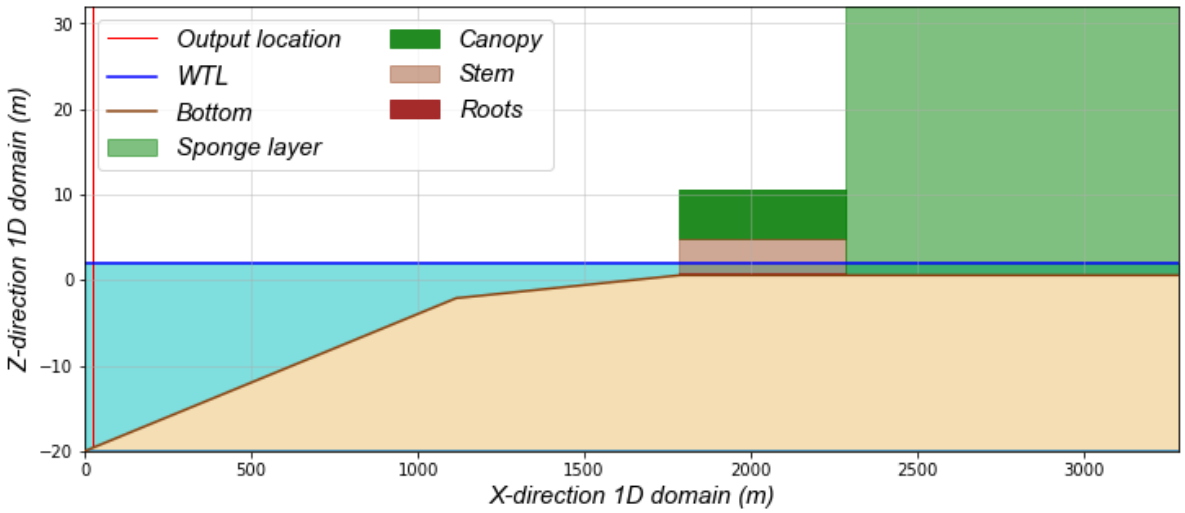

Figure 3.16: *Example of the numerical domain applied in step 2, with a mangrove belt of 500 m located at the horizontal plane.*

The SWASH model produces for every 10 m of vegetation the time-series of the water level. These are used to define the transformation of the two parameters within the mangrove forest. The output locations are indicated with red lines in figure 3.17, which is a part of the domain of figure 3.16. At these output locations the $H_{s,on}$ and $T_{m,on}$ are calculated to track the transformation of the two parameters in the mangrove forest. These parameters for every 10 meters are used as input for the safety assessment of step 2.

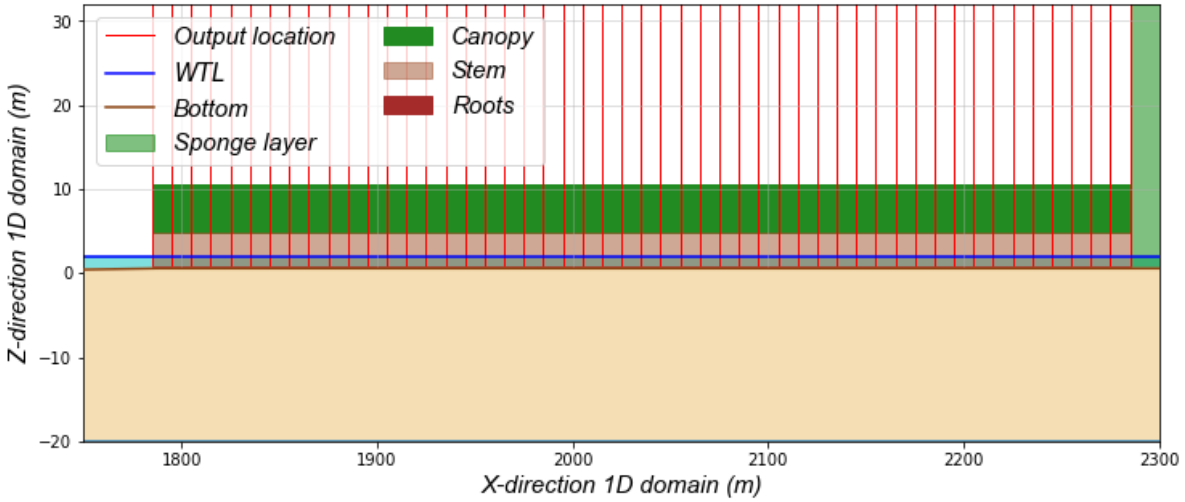

Figure 3.17: *Detail visualization of the distribution of output locations of the SWASH model along the mangrove forest.*

Coastal safety assessment

For all the output locations in the domain, the empirical safety equations of Pullen et al. (2018) are applied to calculated the required R_c. The eventual R_c, including S, is the required crest height of the dike above the $WTL_{MSL+HAT}$. Within the 500 m of mangrove forest the location is searched where the R_c is meeting a required $R_{c,lim}$. This optimization process is to compare the required 1/40-year design condition of 1987 with 2018. With selecting the lowest $R_{c,lim}$, containing a vegetation width for 1987 and 2018, the largest vegetation width is selected. This means that the required crest height results in the ideal case in a vegetation width above the 0 m and below the 500 m for both design conditions. The possible $R_{c,lim}$ values are 1, 2, 3, 4 and 5 m.

4

Results

This chapter elaborates on the results from the study of the non-stationary extreme value analysis, the statistical upscaling and the impact this could have on the coastal safety at the mangrove locations.

4.1. Extreme value analysis

From the data collection, 5809 different mangrove environments were defined to represent the hydrodynamic conditions in mangrove areas. These 5809 hourly time-series of the past 32 years contained 280512 data points for the parameters H_s, T_m, and S. With the use of the Proxy of Stockdon et al. (2006), the trend of the multivariate extreme event was tracked between 1987-01-01 till 2018-12-31. This Proxy neglected the direction of the extreme events. Insight in the result of neglecting this parameter is created in B.3. This identified that applying only the wind direction and the transect orientation, would not completely cover the processes that occur during tropical cyclones. For that reason, this study used the conservative approach to consider the parameters H_s, T_m and S. The introduction of the non-stationary approach of Mentaschi et al. (2016) for the POT analysis, resulted in a method to test the hypothesis. 56.9% of the 5809 mangrove environments meets the desired GPD within the requirements set. At the other 43.1%, N_s was the limiting factor.

The linear time-dependency of the location parameter, T_μ, identified the non-stationarity of the multivariate extreme events. At 87.5% of the locations a positive trend was observed, indicating that the threshold and thus the extreme events are increasing at these locations in the researched period of 32 years. The distribution of this parameter for the 5809 mangrove environments is given in figure 4.1, with a minimum of -0.0018 m/year till a positive maximum of 0.0041 m/year. On average the parameter T_μ was positive with a value of 0.0006 m/year.

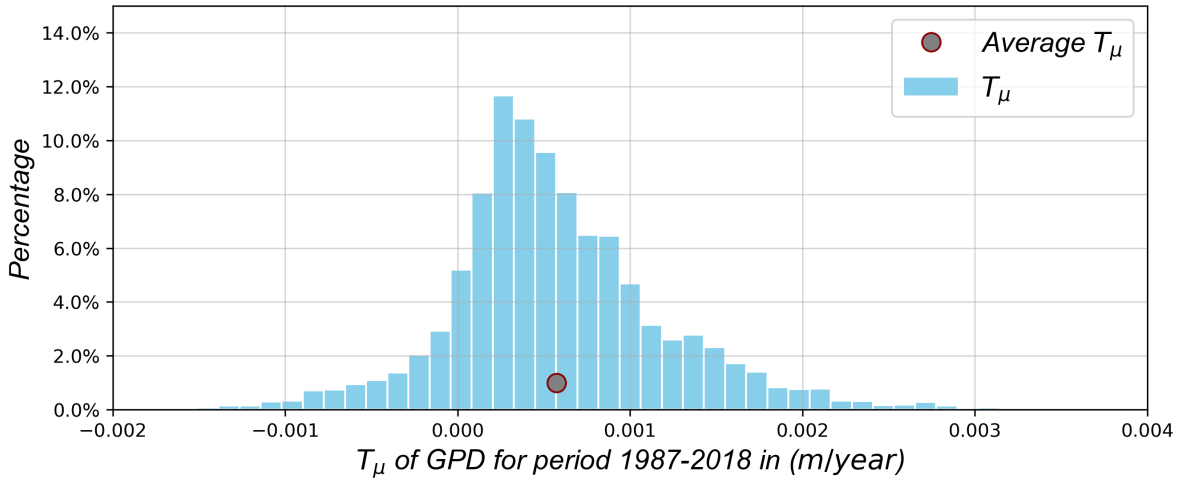

Figure 4.1: *Observed trend in μ of P_{xy} representing the non-stationary of the empirical flood levels, resulting from the multivariate input.*

The global spatial distribution of this parameter is visualized in figure 4.2. Areas with a decrease are found along the West coast of Central-America and the Northern part of Vietnam. However, overall a positive trend can be observed indicating an increase in the impact of the extreme events over the past 32 years.

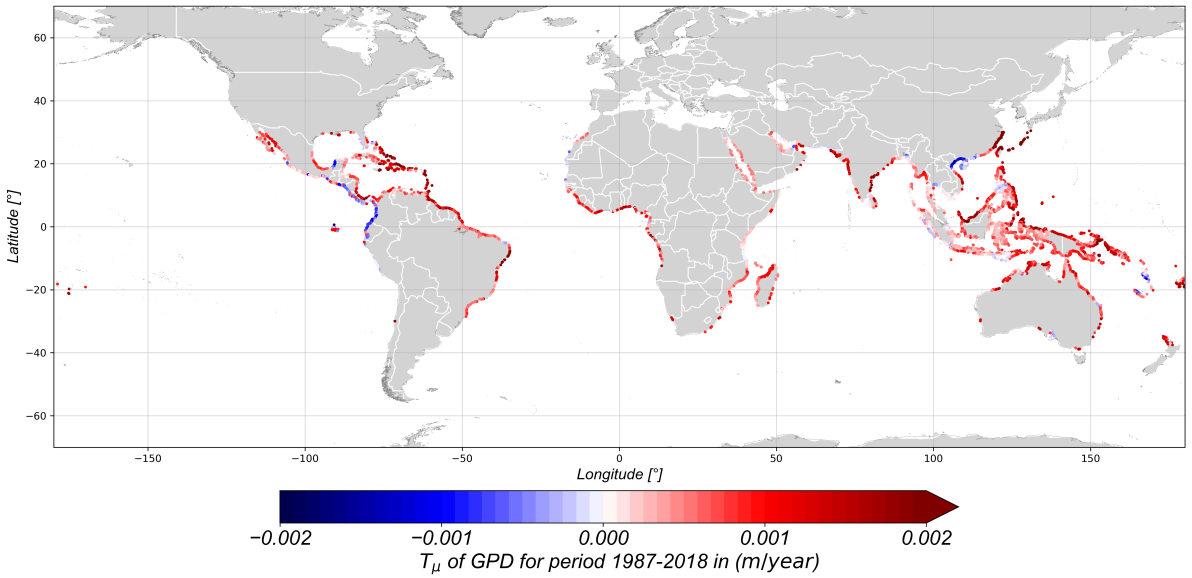

Figure 4.2: *Global distribution of the trend observed in the location parameter, μ, of the Generalized Pareto distribution of the proxy, P_{xy}.*

With the use of the non-stationary assumption and the POT analysis, the number of extreme events was identified over time. The results of this analysis are presented in figure 4.3. This figure shows the distribution of the mean number of storms, N_s, of the 5809 environmental locations for the period of 1987 until 2002 and 2003 until 2018. The horizontal axis displays the N_s found in this period. The vertical axis indicates the percentage of locations at a particular bin. With the two dots in this plot the mean N_s for the 5809 environmental locations is indicated for the two observed time periods. An increase in the mean number of extreme events was identified at 59.8% of the environmental locations, the other locations a decrease was observed. Furthermore, the mean N_s of all the environmental locations increased from 4.16 till 4.32 for respectively the time periods 1987-2002 and 2003-2018. This is an increase of 3.78 % for the average N_s in mangrove areas.

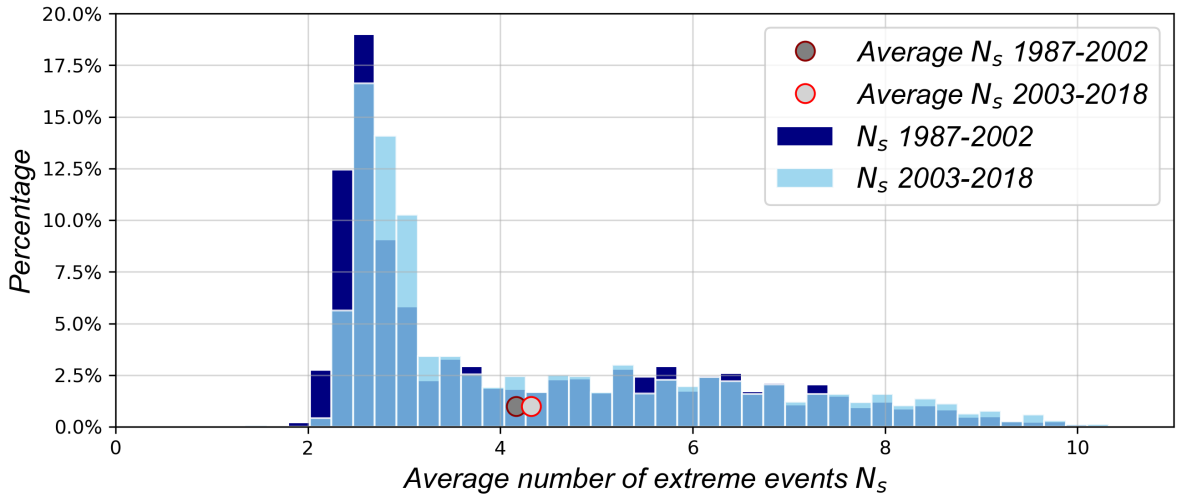

Figure 4.3: *Visualization of the stationarity of N_s, by comparing the time periods 1987-2002 and 2003-2018.*

With the proposed methodology in this study to track the non-stationarity of multivariate extreme events, the evolution of the parameters H_s, T_m and S were defined. This non-stationarity was tracked with the trend in the long-term mean and standard deviation to track the slowly varying tendency of the series of the extremes over the past 32 years. The parameters T_T and T_S tracked the tendency of the multivariate extreme events in the 3 dimension of H_s, T_m and S.

Table 4.1 presents the calculated percentages of mangrove environments with a positive trend in the period 1987-2018. The results indicate that the transformation of the T_T was more significant then T_S. The T_T over the past 32 years changed in H_s direction from -0.025 til 0.041 m/year, for T_m the range was -0.053 til 0.051 s/year and S ranged between -0.49 and 0.57 cm/year. The average extreme event in a mangrove environment increased in the past 32 years with 0.06 m, 0.16 sec and 0.7 cm for respectively the parameters H_s, T_m and S.

	H_s	T_m	S
Positive trend T_T	70.6%	72.6%	64.6%
Positive trend T_S	51.5%	56.6%	48.9%

Table 4.1: *Percentage of locations with a positive* $T_{T_{H_s}}$, $T_{T_{T_m}}$ *and* T_{T_S} *or* $T_{S_{H_s}}$, $T_{S_{T_m}}$ *and* T_{S_S}.

The distributions of the parameter T_T for the three parameters are given in figure 4.4. In this figure the mean tendency of the long-term mean is indicated by a grey dot. These were positive for the three parameters, which implies on average an increase of the three parameters of the design conditions.

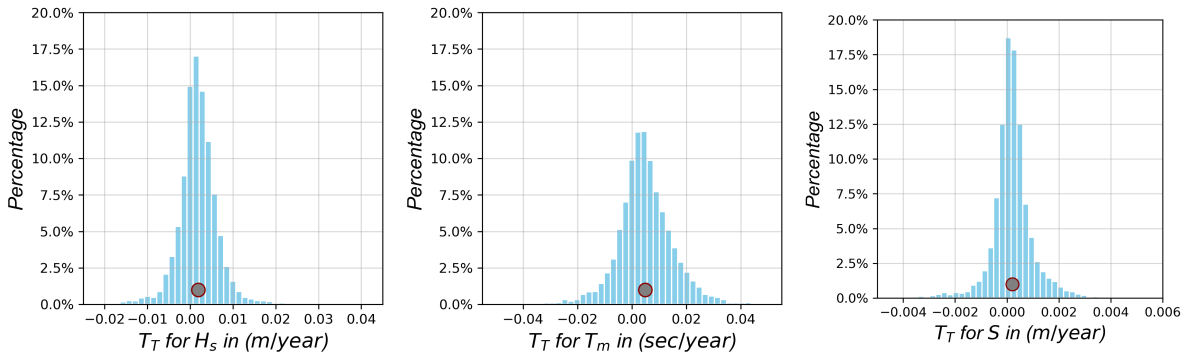

(a) T_T *of* H_s ***(b)*** T_T *of* T_m ***(c)*** T_T *of* S

Figure 4.4: *Distribution of* T_T *of the 5809 mangrove environments for the three parameters of the multivariate extreme event. The grey dot indicates the mean of the parameter of the environments.*

The global distribution of the parameter T_T of the parameters H_s, T_m and S are respectively visualized in the figures 4.5, 4.6 and 4.7. The observation can be made that the designed model produces stable result based on the tendency of the gentle trends along the coastlines of mangrove areas.

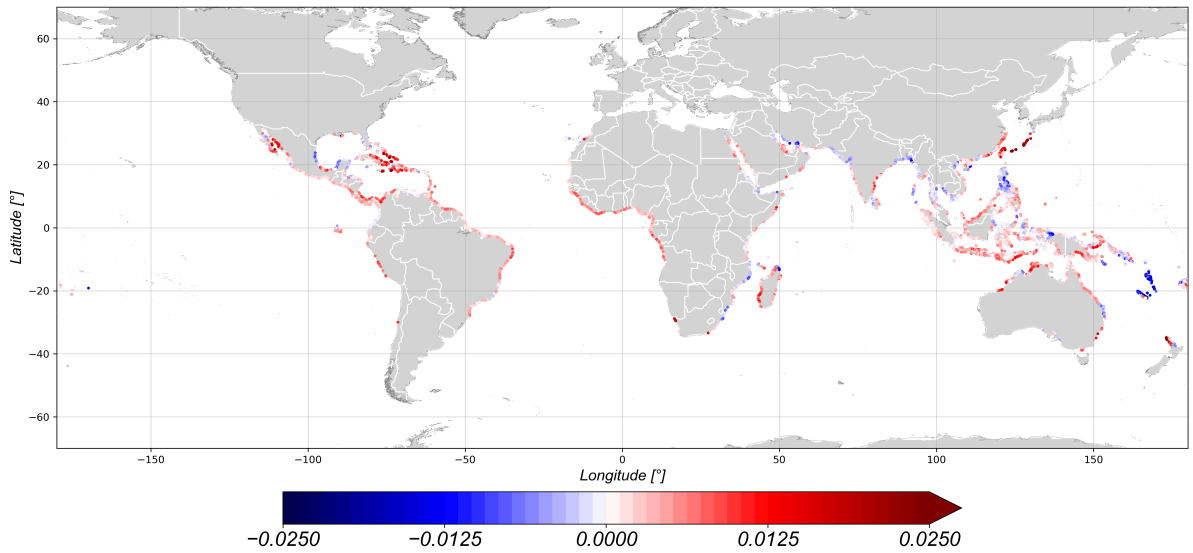

Figure 4.5: *Global distribution of the T_{TH_s} in the period of 1987-2018 during the multivariate extreme events in $m/year$.*

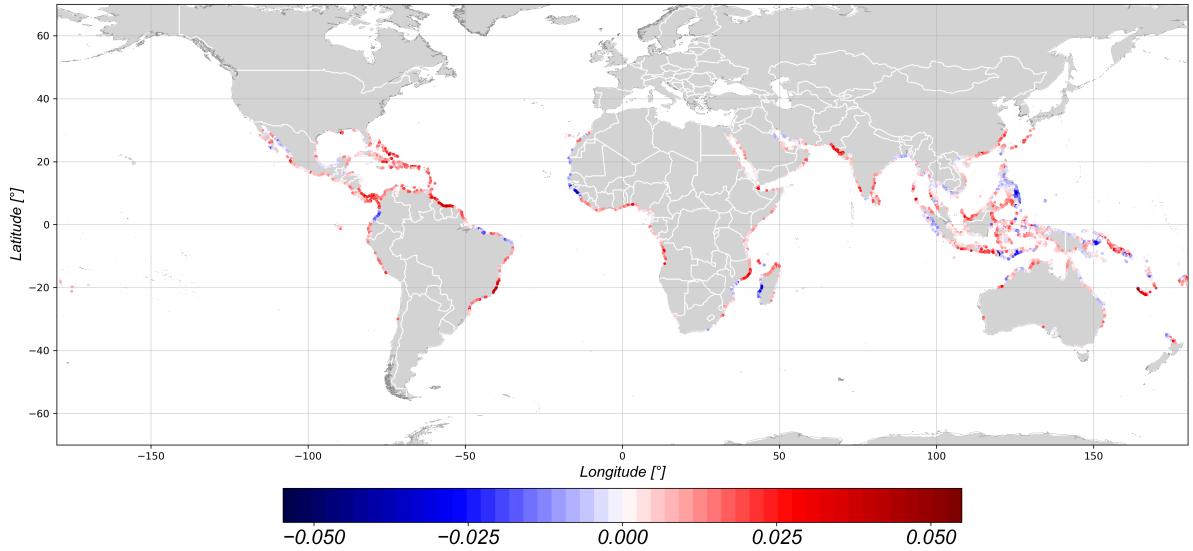

Figure 4.6: *Global distribution of the T_{TT_m} in the period of 1987-2018 during the multivariate extreme events in $sec/year$.*

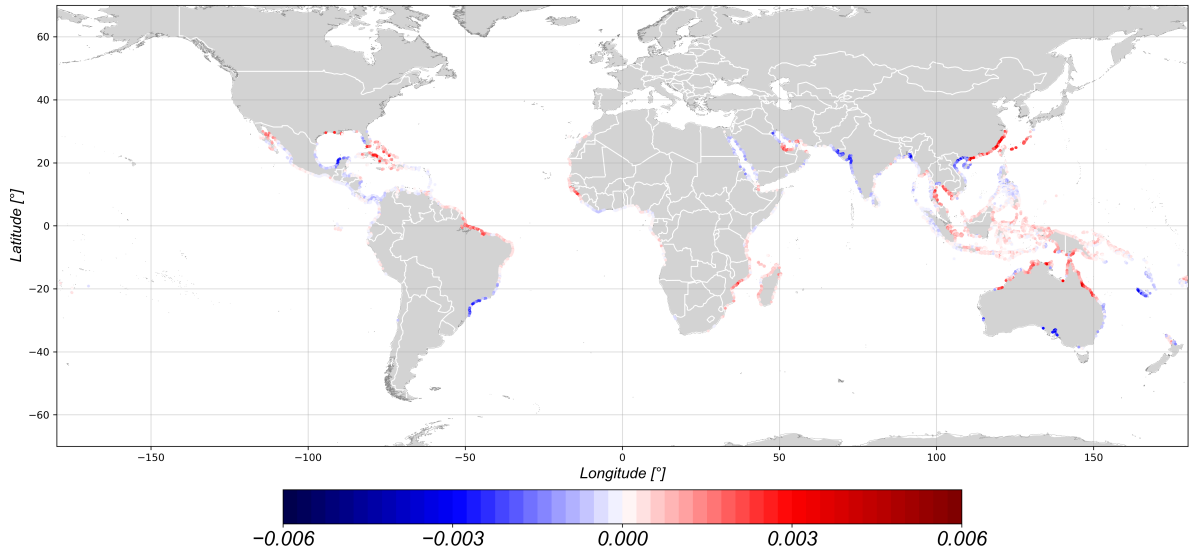

Figure 4.7: *Global distribution of the T_{TS} in the period of 1987-2018 during the multivariate extreme events in $m/year$.*

4.2. Statistical upscaling

This non-stationarity of the multivariate extreme events was used to eventually define the impact of this non-stationarity on design conditions and the coastal safety at mangrove locations. To make this translation without demanding a large amount of computational power, the K-means method was applied.

Representative mangrove environments

The first result of this part is the number of representative mangrove environments that were used to replace the original 31-dimensional 5809 mangrove environments. The results indicated that 49 clusters were sufficient, based on the Silhouette coefficient and the Error Sum of Squares, called SSE. The Silhouette coefficient reached a local maximum with 49 clusters, see figure 4.8a. This indicator defines how well the clusters are defined from one another.

The other indicator of how well the centroids represent the complete dataset is by determining the eventual SSE, representing the sum of the squared differences between the centroids and the observation allocated to this group. Figure 4.8 shows that the error was reduced by almost 50% between the 16, 25 and 36 applied clusters. The step of increasing the number of clusters from 36 to 49 is no longer halving the SSE score.

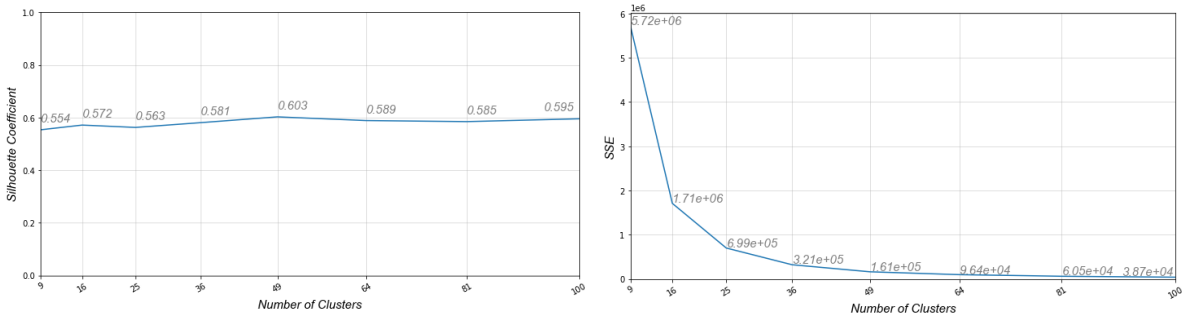

(a) *Silhouette score*

(b) *Error Sum of Squares*

Figure 4.8: *Performances of number of different number of clusters to represent the complete 31-dimensional data set of mangrove climates based on the Sum of Squared Error and the Silhouette coefficient.*

Figure 4.8 indicates that as expected an increase in the number of centroids reduced the SSE. The decrease of the SSE results in a better representation of the original 31-dimensional dataset. To get insight into the implications of the SSE for 36 and 49 clusters, figure 4.9 and 4.10 can be used. In these figures, the results are given of respectively 36 and 49 representative mangrove environments for representation of three of the 31-dimensional non-stationary climates. In these figures the boxplot distribution of the parameter T_T of H_s, T_m and S, is given per cluster. A green background is applied when the median of the boxplot and the centroid of the data have the same sign. When for a parameter the centroid and the median of the boxplot have the same sign, being either positive or negative, a green background is added to the figure.

Figure 4.9 indicates that 8 of 36 clusters had an equal sign for the three different $T_{T_{H_s}}$, $T_{T_{T_m}}$ and T_{T_S} of the median and the centroid representing this cluster. This is indicated with a green bar behind the considered boxplot within the plot. With the use of 49 clusters, 11 clusters have this same sign for the median and the centroid for the three different parameters, as one can observe in figure 4.10.

Every cluster represented a different amount of mangrove environments, therefore the results of figures 4.9 and 4.10 were weighted with the total number of environments combined within these clusters. The results of this analysis is given in table 4.2. The performance of using 49 clusters to represent the 31-dimensional non-stationary climates resulted in a better performance for correctly identifying the sign of the median of the data in 1 dimension. Only in 3 dimensions the 36 clusters performed better. Therefore the application of 49 clusters is preferred on this analysis.

	3 dimensions	**2 dimension**	**1 dimension**
36 Clusters	32.8%	69.8%	89.7%
49 Clusters	30.6%	64.1%	93.2%

Table 4.2: *Percentage of equal sign of the median and centroid of the clusters for the parameters $T_{T_{H_s}}$, $T_{T_{T_m}}$ and T_{T_S}, weighted with the number of environments represented by a cluster.*

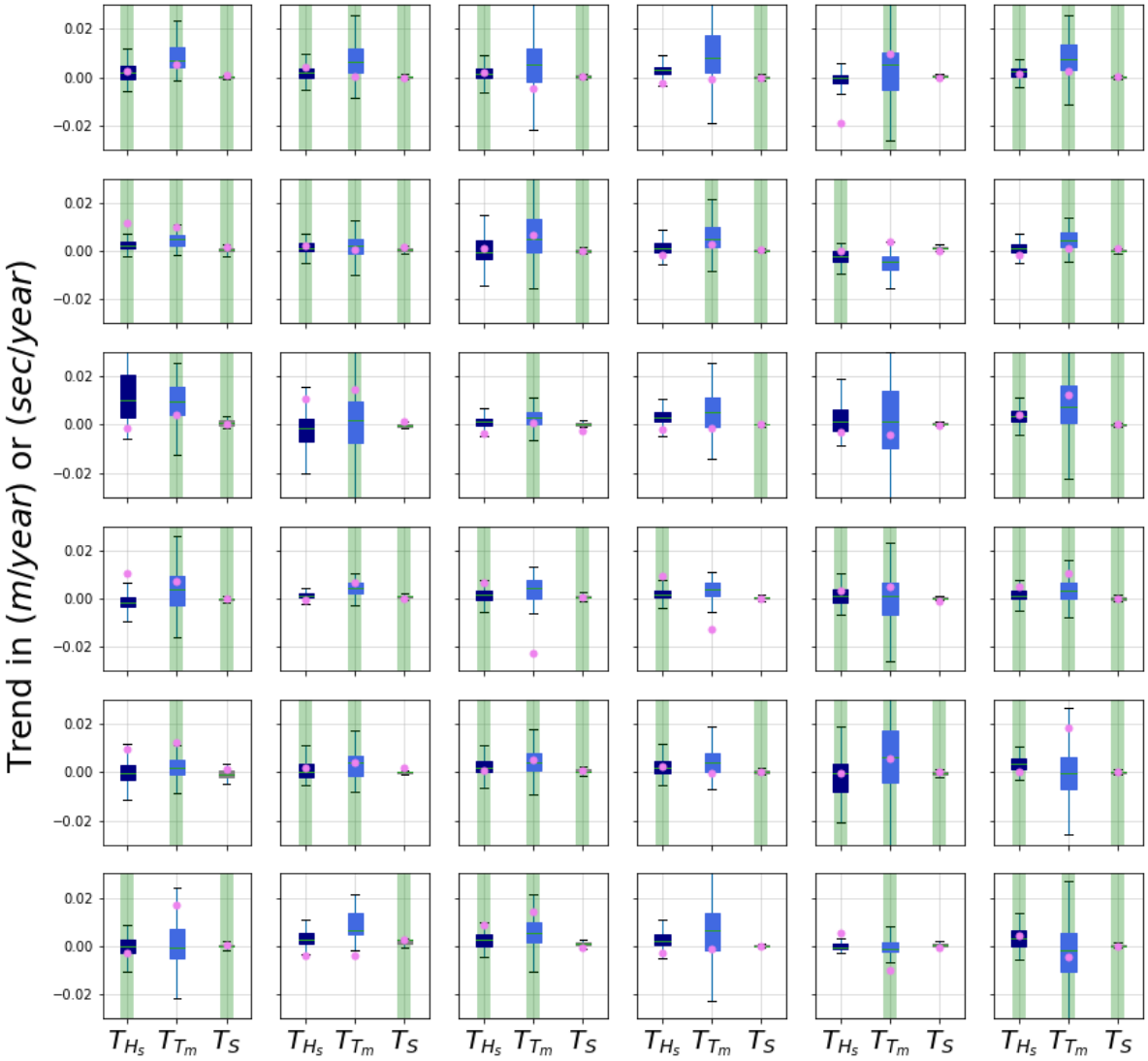

Figure 4.9: *Comparison between median and centroid of cluster for the parameters $T_{T_{H_s}}$, $T_{T_{T_m}}$ and T_{T_S},of the 36 representative climates. The median is indicated with the green line in the boxplot and the centroid for the parameter in the cluster is indicated with a pink dot. When the median and the centroid have the same sign, a green bar is added behind the boxplot.*

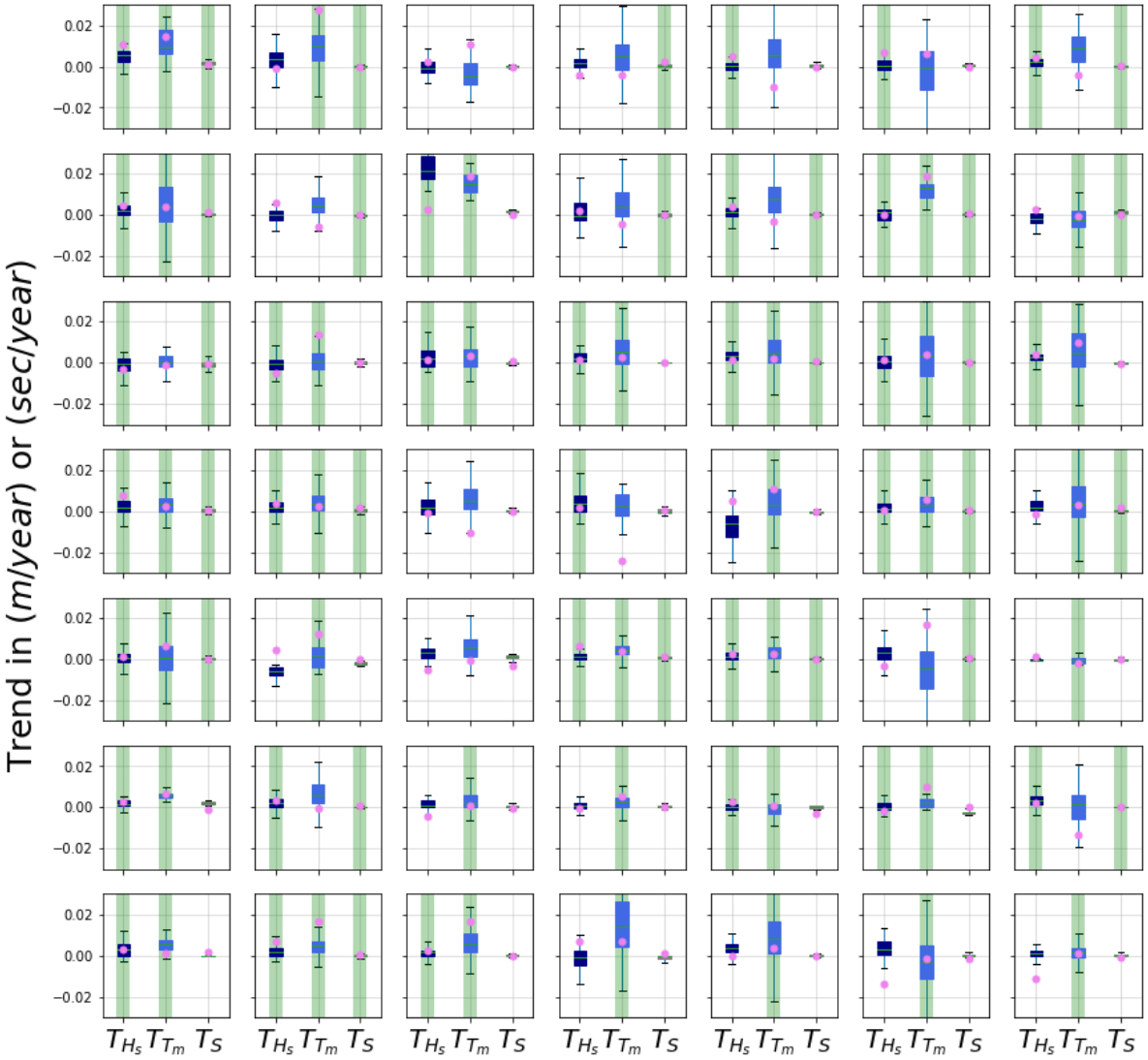

Figure 4.10: *Comparison between median and centroid of cluster for the parameters $T_{T_{H_s}}$, $T_{T_{T_m}}$ and T_{T_S}, of the 49 representative climates. The median is indicated with the green line in the boxplot and the centroid for the parameter in the cluster is indicated with a pink dot. When the median and the centroid have the same sign, a green bar is added behind the boxplot.*

In table 4.3 the weighted percentage of the clusters with a positive trend in the mean of extreme events T_T is given. This percentage were weighted with the number of locations designated to the particular cluster. Initially, the percentage of the dataset was 70.6%, 72.6% and 64.6%, which can be found in table 4.1.

	H_s	T_m	S
36 Clusters	66.9%	61.6%	70.3%
49 Clusters	68.2%	71.4%	61.8%

Table 4.3: *Percentage of equal sign of the median and centroid of the clusters for the parameters $T_{T_{H_s}}$, $T_{T_{T_m}}$ and T_{T_S}, weighted with the number of locations represented by a cluster.*

The 49 clusters had comparable performance in correctly identifying the trend of the T_{0y} in the one, two, and three-dimension in comparison with the 36 clusters, table 4.2. However, the 49 clusters were better at representing the initial percentage of positive trends of T_{0y}. Therefore, 49 clusters were used to represent the 5809 mangrove environments. The spatial distribution of the 49 representative mangrove environments is shown in figure 4.11. The color indicates the representative mangrove climate for the considered mangrove environment.

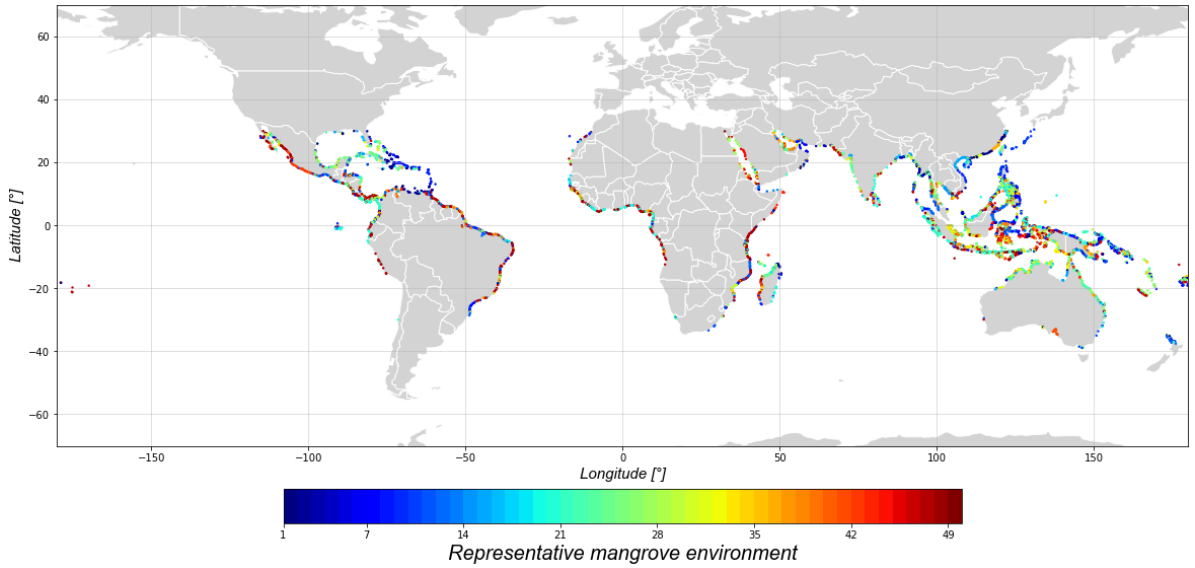

Figure 4.11: *Spatial distribution of the 49 identified representative mangrove environments for the 31-dimensional non-stationary mangrove climates.*

The multivariate dependency model of these different representative mangrove environments were used to define the design conditions. Performances of the statistical representation of the time-dependent sampling procedure are visualized in more detail. The representative environments 5,14 and 33 have a misfitting of the dependency for the representative mangrove environments, based on the results. An example is showed for 5 in figure 4.12, where the orientation of the dependency is limiting in comparison with the original data. The original extreme events identified for this environmental cluster are indicated in grey. The design conditions of 1987 and 2018, are respectively visualized in dark and light blue.

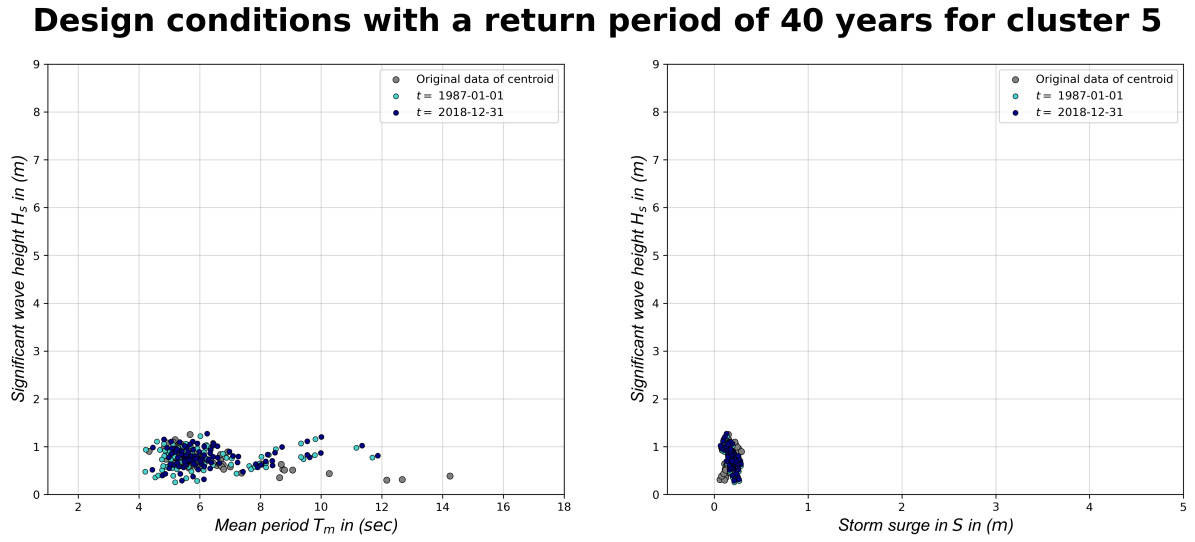

Figure 4.12: *The original and sampled extreme events resulting in the design conditions for the further analysis for environmental cluster 5, for the year 1987 and 2018.*

The results of environment 8 are given in figure 4.13. The light and dark blue dots indicate a underestimation of the extremes in H_s direction in comparison to the original multivariate extreme events, indicated with a grey dot.

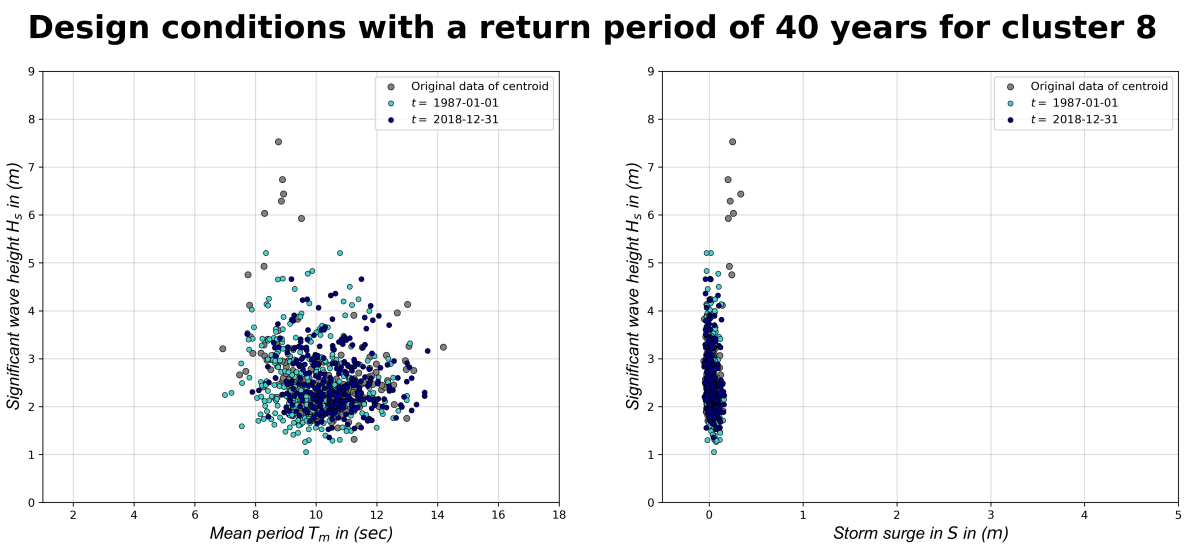

Figure 4.13: *The original and sampled extreme events resulting in the design conditions for the further analysis for environmental cluster 8, for the year 1987 and 2018.*

A better representation of the original dataset can be observed in figure 4.14, where the sampling procedure is capable of defining the edges of the multivariate extreme events itself. These results for representative mangrove environment 10 visualizes the complicated dependency models that can be modelled with the proposed methodology.

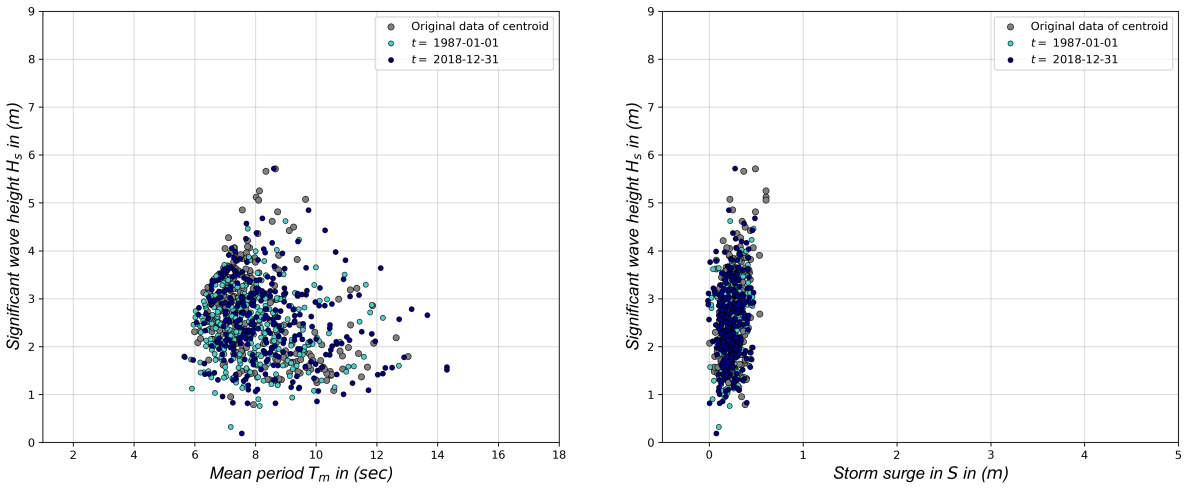

Figure 4.14: *The original and sampled extreme events resulting in the design conditions for the further analysis for environmental cluster 9, for the year 1987 and 2018.*

Representative mangrove locations

The next step in the statistical upscaling was reducing the number of mangrove locations. The data collection resulted in the distributions of figure 4.15, of the six parameters for 274440 mangrove locations. This dataset of mangrove locations was reduced to 289 representative mangrove locations. This selection of the number of representative mangrove locations was based on Silhouette coefficient and the SSE. In figure 4.16a the Silhouette coefficient of the different number of clusters to represent the 6-dimensional mangrove locations is visualized. In figure 4.16b the SSE is given for the different amounts of clusters. The Silhouette coefficients of the different clusters are comparable with one another, for that reason the selection of the number of clusters will be based on the SSE. With a further increase of the number of clusters above the 289, the decrease tended to move towards a linear trend, also known as the elbow method. For that reason 289 clusters were selected to represent the 6-dimensional 27440 mangrove locations in this study. A visualization of the complete statistical upscaling is shown in appendix C.2.

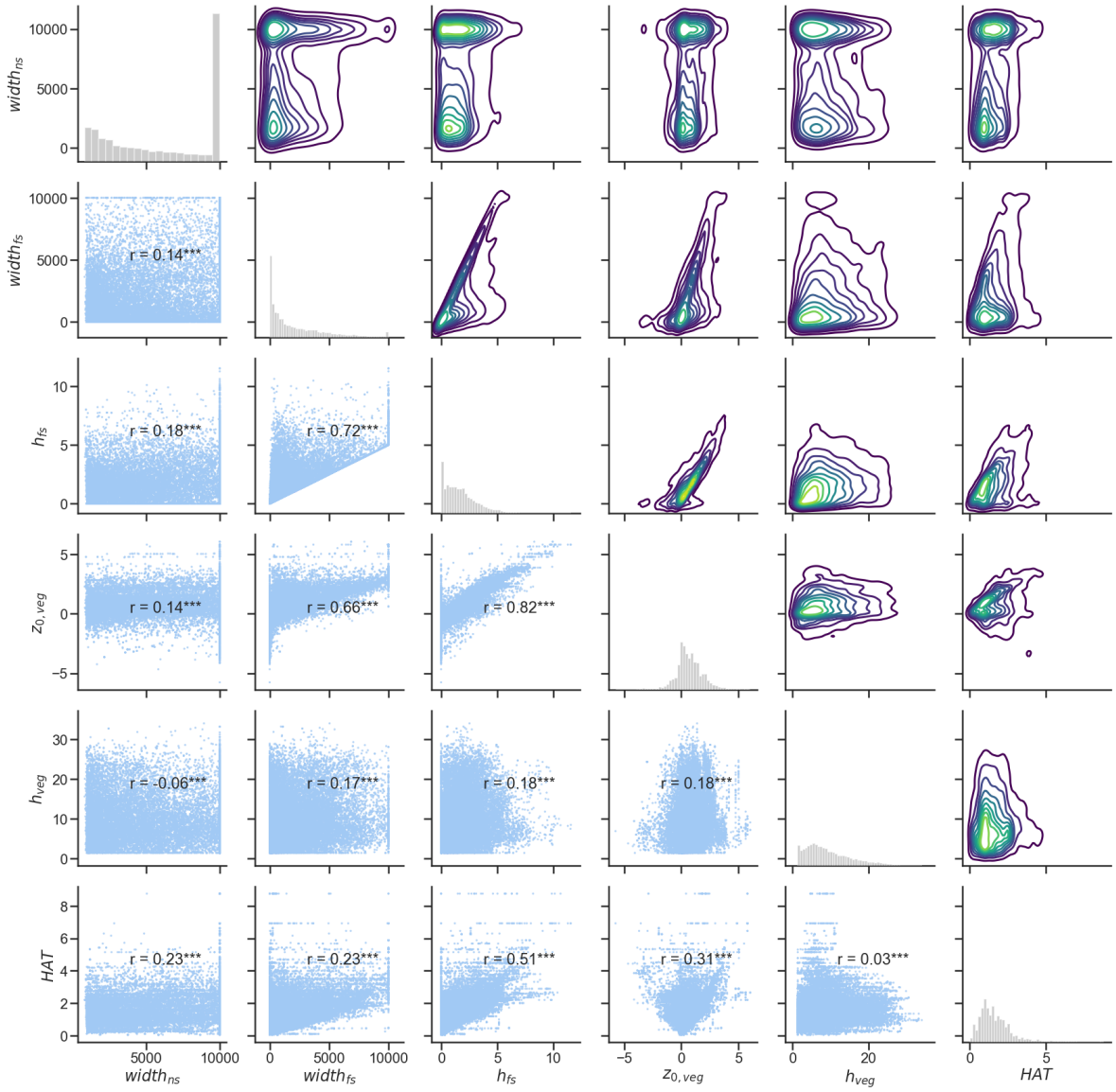

Figure 4.15: *Visualization of the 6-dimensional mangrove locations data set, containing the 27440 mangrove locations. In this figure the lower left part visualizes the spatial distribution of the mangrove locations in 2 dimension, with the Spearmann correlation coefficient between the different parameters given in black. On the diagonal a bar chart is included, which shows the density distribution of the parameter. Above this diagonal the density within the spatial distribution is visualized with a kernel density estimate where the brighter colors represent an area with a higher density. The order of parameters from left to right and top to bottom is* $width_ns$, $width_fs$, h_fs, $z_{0,veg}$, h_veg *and* HAT.

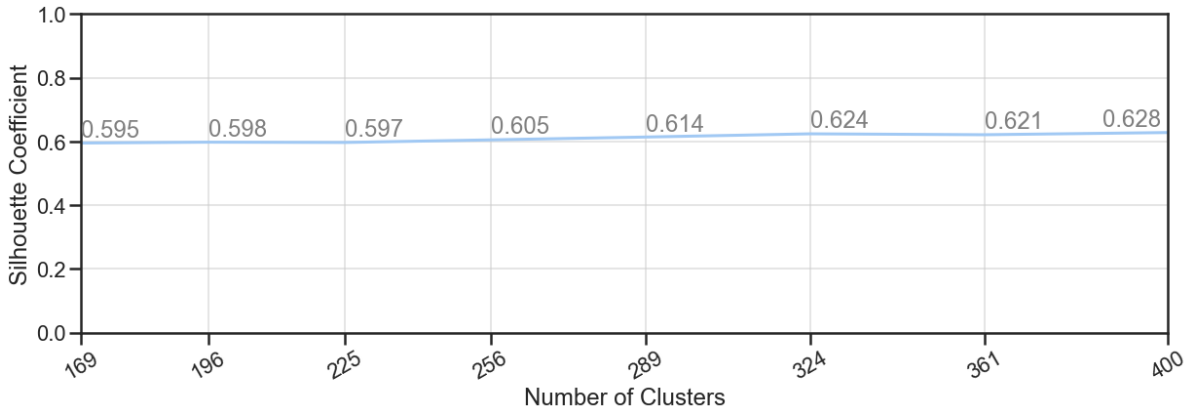

(a) *Silhouette score*

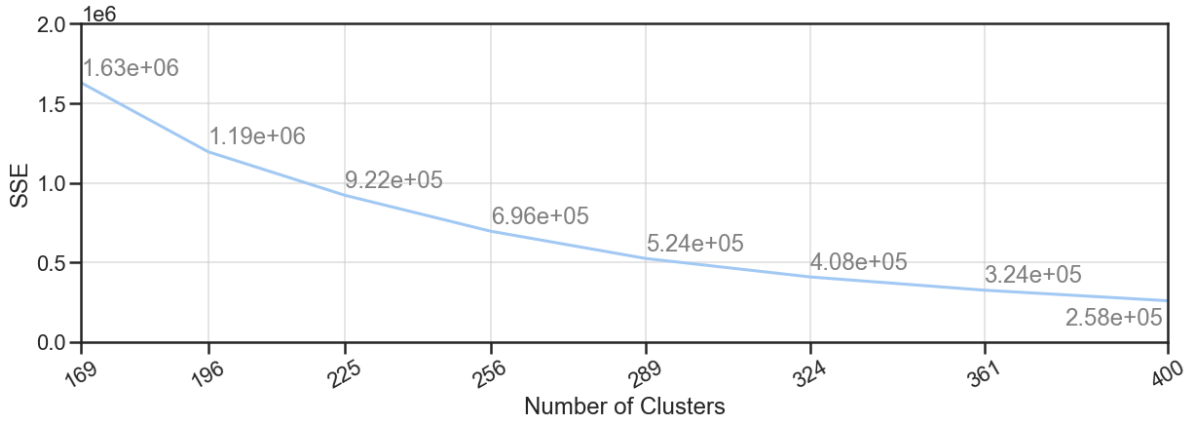

(b) *Sum of Squares Error*

Figure 4.16: *Performances of number of different number of clusters to represent the 6-dimensional data set of mangrove locations based on the Sum of Squared Error and the Silhouette coefficient.*

4.3. Hydrodynamic model & safety assessment

The defined non-stationarity of multivariate extreme events is applied to calculate the impact on the coastal safety. The hydrodynamic model and coastal assessment is used to define the global impact based on the representative mangrove environments and locations.

Step 1: Identifying the extreme event
The first step in this analysis is defining the 1/40 year design condition. The sampling procedure of multivariate extreme events is based on the Vine-D model and the linear time dependencies in the three dimensions H_s, T_m and S. The initial number of 15982 multivariate extreme events for the 49 clusters was reduced to a number of 4038 extreme events based on the discussed pre-processing step. The theoretical framework applied in the hydrodynamic model was not capable to solve 4 events of representative mangrove environment 19. These events had an H_s above 10 m. Therefore, these events were left out of the analysis.

The result of the methodology of step 1 was 49 multivariate extreme events for the analyzed moments in time. The results of the analysis are visualized in figures 4.17 and 4.18, for respectively 1987 and 2018. In the right plot, the H_s and combining T_m are indicated, the left figure shows the accompanying S value in relation to the H_s. The color in the plot indicates the specific representative mangrove environment the design condition originates from.

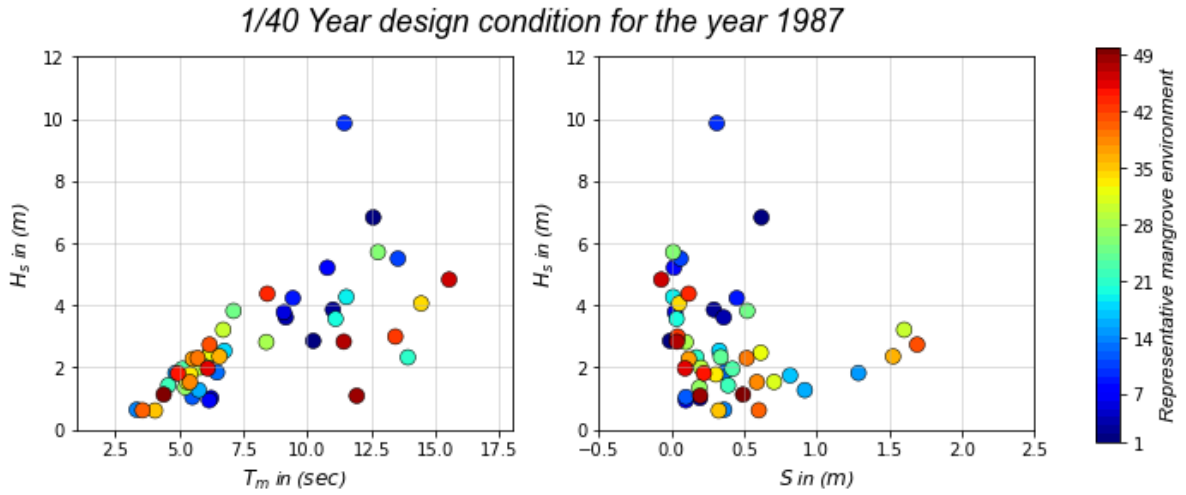

Figure 4.17: *Left panel shows the mean wave period versus significant wave height. Right panel shows the storm surge versus significant wave height. The color bar indicates the cluster to which the multivariate 1/40-year design condition of 1987 belongs.*

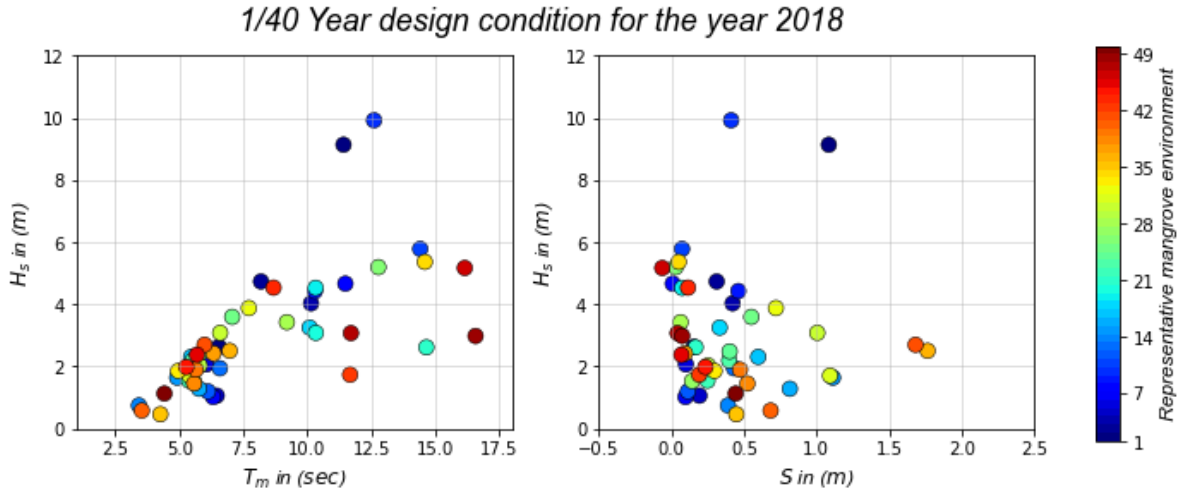

Figure 4.18: *Left panel shows the mean wave period versus significant wave height. Right panel shows the storm surge versus significant wave height. The color bar indicates the cluster to which the multivariate 1/40-year design condition of 2018 belongs.*

The changes in design conditions, are shown using scalars in figure 4.19a. The difference between the two design conditions per representative mangrove environment are visualized in the figure 4.19a. The event of 1987 is located in the origin and the transformation towards the 2018 event is indicated with a line. The left plot indicates the transformation in H_s and T_m direction and the right plot indicate the transformation of H_s and S. These two plots combined represent the absolute change of the multivariate extreme event between the two time periods. The hue of red indicates the weight it has in the total determination of the weighted mean, based on the number of environmental locations represented by this specific mangrove environment. In figure 4.19b, the same procedure is performed but weighted by the number of mangrove locations it is representing instead of environments.

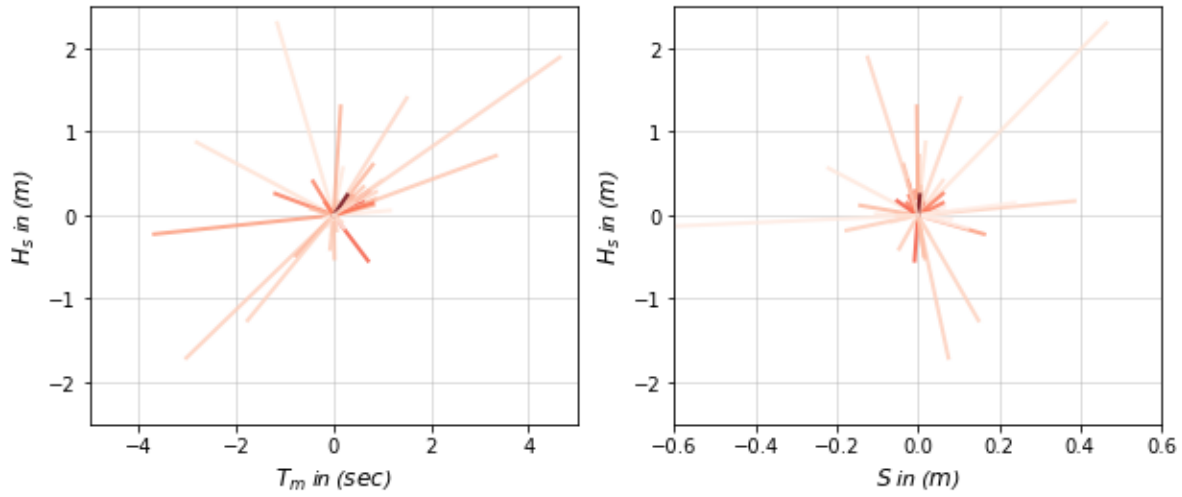

(a) *Transformation weighted by the 5809 environmental climates.*

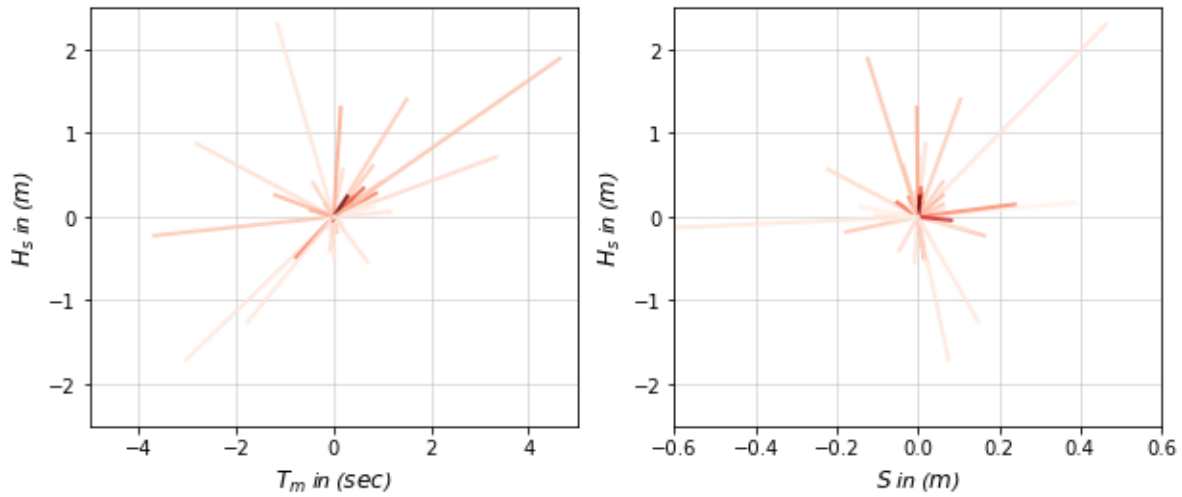

(b) *Transformation weighted by the 27440 environmental locations*

Figure 4.19: *Absolute difference between the 1987 and 2018 design conditions for the 1/40 year event, with the 1987 event located in the origin. The hue of red indicates the weight of the specific representative mangrove environments.*

These different weights and the accompanying changes resulted in different average transformation of the multivariate extreme event in the three directions, given in table 4.4. While the storm surges can be either negative or positive, the percentage transformation over time does not provided insight into the change. For that reason, this percentage is not given. The results indicate that the 1/40 year design condition was on average increasing with 8.75% in H_s direction and 2.57% in T_m and a increase of 0.01 m in S direction. These environmental climates were as a result of the GTSM model more evenly distributed in comparison with the mangrove locations. The transformation weighted by the mangrove locations was more extreme in the three dimensions.

Weighted by	H_s	T_m	S
5809 environmental climates	+0.15 m +8.75%	+0.13 sec +2.57%	+0.01 m
27440 mangrove locations	+1.04 m +46.9%	+0.86 sec +11.83%	+0.08 m

Table 4.4: *Relative and absolute average weighted increases for the parameter H_s, T_m and S for the 1/40-year design condition in the period 1987-2018.*

The eventual set of 1/40 year design conditions was depending on the complete proposed methodology in this study. One can observe the H_s during the 1/40 year design condition identified based on the sampled events in 1987 and 2018 in figure 4.20. The color indicates, in accordance with the color bar, the H_s, with a maximum of 9.86 m in 1987 and 9.92 m in 2018. The parameters of the accompanying T_m and S of these multivariate extreme events can be found in appendix E.1.

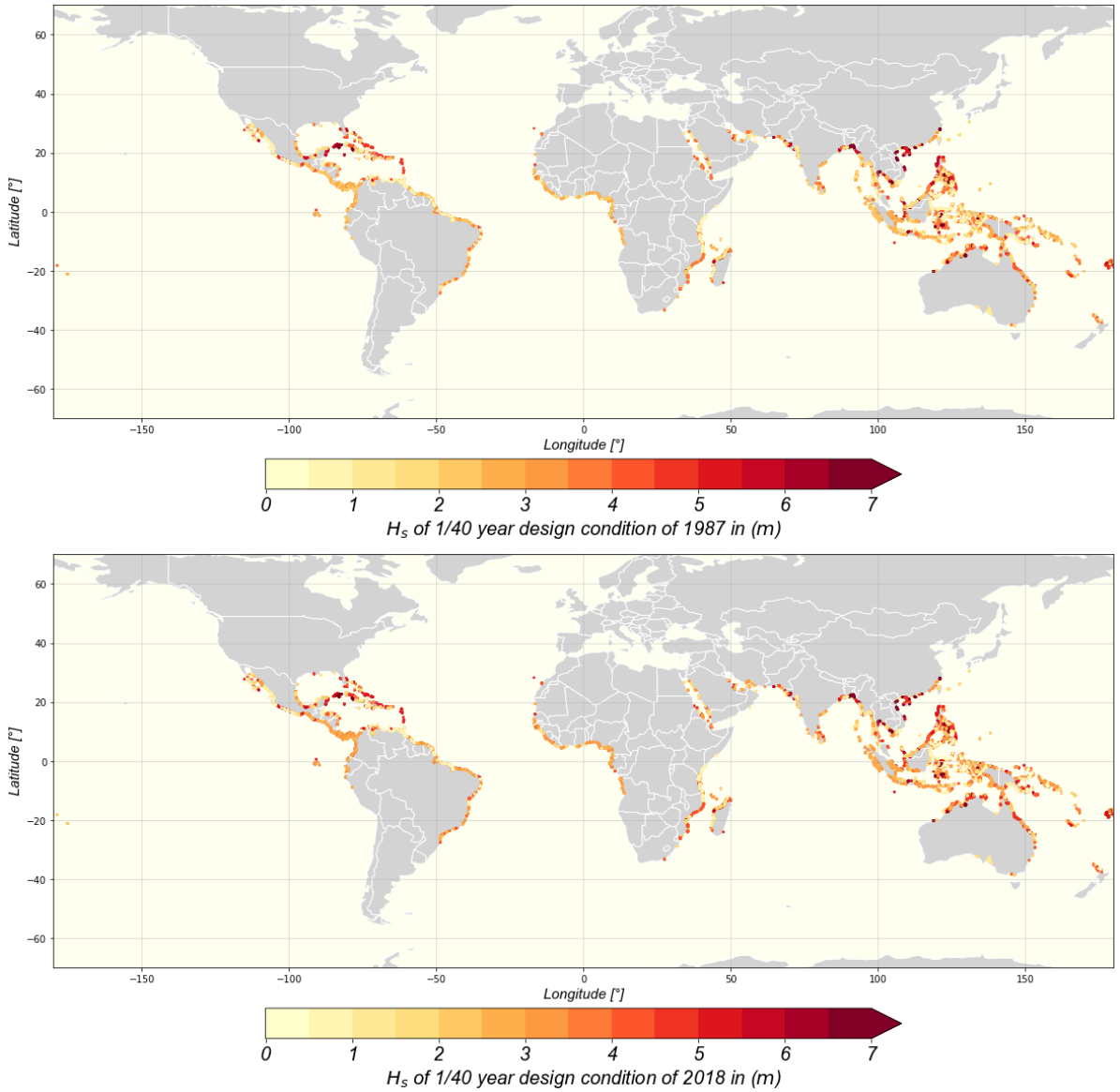

Figure 4.20: *Global spatial distribution of H_s of the multivariate extreme 1/40 year design condition of 1987-01-01 and 2018-31-12*

Step 2: Identifying required mangrove width
The second step was to define the required vegetation width, $width_{veg}$ for the 1/40-year design condition of 1987 and 2018. In appendix D.2 a sensitivity analysis of the coastal safety with respect to the water level is given, to elaborate on the performance of a mangrove tree as coastal protection in the defined theoretical framework. These results indicated that the location of the water level with respect to the canopy is of importance during these extreme conditions in mangrove environments.

An important difference in model set-up between step 1 and step 2 is the space-discretization of 2 m applied instead of 1 m. This decision was made to meet the limited available computational resources of this study. SWASH advises the use of 15-20 computational grid cells per wavelength to accurately resolve the processes. With the assumption of the shallow water, the period of waves accurate solved was calculated with equation 4.1.

$$T = \frac{20\Delta x}{\sqrt{g \cdot h}} \tag{4.1}$$

The coarser resolution on the longer foreshores resulted in a energy concentration in the long-period waves. Four cases with different representative mangrove locations were selected to create more insight in the results of this process and are visualized in appendix D.6. The wave speed is depending on the water depth, and due to friction also on the length of the foreshore, influencing the number of computational grid cells per wavelength. The results of the appendix created the expectation that there could be a relation between the concentration of energy at the long-period waves and the water level at the horizontal plane.

In figure 4.21, the distribution of the water depth on the 500-meter-long horizontal plane is visualized in a histogram. On the horizontal axis, the water level at the horizontal plane of vegetation is given ranging from 0 to 6, neglecting the small number of extremes up to a depth of 10.9 meters. At the left vertical axis, the percentage in the different bins can be observed and at the right vertical axis, the wave period of the waves is given in seconds. The red area in the plot indicates the wave periods that are not solved correctly in this water depth. The light blue line indicates the requirement of 15 grid cells per wavelength and the dark blue line the requirement of 20 grid cells per wavelength.

In figure 4.22, the 9864 combinations of the water level at the horizontal plane and $width_{fs}$ are given. With the color the density of the location within the 2D plot is visualized. Yellow indicates a dense area and blue the opposite. A concentration of runs was observed in the area between 0.5 and 1 m water depth.

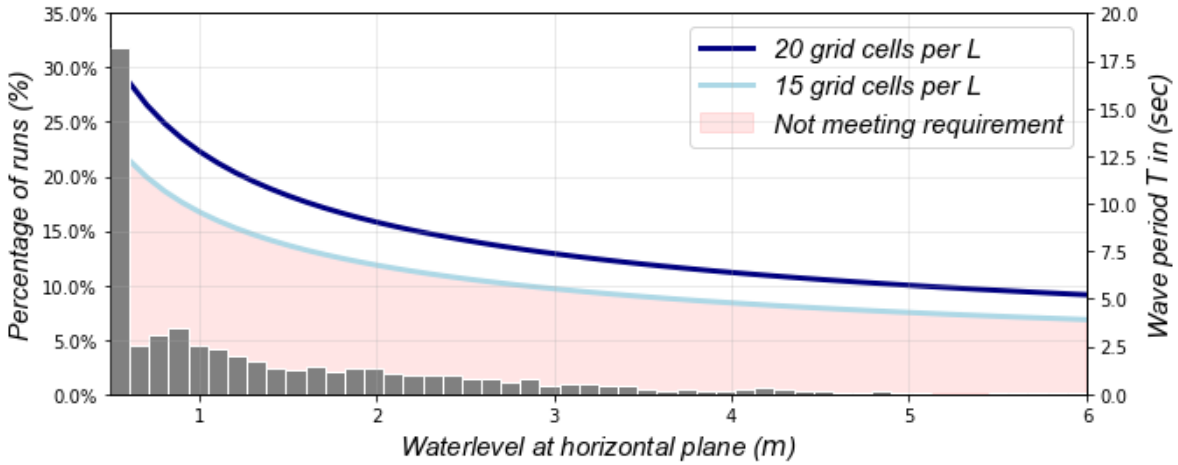

Figure 4.21: *The left vertical axis indicate the percentage in a specific bin. The right vertical axis indicate the period of the waves that can be solved in the system based on equation 4.1 with a Δx of 2 meter, the horizontal axis indicate the water level on the horizontal plane.*

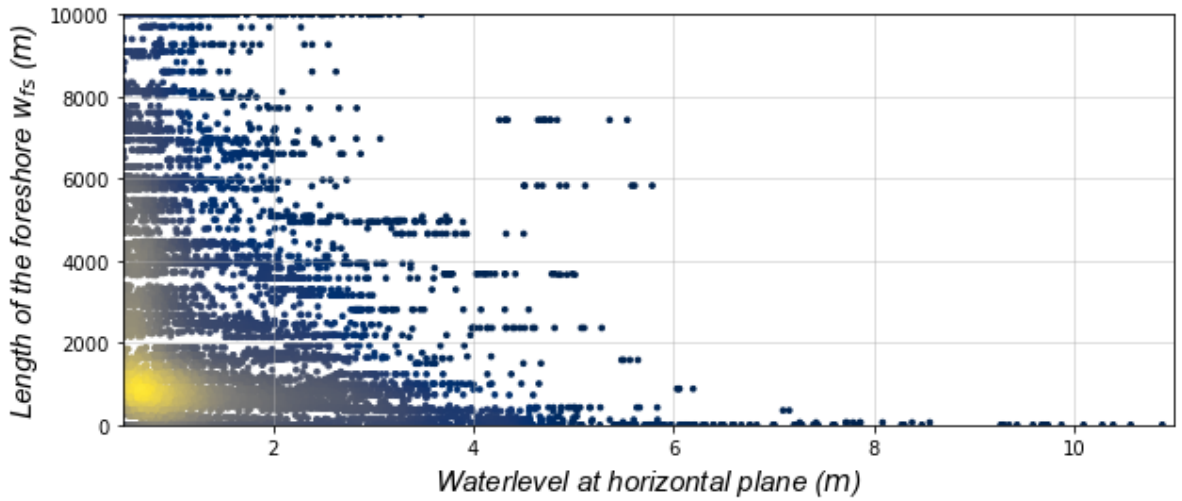

Figure 4.22: *Combinations of widths of the foreshore and waterelevels at the horizontal plane for the 9864 SWASH runs for step 2 of the analysis.*

The concentration of energy in the long-period waves was tracked for the SWASH runs of step 2. This was performed with measuring the percentage of energy concentrated between 0 and 0.0086 in respect to the energy of the total spectrum. This calculation was performed based on the 0-order of moment of $E(f)$. In figure 4.23, the energy concentration in the lowest bin is visualized as a percentage of the energy in the complete 0-order of moment of $E(f)$.

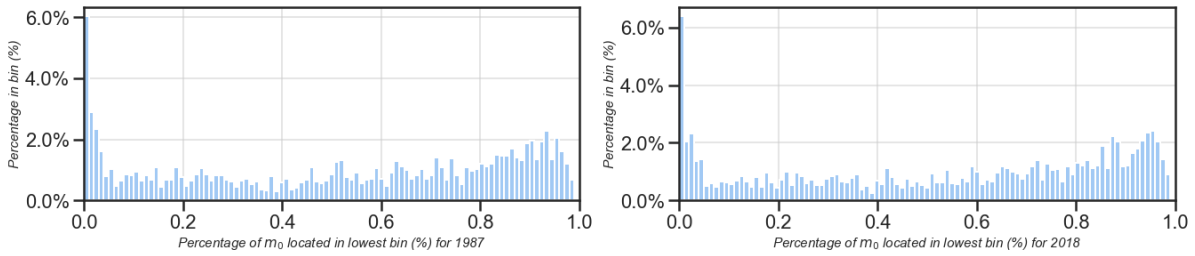

(a) *1987* ***(b)*** *2018*

Figure 4.23: *The described energy concentration in the lowest bin 0.0086 of the spectrum plotted against the percentage of the in total 27440 locations for the SWASH runs of the design condition of 1987 and 2018.*

After mentioning this limitation of step 2 found in the results, the results of the safety assessment of this step are presented. A total of 9864 mangrove runs were performed. This resulted in 4932 different combinations of a representative mangrove location and environment. For these combinations the design condition of 1987 and 2018 were modelled. If at one of two SWASH runs the vegetation width exceeded 500 m, a higher crest height, hereafter referred to as R_c, was applied in the hybrid coastal protection. The distribution of the applied crest heights is listed in table 4.5.

Crest height, R_c, above WTL_{1987}	*1 m*	*2 m*	*3 m*	*4 m*	*5 m*
4932 Combinations	4494 91.1%	412 8.4%	20 0.4%	5 0.1%	1 0.0%

Table 4.5: *The applied dike heights above the WTL of 1987 to meet the requirement of a maximum $width_{veg}$ of 500 m.*

The results of the calculated difference in vegetation width between 1987 and 2018 are listed in table 4.6. When the 27440 mangrove locations are considered, the methodology applied resulted in a required vegetation width increase at 53.3% and a decrease at 22.1% of the locations. At 24.6% of the locations the change in the 1/40 design condition did not influence the required vegetation width. The average difference in required vegetation width of 1987 and 2018 is an increase of 15.6 m for the 4932 SWASH combinations, resulted in 16.8 m when

weighted by the 27440 mangrove locations. At a total of 20709 (75.4%) of the mangrove locations required vegetation width had changed over time, $\Delta_{veg} \neq 0$, emphasizing the importance of determining the coastal safety with a non-stationary approach. Of the non-stationary locations, 70.7% of the locations showed an increase in vegetation width and 29.3% of the locations showed a decrease in required vegetation width, with a respective average increase of 55 m and an average decrease of 58 m.

	Increase	*Decrease*
All 27440 location	53.3%	22.1%
20709 locations, where $\Delta_{veg} \neq 0$	70.7% 55 m	29.3% -58 m

Table 4.6: *The percentage of mangrove locations with a positive or negative difference in required vegetation width, $\Delta width_{veg}$, between the 1987 and 2018 1/40 year design condition. Defined for the all the 27440 locations and for the 20709 non-stationary locations*

Figure 4.24 shows the impact of the non-stationarity of the 1/40 year event in a spatial distribution, by visualizing $\Delta width_{veg}$. The color bar beneath the figure indicates the identified changes in vegetation width, where a blue hue indicates a decrease and a red hue indicates an increase. The limits of the color bar for $\Delta width_{veg}$ range between -150 and 150 m. $\Delta width_{veg}$ was between these limits at 92.3% of the locations. The maximum decrease observed was 500 m and the maximum increase was 410 m. The figure expresses the importance of the non-stationarity of the multivariate extreme events. The required width of the coastal mangrove vegetation had increased especially at the coastline of North and South Brazil, West Central Africa, the Southern islands of Japan, and West and Central Indonesia. Further insights in the data can be obtained in appendix E.1 and within the discussion.

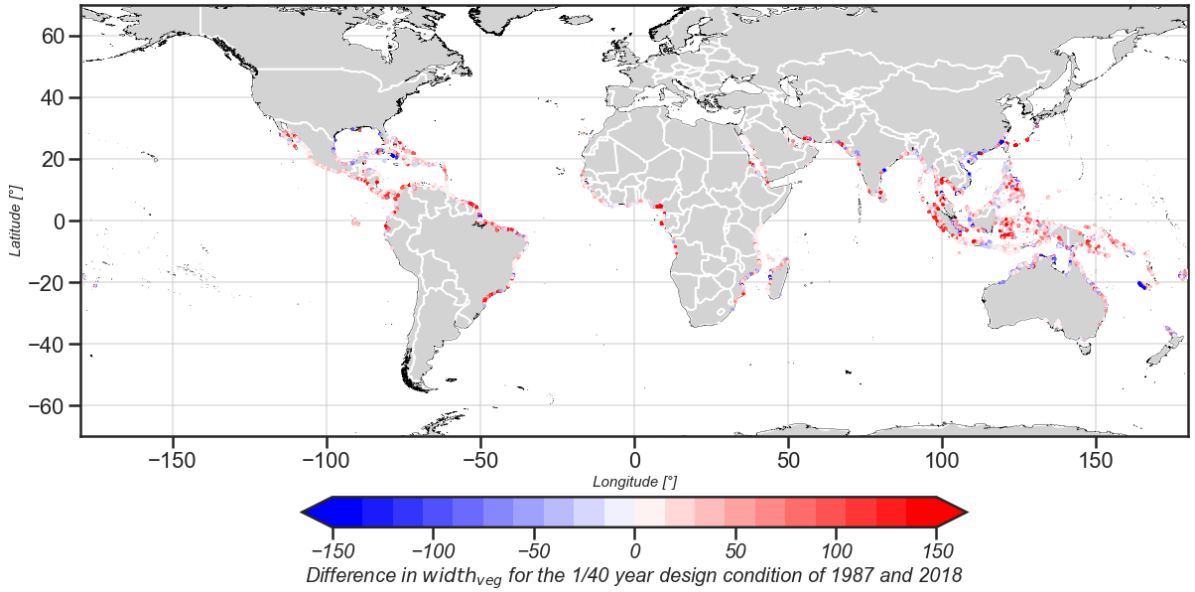

Figure 4.24: *Spatial distribution of $\Delta width_{veg}$ between the 1987 and 2018 1/40 year design condition in meter*

However, the water depth on the horizontal plane was replaced with a minimum of 0.5 m at a large number of the SWASH runs, as a result of the applied methodology. This means that the sensitivity of the transformation of S was not completely represented in the results. Therefore the results of these 27440 mangrove locations are post-processed by only selecting the locations where $\Delta width_veg \neq 0$ and the water level at the horizontal plane being at least 1 m. This resulted in 7722 mangrove locations. These represented 28.1% of all the locations and 37.3% of the non-stationary locations. The energy concentration in the lowest bin of the energy spectrum for these runs is given in figure 4.25. If these distributions of the energy concentration are compared with figure 4.23, the conclusion can be made that these results of 7722 are less influenced by the described concentration of energy in the long-period waves.

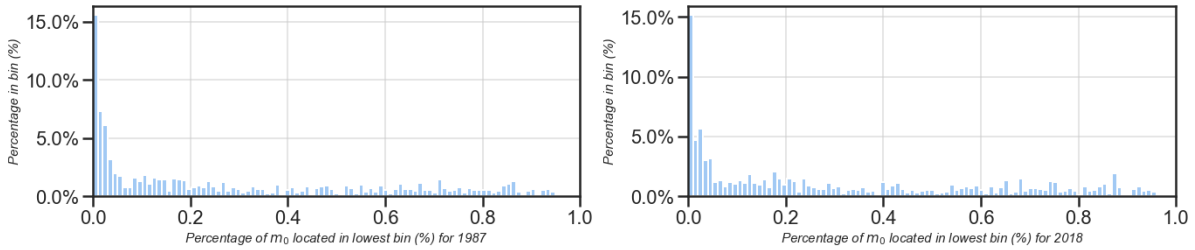

(a) *1987* **(b)** *2018*

Figure 4.25: *Percentage of energy in the lowest bin (0-0.0086Hz), plotted against the percentage of the in total 7722 with minimal waterdepth of 1 m at horizontal plane and a $\Delta_{veg} \neq 0m$ of the design conditiono of 1987 and 2018.*

Figure 4.26 visualizes the sensitivities of $\Delta width_{veg}$ with respect to the three parameters. This is only for the post-processed 7722 mangrove locations. The figure indicates that the impact in terms of $\Delta width_{veg}$ is a combination of the transformation of H_s, T_m and S. This is indicated with the Spearman correlation coefficient between $\Delta width_{veg}$ and ΔH_s of 0.39, between $\Delta width_{veg}$ and ΔT_m of 0.39 and $\Delta width_{veg}$ and ΔS of 0.35.

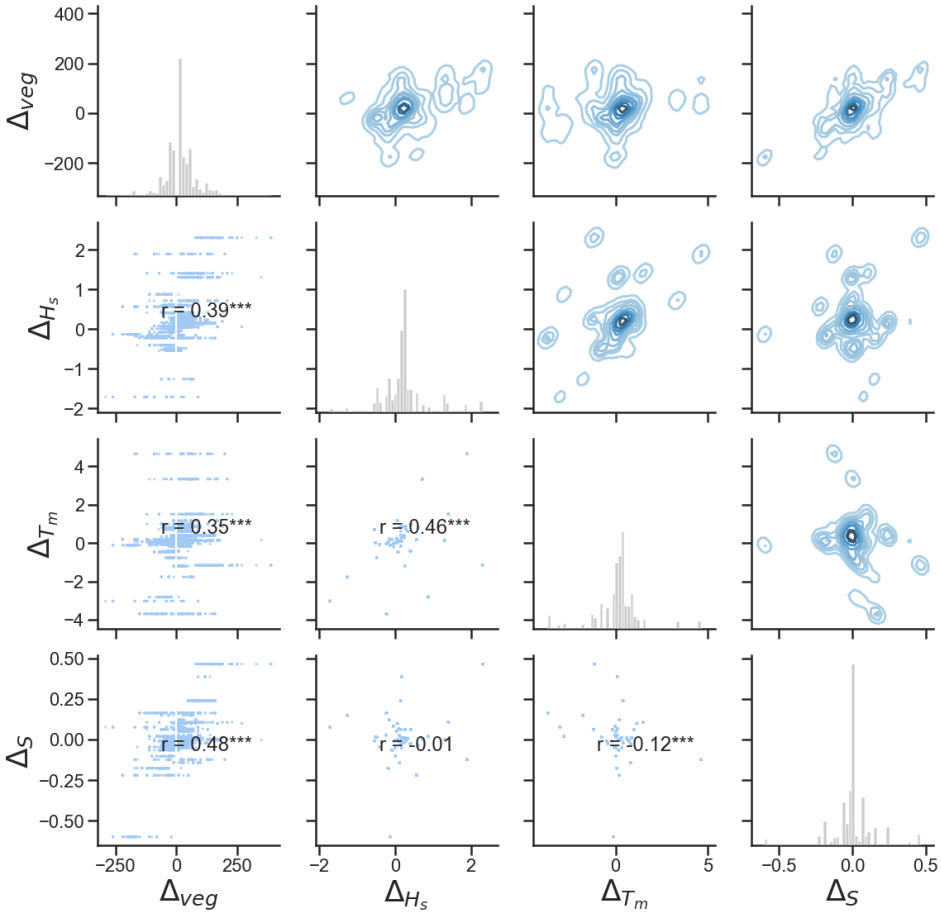

Figure 4.26: *Pair plot representation of the non-stationary vegetation results of the in total 7722 locations with waterlevel of at least 1 m at horizontal plane and $\Delta_{veg} \neq 0m$. The plots in the lower left show the scatter combinations, with the Spearman rank coefficient between the parameters. The diagonal indicates the distribution of the four parameters and the right upper part are the density plots, where the darker blue colors indicate an area with a higher density.*

5 Discussion

This chapter further elaborates on the results in contrast to previous studies regarding the coastal protection offered by mangrove vegetation now and in the future. By critically reflecting on the applied methodologies, this chapter discusses the limitations of the current methodology applied.

5.1. Reflection on main results

The main result from the study is that on average an increase of the multivariate extreme events was observed in mangrove environments between 1987-01-01 and 2018-12-31. At 87.5 % of the in total 5809 environments, a positive trend of the location parameter was calculated. This location parameter defines the location of the Generalized Pareto Distribution, hereafter referred to as GPD, of the extreme events defined by the Proxy of Gouldby et al. (2014). The eventual global impact assessment with this non-stationary multivariate extreme events, resulted in an required average increase of 16.8 m $width_{veg}$ between 1987 and 2018. This is needed to ensure the coastal safety against the 1/40 year design condition at the 27440 mangrove locations. This design conditions has the probability to occur ones per 40 year.

Non-stationary extreme value analysis

The extreme value analysis showed that the extreme events in mangrove environments are becoming more extreme and the average number of extreme events per year is increasing. At 87.5% of the environments an increase in the location parameter of the multivariate GPD was identified, with average number of extreme events per year, hereafter referred to as N_s, increasing in 59.8% of the cases. The average N_s increased from 4.16 to 4.32 between the time-periods 1987-2002 and 2003-2018. The multivariate extreme event increased on average with 0.06 m, 0.16 sec and 0.7 cm for respectively the parameters H_s, T_m and S. The transformation of the average extreme event, T_T, was positive at 70.6%, 72.6% and 64.6% for the three parameters at the 5809 investigated mangrove environments.

Previous studies identified that the coastal protection offered by mangroves is depending on the water level and the vulnerability to long-period waves (Quartel et al., 2007; Gijsman et al., 2021). However, in the global impact assessment of coastal mangrove vegetation, a univariate extreme value analysis is commonly applied (van Zelst et al., 2021; Menéndez et al., 2020). In the study of Marcos et al. (2019), it was pointed out that neglecting the multivariate dependency could lead to an underestimation of the risk. The proposed methodology in this study incorporated these limitations identified in previous studies. Based on the studies of Gouldby et al. (2014) and (Mentaschi et al., 2016), the methodology is capable of taking into account the non-stationarity of multivariate extreme events. These multivariate extreme events take into account the dependency of the water level and the vulnerability to long-period waves for the coastal protection offered by mangroves.

The hypothesis of this study was that the non-stationarity of extreme events in mangrove areas could be observed in historical data. To test this hypothesis an analysis over a period of 32 years was performed, from 1987-01-01 till 2018-12-31. The findings of the extreme value analysis are based on 280512 hourly combinations of H_s, T_m and S per mangrove environment. The significance of the percentage of environmental locations with a positive trend implied that the dependency and non-stationary extreme events in these regions are important in the determination of design conditions. The increase of N_s indicated that besides the non-stationarity of the extreme events itself, the number of extreme events could be of importance. This increases the probability of extreme events to occur in these mangrove regions.

Step 1: Identifying the extreme

The next step for the global impact assessment was to define the impact of the non-stationarity for design conditions. The method was defined by applying the detrending equations of Mentaschi et al. (2016) and a multivariate dependency model. The result was that on average the 1/40 year design conditions increased with 0.15 m (8.75%) for H_s, 0.13 sec (2.57%) for T_m and a increase of 0.01 m for S. The higher location weighted averages in table 4.4, created the expectation that mangroves are concentrated in areas that are subjected to a more extreme increase in design conditions over the studied period of 32 year.

The average increase of these multivariate extreme events are moderate. However, this increase in hydraulic loads on the vegetation belt can influence the persistence of the mangrove vegetation. Mangrove forests are capable to recover from damage caused by extreme events, but the rate of recovery and success declines when the damage itself is increasing (Gijsman et al., 2021). This moderate increase of the average conditions, can therefore influence the persistence of forests that already are at their limit.

Step 2: Identifying required mangrove width

The transformation of the 1/40 year design condition between 1987 and 2018 was in the last step transformed to the impact it had on the coastal safety. The theoretical framework for the global analysis resulted in the possibility to take the parameter $width_{veg}$ as optimization parameter. The analysis showed an increase of the required vegetation width of on average 16.8 m, with an increase at 53.3% of the 27440 mangrove locations.

The second main result from step 2 of the assessment is the sensitivity of $\Delta width_{veg}$ with respect to the three different parameters. This was indicated with the Spearman correlation coefficient between $\Delta width_{veg}$ and ΔH_s of 0.39, $\Delta width_{veg}$ and ΔH_s of 0.35 and $\Delta width_{veg}$ and ΔS of 0.48, visualized in figure 4.26. These values were defined with 7722 locations, meeting the post-process requirements. The Spearman correlation coefficient implied that the coastal protection offered by mangrove vegetation is a result of the transformation of these three parameters. This follows literature that argues that the wave attenuation of this coastal vegetation is depending on these parameters (Quartel et al., 2007; Gijsman et al., 2021).

5.2. Materials and Methods

The main results of the study are defined with the applied materials and methods as stated in the methodology part of this thesis. This part of the chapter discusses these applied methods and assumption to define the context for interpretation of the main results of this study.

5.2.1. Data sources

The extreme value analysis was based on hydrodynamic conditions from the globally covering ERA5 data and GTSM. The last model had been updated with ERA5 as forcing conditions. However, it is known that the ERA products underestimate the extreme conditions during tropical cyclones. In the paper of Shanas and Kumar (2015), it is argued that ERA-I data underestimated tropical cyclones with 33%. The observation of an underestimation of tropical cyclones is also observed in the ERA5 model (Bian et al., 2021). The influence of this is limited for the determination of the non-stationarity of the extreme events itself, while this underestimation is expected for all of the tropical cyclones. Therefore the data sources used for identifying the non-stationarity of the climate were applicable to create a global image.

The global impact assessment used data from the three studies of Van Zelst (2018), Athanasiou et al. (2019) and Simard et al. (2019), besides the extreme conditions from the previous analysis. Indicated in figure 4.15 the 27440 mangrove locations represent a large spread of data. As stated in section 3.1.3, the accuracy of these data sets was in some cases limited. One example is that the data of Van Zelst (2018) contained 20 locations where $z_{0,veg}$ was located beneath -10 m in respect to the mean sea level, with an extreme of -38.5 m. Furthermore, the dataset of Athanasiou et al. (2019), contained steep nearshore slopes above 1 in mangrove regions. The mentioned limitation of the data collection of parameters from Simard et al. (2019), with the locations of Van Zelst (2018), will partly influence the accuracy of this data set. These limitations of the different data sets were solved with the discussed pre-processing of the different data sets.

With the introduction of the theoretical framework, the focus was on the relative change in $width_{veg}$, and no longer the absolute change. Therefore the study revealed valuable insights in the impact of non-stationarity and points out that further research should be performed to identify the extend of the impact of non-stationarity on the coastal safety of the mangrove regions.

5.2.2. Non-stationary extreme value analysis

Limitations were introduced with the applied methodology of the non-stationary extreme value analysis. First of all, the Proxy of Gouldby et al. (2014) resulted in already imposed contribution of the different parameters to an extreme event. While it is defining the extreme flood events, it is expected that it is capable of defining the critical region. It is advised to further study the performances of this Proxy on the identification for the coastal protection offered by mangrove vegetation.

Secondly, the case-study of appendix B.3 showed the capability to take into account the tropical cyclones. The complex wind driven orientation of these events is left out of the scope of this study. By neglecting the orientation in the extreme value analysis, events at the coastline could be less extreme than the currently applied assumption of an oblique orientation defines. This could be implemented with further case studies and for example the methodology proposed in the study of Menéndez et al. (2020).

5.2.3. Statistical upscaling

The results of the statistical upscaling method are discussed in more detail in figure 4.10. The differences between the median of the boxplot and the centroid of the data visualizes that the upscaling method had, with the current application, limited capacity to reduce the Error Sum of Squares, hereafter referred to as SSE, correctly for the study. The green bars and their weights showed that only 30.6% of the mangrove environments the centroid and the median of all the three boxplots had the same sign. This was a result of the large spatial differences of the mangrove environments and the 31-dimensions to represent these environments. The percentages of equal sign presented in table 4.1 and table 4.3, implied that the averages are comparable. Therefore the study will give an insight in the global transformation, however further studies are needed. These studies should represent the original data set with more clusters or less parameters, to reduce the SSE.

It is therefore advised to reduce the number of parameters for clustering of the mangrove environments. A proposed solution for this is to replace the 9-dimensional multivariate dependency model with Spearman correlation coefficients. Besides the reduction of parameters, the number of clusters to further reduce SSE is possible. This second solution was not applied in this study, because of the limited computational resources.

5.2.4. Step 1: Identifying the extreme

The limitation of step 1 of the analysis are divided in three sections, to elaborate on the different limitations of the applied methodology.

Sampling procedure

The first limitation to identify the extreme is the applied methodology for the sampling procedure. Figure 4.12 represents one of the current limitations of the sampling procedure applied. The complex dependency structure was at three of the representative mangrove environments modelled with a dependency direction that was not in coherence with the identified extreme events. Another limitation of the sampling procedure is the selected distribution, visualized in figure 4.13. The extreme events were not covered by the generated cloud of extreme events, which should be to represent the original design conditions of this specific representative mangrove environment.

The cause of the orientation of the different dependency direction at these three clusters, is explained first. The selection of the best fitting copula was based on the sum of the error of the upper and lower tail between the empirical cumulative distribution function and the candidates for the copula. This is already a step forward in comparison to the commonly used visual inspection (Lira-Loarca et al., 2020; De Michele et al., 2007). However, a further study in properly representing the dependency is advised. This should result in a better framework to test the goodness of fit of the dependency model. The dependency model itself was fitted on the stationary parameters H_s^*, T_m^*, and S^*, this implied a stationary dependency, which could be questionable for longer time scales (Bender et al., 2014).

The cause of the underestimation of extremes is explained next. This is expected to be a result of the detrending procedure and the fitted distributions. The first limitation in this approach is that a linear trend was fitted for T_T and T_S. Especially the linear trend of T_S could be sensitive to outliers, considering the number of extreme events. The sensitivity of this parameter is pointed out in previous research (De Leo et al., 2021). The sensitivity was reduced by increasing the time window to 18 years as discussed in appendix B.2. However, the large percentages of the transformation of H_s for the design condition, indicates that further research is needed. This could be caused by the fact that the analysis had been performed in regions that are known for tropical cyclones. These result in large outliers influencing the T_S. Furthermore, the sampling procedure sampled the stationary H_s^*, T_m^*, and S^* from the Log-Norm distribution. This distribution was primarily fitted on the large weight of the central regime, misfitting the extremes, visualized in appendix C. In the studies of Rozas Rojas (2017) and Lira-Loarca et al. (2020) this problem is solved by introducing a mixed distribution. The current length of the original time-series in this study was to short for this analysis. The 32 years of data, would result in a limited amount of extreme events on which the tails of the extreme value distribution could be fit, making it for this study to sensitive.

Applied framework

The second limitation is that in the framework the influence of vegetation was neglected to identify the design condition. The test cases resulted that the extreme design condition at the edge of the horizontal plane were calculated at one particular transect. This approach reduced the computational demand, however neglected the sensitivity of the water level with respect to the efficiency of the mangrove vegetation to attenuate the waves. For local studies, it is therefore advised to include the vegetation at the local transect.

Spatial coherence

Besides these limitations, one can observe in figure 4.20, that the global distribution of the largest H_s follows the expected distribution. The spatial differences identified in the study of Marois and Mitsch (2015). The map indicates that the procedure sampled the largest extreme H_s parameters around the Caribbean sea and the South-Chinese sea, these areas are known to be crossed by the common cyclone pathways.

5.2.5. Step 2: Identifying required mangrove width

The discussion of the second step of the hydrodynamic model and the safety assessment is divided in three parts. First the discussion will be focused on the theoretical framework applied. Second, the application of the applied hydrodynamic model for the frame work. Third and last, the representation of wave-vegetation interaction within the model is discussed.

First, the framework defined introduced the possibility to define $\Delta width_{veg}$ as optimization parameter. This neglected the wave reduction of a decreasing water depth. The differences in $\Delta width_{veg}$ were therefore higher than they would be with the observed sloping bathymetery (van Zelst et al., 2021). This has to be kept in mind with the observed difference in vegetation width.

The second part of this discussion focuses on the applicability of the hydrodynamic model applied. SWASH is tested and validated on shallow and very shallow foreshores, with slopes ranging between 1/35 and 1/50 (Suzuki et al., 2017). However, the length of the domain and the space-discretization were limited to respectively 35 m and 0.02 m. In this study, slopes with a maximum of 1/620 for the nearshore and 1/2000 for the foreshore were examined. The results of the hydrodynamic model showed a concentration of energy in the long-period waves, comparable with the energy concentration of the step 1 in appendix D.5. This was solved for step 1 by decreasing the space-discretization step. However, due to the computational demand this was not possible for step 2. This energy concentration on long shallow foreshores was previously observed in the study of (Bakker, 2017). Their explanation was numerical resonance of the hydrodynamic model itself, causing a concentration of energy in the long-period waves. The results from the second step of the hydrodynamic model needs further research to validate this cause of the phenomena and the influence of it on the results of the SWASH model.

The third and last discussion point is the wave-vegetation interaction that is modeled in the hydrodynamic model. The parameterization of the mangrove trees in this study was based on literature (Narayan et al., 2011; Janssen, 2016). Appendix D.7 visualizes for four runs the wave attenuation in the mangrove forest. The average dissipation of H_s within the forest ranged between 0.25 till 0.51 %/m. In literature, it is stated that H_S decreases with 0.14 till 1.1%/m vegetation (Mcivor et al., 2012). This validates that the modelled energy dissipation was within the ranges of literature. Only the wave vegetation interaction during extreme conditions is not completely represented in the hydrodynamic model. Interaction as swaying, breaking and uprooting of the vegetation during extreme events were not included. These wave-vegetation interactions reduce the efficiency of the mangrove vegetation to attenuate the waves. The uprooting and breaking of mangrove trees, point out that mangrove trees have a limiting amount of wave attenuation capacity (Kovacs et al., 2001; Smith et al., 2009; Yanagisawa et al., 2009; van Hespen et al., 2021). However, limits for the degradation of the functionality of a mangrove tree are currently not defined. Furthermore, the model setup did not allow to include the spatial difference along the transect, with dense young vegetation located at the coastline and older higher trees in the upper regions of the transect (Janssen, 2016). This will underestimate the wave attenuation, while the young pioneers will reduce the waves passing through the vulnerable stem regions of the higher trees.

5.3. Main limitations

From the discussed limitation, some main limitation are mentioned below. This section therefore summarizes the discussion of the applied methodology to place the results in the appropriate context.

Sampling procedure design conditions

The design conditions were sampled from the fitted time-dependencies, the Log-Norm distributions and the multivariate dependency model. This procedure was sensitive to outliers in the extreme events, resulting in extreme design conditions. A cause of this is the large amount of environmental locations where tropical cyclones are present, influencing the linear fittings of the model. This results in the transformation of the design conditions that need further research to validate these values.

Choice hydrodynamic model

The SWASH model was applied in the methodology of this study to better track the transformation of energy from short-period waves to long-period waves on the long and shallow foreshores. However, as pointed out in this study the limitations in space-discretization with the computational resources available reduced the accuracy of the results. It is therefore advised to compare the results with a simplified hydrodynamic model or with measurements from field studies, to validate the results of this study.

Theoretical framework

The applied theoretical framework made it possible to choose the width of the mangrove vegetation as optimization parameter. This neglects the impact of the bathymetery and the commonly natural appearance of mangrove vegetation on a sloping bed. The found differences in required vegetation width are therefore more an identification of the impact of non-stationarity.

5.4. Relevance

The results of this study are based on the 5809 mangrove environments spread over the mangrove regions. The large amount of data and the therefore represented part of the global coastline, creates the confidence that the non-stationarity of the multivariate extreme events observed is of importance at a broader scale. The defined increase in design conditions in the mangrove environments and the observed increase in N_s points out that the hydrodynamic loads in mangrove areas have increased in the analyzed period of 32 years. This observed increase in multivariate extreme events and the number of extreme events may reduce the persistence of mangroves. It is therefore advised to study and monitor the condition of the coastal mangrove vegetation and to take action when mangrove vegetation is decreasing.

This study proved that an increase in the extreme storm-induced events is observed in the period of 1987 till 2018, a period of 32 years. The historical sea level rise implemented in the GTSM model is subtracted, to only take into account the storm-induced skew-surge (Batstone et al., 2013). The observed historical increase in the 32 years had a minimum increase of 0.4 cm and a maximum of 10.0 cm. The average transformation of S was 0.7 cm for an extreme event and 1 cm for the 1/40 year design condition. The eventual impact assessment would with the transformation of this parameter be more extreme, than the currently defined average increase of 16.8 m of mangrove vegetation at the 27440 locations.

Mangrove trees may be damaged during extreme conditions and need time to recover from these events to survive (Kovacs et al., 2001; Smith et al., 2009; Yanagisawa et al., 2009; van Hespen et al., 2021). The observed increase of the average extreme event, results in an expected increase in recovery time to keep surviving. However, the increase of N_s reduces the time between the extreme events. Based on the results of this study it is therefore advised to monitor the evolution of the coastal mangrove vegetation and the impact this may have on the coastal protection for the 15 million people defined in the study of Menéndez et al. (2020).

The large extend of this study in the tropical regions, further indicates that multivariate extreme events are increasing over time. This will increase the risk for floods in these coastal areas, especially when the historical sea level rise is considered as well, defined in Muis et al. (2016).

6

Conclusion and recommendations

This chapter answers the research questions defined in the introduction of this research. First, the main research question is answered followed by the sub-research questions. Finally a section with recommendations for further research following from the performed research work of this study is given.

6.1. Conclusion

Main research question

What is the impact of the non-stationarity of multivariate extreme events on the coastal safety in the mangrove areas with respect to the wave attenuation capacity of mangroves?

The hypothesis of this study was that the extreme events in mangrove areas have increased. The results of this study showed that at 87.5% of the mangrove environments an increase in the location parameter of the Generalized Pareto Distribution of the extremes was observed. On average the increase of this parameter was 0.02 m between 1987 and 2018. The transformation of these multivariate extreme events was tracked in three dimensions. Conclusion from this is that the average H_s, T_m and S increased in 70.6%, 72.6% and 64.6% of the mangrove environments. The average multivariate extreme event in mangrove environments increased with 0.06 m, 0.16 sec and 0.7 cm for the the parameters H_s, T_m and S. Furthermore, the number of extreme events increased on average between the period 1987-2002 and 2003-2018, from 4.16 to 4.32 per year.

The global impact assessment of this non-stationary multivariate extreme events resulted in a required average increase of 16.8m mangrove width at the 27440 assessed mangrove locations. This vegetation width is defined in a theoretical framework, as an optimization parameter to secure the coastal safety between the design conditions of 1987 and 2018 for a 1/40-year design condition. The post-processed results from the hydrodynamic SWASH model resulted in the Spearman rank correlation coefficients between the difference in required vegetation width and the three parameters of 0.39, 0.35 and 0.48, for respectively ΔH_s, $\Delta T_m s$ and ΔS. This validated that extreme events for the coastal protection of coastal mangrove vegetation should be assessed as a multivariate extreme event. The observed increase in the multivariate extreme events and the number of extreme events may reduce the persistence of mangroves and therewith their ability as coastal protection.

Sub-research question

How to identify an extreme event in respect to coastal safety offered by mangroves?

In this study an extreme event has been examined as a multivariate event. This is based on the assumption that the wave attenuation is depending on the wave characteristics and the accompanying water level. The Spearman rank correlation coefficients between the difference in required vegetation width and the three parameters 0.39, 0.35 and 0.48 with ΔH_s, $\Delta T_m s$ and ΔS validated this approach. The application of a Proxy resulted in a methodology feasible to define these extreme events.

How to identify and incorporate non-stationary of a multivariate extreme event?

A large part of this study dealt with defining a new methodology for filling the knowledge gap to incorporate non-stationary multivariate extreme events in the calculation of design conditions. The results from the methodology seems promising, but further research is needed to identify the sensitivity of the methodology to the extreme tropical cyclones in mangrove regions. In this research, the methodology was applied to the complex wave attenuation processes of mangroves in the expected non-stationary tropical mangrove environments. The identified workflow

could be translated to global studies or even local assessments to identify the impact of non-stationarity in preventing under- or overestimating of extreme events.

The study identified the potential of the non-stationary Peak over Threshold analysis and the identification of the non-stationarity. With a further focus on the parameters themselves, the transformation of these extreme events can be tracked. An overview of the workflow proposed is listed in the 5 steps below:

1. *Identify with a non-stationary Peak over Threshold analysis the combinations of multivariate extreme events.*
2. *Identify the trends of the univariates found during the multivariate extreme events, to transform the non-stationary univariates towards stationary univariates.*
3. *Define the dependency of the stationary univariates by implementing a Vine-D model.*
4. *Sample the design conditions in the stationary distributions.*
5. *Transform the stationary design conditions towards the desired moment in time.*

How did the extreme events transform in the considered period using a multivariate extreme value analysis?

The multivariate extreme event was a combination of H_s, T_m and s. The mean of the considered three parameters during extreme events increased in the three dimensions in 70.6%, 72.6%, and 64.6% of the mangrove environments. Resulting in a maximum increase in T_{0y} of 1.3 m for H_s, 1.6 sec for T_m and 0.2 m for S over the past 32 years. On average an extreme event at a mangrove location increased with 0.06 m, 0.16 sec, and 0.7 cm for the three parameters.

The sampling procedure of the time-dependent 1/40-year design condition resulted in an average increase of 0.15 m, 0.13 sec and 0.01 m. The difference in weighted averages between the mangrove environments and mangrove locations, brought the expectation that the coastal mangrove vegetation is concentrated in regions with a more extreme positive increase of the multivariate extreme event. This needs further research, due to the limitations of the sampling procedure.

The research furthermore emphasized the importance of the application of the Peak over Threshold analysis, which resulted in the observation of a mean increase in N_s between the first and second half of the period 1987 to 2018. The increase from 4.16 to 4.32 of this parameter, results in the conclusion that the probability of these extreme events occurring is increasing. This emphasizes the vulnerability of the coastal safety in the tropical region.

Which sensitivities of the coastal protection offered by mangroves can be identified from the results and what is the influence of these sensitivities?

As indicated in previous research, the water level influences the wave attenuation capacity of mangrove trees. The sensitivity of the wave attenuation capacity of mangroves with respect to the water level is emphasized further by identifying the differences in required vegetation width needed to meet the safety requirements for overtopping and run-up of the different water levels. The conclusion from this analysis is that higher water levels increase the required width of vegetation needed, which has been validated by comparing seven different mangrove trees.

This study showed that the coastal protection offered by mangrove vegetation is depending on the parameters H_s, T_m and S during the extreme conditions. This is based on the results from the post-processed SWASH results of 7722 mangrove locations. The Spearman rank correlation coefficients between the difference in required vegetation width and the three parameters 0.39, 0.35 and 0.48 with ΔH_s, $\Delta T_m s$ and ΔS. This means that the impact of non-stationary multivariate extreme events on the coastal safety in mangrove areas is depending on the combination of these parameters during the extreme events. Emphasizing the importance of taking into account the combination of these parameters during the multivariate extreme events.

6.2. Recommendations

The recommendations of this study are divided in two parts. First the scientific recommendations for further research will be examined. Second, the recommendations for engineering purposes will be discussed.

6.2.1. Scientific recommendation

Stability of the mangrove ecosystem

The first key-message of this research is the focus to the expected increase in vulnerability of the coastal protection offered by mangrove. In this research, mangroves were represented as static rigid structures, which is not influenced by the extreme conditions. However, mangrove is a living vegetation with a complex root structure. With the identified non-stationarity on the loading part of these coastal systems, the hypothesis is that the coastal safety is decreased. With more frequently and more extreme events subjected on the mangrove vegetation in 2018 in respect to 1987, it is emphasized that further research is needed to secure this important natural coastal protection will survive. Especially when the increase of N_s turns out to be significant, the recovery time for the coastal vegetation between the extreme loads decreases. It is therefore recommended to monitor the condition of the global mangrove forests more closely and to take action when mangrove vegetation is decreasing. Important is to measure the wave attenuation capacity to validate the results further and to identify the response to extreme events. It is furthermore recommended to focus on the non-stationarity in global impact assessments, while with the transformation of multivariate extreme events, the risk may increase with respect to a stationary univariate analysis. This while a combination of moderate values for the different parameters already can lead to an extreme.

Global non-stationarity of multivariate extreme events

Secondly, this study processed hydrodynamic conditions of 5809 mangrove environments. These are distributed along a large part of the global coastline. The therefore identified non-stationarity of 87.5% of only the storm-induced multivariate extreme events requires more attention. Especially when the consideration is made that within these regions mangroves protect a hinterland against annual flooding where globally 15 million people live Menéndez et al. (2020). The extreme events are neglecting the already observed historical sea level rise. When this sea level rise of a calculated maximum of 10 cm in the mangrove regions, the impact on the coastal safety is expected to increase.

It is furthermore possible that the observed non-stationarity of multivariate extreme events can be observed at other coastlines, based on the significance of the observation. Therefore it is recommended to extend this study to identify the non-stationarity of extreme flood events in coastal regions. The limitations of the applied model given in the discussion, should therefore be considered.

Mangrove during extreme events

Third and last, this study identified the wave-attenuation capacity of mangroves during extreme conditions. Measuring campaigns to validate the performances and persistence of mangrove vegetation and coastlines during these extreme events are limited. It is therefore advised to extend the monitoring of these coastlines and deploy measuring campaigns in mangrove areas during extreme conditions. This will increase the knowledge, which can be used to identify the impact of the non-stationarity of multivariate extreme events in these regions.

6.2.2. Engineering recommendations

Methodology of non-stationary multivariate extreme value analysis

The application of this study for further research and engineering purposes is mainly focused on the proposed multivariate extreme value analysis. The research identified the implication of the commonly used stationary assumption and proposed a methodology to prevent the under- or overestimation of the probability of extreme events. By identifying the trend, coastal protection can be designed more accurately to secure the safety of the hinterland. And while the results of the extreme value analysis are used to define the design conditions, this non-stationarity of the extreme events itself should be kept in mind with great importance. Neglecting the dependency of the different parameters of a multivariate extreme event, could result in an underestimation of the probability of occurrence of these extreme events.

Importance multivariate extreme events

The research furthermore pointed out that the approach of univariate extreme value analysis could result in limitations of the insight created. For some coastal protection structures, it could for example be that a single extreme parameter is not resulting in an extreme impact. However, the combination of semi-extreme parameters with a larger probability could result in a more extreme impact. The described methodology in this study could be applied to identify the critical regions of parameter combinations, which should be considered during the design or assessment phase of coastal structures. This approach is especially of importance in regions where mangrove offers a coastal protection function.

Bibliography

P. Athanasiou, A. Van Dongeren, A. Giardino, M. Vousdoukas, S. Gaytan-Aguilar, and R. Ranasinghe. Global distribution of nearshore slopes with implications for coastal retreat. *Earth System Science Data*, 11(4), 2019. ISSN 18663516. doi: 10.5194/essd-11-1515-2019.

S. A. Bakker. Coastal protection in the Mekong Delta Investigation of shore nourishment and mangroves as Building with Nature solutions. Technical report, 2017. URL `http://repository.tudelft.nl/`.

C. Batstone, M. Lawless, J. Tawn, K. Horsburgh, D. Blackman, A. McMillan, D. Worth, S. Laeger, and T. Hunt. A UK best-practice approach for extreme sea-level analysis along complex topographic coastlines. *Ocean Engineering*, 71:28–39, 2013. ISSN 00298018. doi: 10.1016/j.oceaneng.2013.02.003.

T. Bedford and R. M. Cooke. VINES-A NEW GRAPHICAL MODEL FOR DEPENDENT RANDOM VARIABLES. Technical Report 4, 2002.

J. Bender, T. Wahl, and J. Jensen. Multivariate design in the presence of non-stationarity. *Journal of Hydrology*, 514:123–130, 6 2014. ISSN 00221694. doi: 10.1016/j.jhydrol.2014.04.017.

G. F. Bian, G. Z. Nie, and X. Qiu. How well is outer tropical cyclone size represented in the ERA5 reanalysis dataset? *Atmospheric Research*, 249, 2 2021. ISSN 01698095. doi: 10.1016/j.atmosres.2020.105339.

R. M. Brinkman. Wave attenuation in mangrove forests: an investigation through field and theoretical studies. Technical report, James Cook University, 2006. URL `http://eprints.jcu.edu.au/1351/`.

S. Caires and A. Sterl. 00-Year Return Value Estimates for Ocean Wind Speed and Significant Wave Height from the ERA-40 Data. Technical report, 2005. URL `http://data.ecmwf.int/data/d/era40`.

P. Camus, F. J. Mendez, R. Medina, and A. S. Cofiño. Analysis of clustering and selection algorithms for the study of multivariate wave climate, 6 2011. ISSN 03783839.

L. Carrère, F. Lyard, M. Cancet, . A. Guillot, and L. Roblou. 20 Years of Progress in Radar Altimetry' 24-29. Technical report, 2012.

R. Chen and R. R. Twilley. A gap dynamic model of mangrove forest development along gradients of soil salinity and nutrient resources. *Journal of Ecology*, 86(1), 1998. ISSN 00220477. doi: 10.1046/j.1365-2745.1998.00233.x.

Y. Chen. Mangrove Tree, 1 2013.

S. Corbella and D. D. Stretch. Simulating a multivariate sea storm using Archimedean copulas. *Coastal Engineering*, 76:68–78, 6 2013. ISSN 03783839. doi: 10.1016/j.coastaleng.2013.01.011.

F. De Leo, G. Besio, R. Briganti, and E. Vanem. Non-stationary extreme value analysis of sea states based on linear trends. Analysis of annual maxima series of significant wave height and peak period in the Mediterannean Sea. *Coastal Engineering*, 167, 8 2021. ISSN 03783839. doi: 10.1016/j.coastaleng.2021.103896.

C. De Michele, G. Salvadori, G. Passoni, and R. Vezzoli. A multivariate model of sea storms using copulas. *Coastal Engineering*, 54(10):734–751, 10 2007. ISSN 03783839. doi: 10.1016/j.coastaleng.2007.05.007.

N. Duke, M. Ball, and J. Ellison. Factors influencing bio-diversity and distributional gradients in mangroves. *Global Ecol Biogeogr.*, 7:27–48, 1998.

ECMWF. ERA5, 2021.

ESA and UCLouvain. Globcover, 2010.

K. B. Gedan, M. L. Kirwan, E. Wolanski, E. B. Barbier, and B. R. Silliman. The present and future role of coastal wetland vegetation in protecting shorelines: Answering recent challenges to the paradigm, 5 2011. ISSN 01650009.

N. Geißler, R. Schnetter, and M. L. Schnetter. The pneumathodes of Laguncularia racemosa: Little known rootlets of surprising structure, and notes on a new fluorescent dye for lipophilic substances. *Plant Biology*, 4(6), 2002. ISSN 14358603. doi: 10.1055/s-2002-37404.

R. Gijsman, E. M. Horstman, D. van der Wal, D. A. Friess, A. Swales, and K. M. Wijnberg. Nature-Based Engineering: A Review on Reducing Coastal Flood Risk With Mangroves, 7 2021. ISSN 22967745.

C. Giri, E. Ochieng, L. L. Tieszen, Z. Zhu, A. Singh, T. Loveland, J. Masek, and N. Duke. Status and distribution of mangrove forests of the world using earth observation satellite data. *Global Ecology and Biogeography*, 20 (1):154–159, 1 2011. ISSN 1466822X. doi: 10.1111/j.1466-8238.2010.00584.x.

B. Gouldby, F. J. Méndez, Y. Guanche, A. Rueda, and R. Mínguez. A methodology for deriving extreme nearshore sea conditions for structural design and flood risk analysis. *Coastal Engineering*, 88:15–26, 6 2014. ISSN 03783839. doi: 10.1016/j.coastaleng.2014.01.012.

B. Gouldby, D. Wyncoll, M. Panzeri, M. Franklin, T. Hunt, D. Hames, N. Tozer, P. Hawkes, U. Dornbusch, and T. Pullen. Multivariate extreme value modelling of sea conditions around the coast of England. *Proceedings of the Institution of Civil Engineers: Maritime Engineering*, 170(1):3–20, 3 2017. ISSN 17517737. doi: 10.1680/jmaen.2016.16.

B. Gräler, M. J. Van Den Berg, S. Vandenberghe, A. Petroselli, S. Grimaldi, B. De Baets, and N. E. Verhoest. Multivariate return periods in hydrology: A critical and practical review focusing on synthetic design hydrograph estimation, 2013. ISSN 10275606.

K. Hasselmann, T. P. Barnett, E. Bouws, H. Carlson, D. Cartwright, K. Enke, J. Ewing, H. Gienapp, D. Hasselmann, P. Kruseman, A. Meerburg, P. Müller, D. Olbers, K. Richter, W. Sell, and H. Walden. Measurements of Wind-Wave Growth and Swell Decay during the Joint North Sea Wave Project (JONSWAP). *Ergnzungsheft zur Deutschen Hydrographischen Zeitschrift Reihe*, 8(12):95, 1973.

J. Hinkel, D. Lincke, A. T. Vafeidis, M. Perrette, R. J. Nicholls, R. S. Tol, B. Marzeion, X. Fettweis, C. Ionescu, and A. Levermann. Coastal flood damage and adaptation costs under 21st century sea-level rise. *Proceedings of the National Academy of Sciences of the United States of America*, 111(9):3292–3297, 3 2014. ISSN 00278424. doi: 10.1073/pnas.1222469111.

L. H. Holthuijsen. *Waves in oceanic and coastal waters*, volume 9780521860284. 2007. doi: 10.1017/CBO9780511618536.

E. M. Horstman, C. M. Dohmen-Janssen, P. M. Narra, N. J. van den Berg, M. Siemerink, and S. J. Hulscher. Wave attenuation in mangroves: A quantitative approach to field observations. *Coastal Engineering*, 94:47–62, 12 2014. ISSN 03783839. doi: 10.1016/j.coastaleng.2014.08.005.

M. P. J. Janssen. Flood hazard reduction by mangroves. Technical report, 2016. URL `http://repository.tudelft.nl/`.

A. F. Jenkinson. The frequency distribution of the annual maximum (or minimum) values of meteorological elements. *Quarterly Journal of the Royal Meteorological Society*, 81(348), 1955. ISSN 1477870X. doi: 10.1002/qj.49708134804.

A. Kazemi, K. Van De Riet, and O. M. Curet. Drag coefficient and flow structure downstream of mangrove root-type models through PIV and direct force measurements. *Physical Review Fluids*, 7(3), 2018. ISSN 2469990X. doi: 10.1103/PhysRevFluids.3.073801.

J. M. Kovacs, M. Blanco-Correa, and F. Flores-Verdugo. A logistic regression model of hurricane impacts in a mangrove forest of the Mexican Pacific. *Journal of Coastal Research*, 17(1), 2001. ISSN 07490208.

D. Kurowicka and H. Joe. *Dependence modeling: Vine copula handbook*. 2010. doi: 10.1142/7699.

F. Li, J. Zhou, and C. Liu. Statistical modelling of extreme storms using copulas: A comparison study. *Coastal Engineering*, 142:52–61, 12 2018. ISSN 03783839. doi: 10.1016/j.coastaleng.2018.09.007.

A. Lira-Loarca, M. Cobos, M. □. Losada, and A. Baquerizo. Storm characterization and simulation for damage evolution models of maritime structures. *Coastal Engineering*, 156:103620, 3 2020. ISSN 0378-3839. doi: 10.1016/J.COASTALENG.2019.103620.

S. Maneewongvatana and D. M. Mount. It's okay to be skinny, if your friends are fat. *Center for Geometric Computing 4th Annual Workshop on Computational Geometry*, (October), 1999.

M. Marcos, J. Rohmer, M. I. Vousdoukas, L. Mentaschi, G. Le Cozannet, and A. Amores. Increased Extreme Coastal Water Levels Due to the Combined Action of Storm Surges and Wind Waves. *Geophysical Research Letters*, 46(8):4356–4364, 4 2019. ISSN 19448007. doi: 10.1029/2019GL082599.

R. Marijnissen, M. Kok, C. Kroeze, and J. van Loon-Steensma. The sensitivity of a dike-marsh system to sea-level rise-a model-based exploration. *Journal of Marine Science and Engineering*, 8(1), 2020. ISSN 20771312. doi: 10.3390/JMSE8010042.

D. E. Marois and W. J. Mitsch. Coastal protection from tsunamis and cyclones provided by mangrove wetlands - A review, 1 2015. ISSN 21513740.

G. McGranahan, D. Balk, and B. Anderson. The rising tide: Assessing the risks of climate change and human settlements in low elevation coastal zones. *Environment and Urbanization*, 19(1):17–37, 4 2007. ISSN 09562478. doi: 10.1177/0956247807076960.

A. Mcivor, I. Möller, T. Spencer, and M. Spalding. Reduction of Wind and Swell Waves by Mangroves Natural Coastal Protection Series: Report 1. Technical report, 2012. URL http://www.naturalcoastalprotection.org/documents/reduction-of-wind-and-swell-waves-.

F. J. Méndez, M. Menéndez, A. Luceño, and I. J. Losada. Estimation of the long-term variability of extreme significant wave height using a time-dependent Peak Over Threshold (POT) model. *Journal of Geophysical Research: Oceans*, 111(7), 7 2006. ISSN 21699291. doi: 10.1029/2005JC003344.

P. Menéndez, I. J. Losada, S. Torres-Ortega, S. Narayan, and M. W. Beck. The Global Flood Protection Benefits of Mangroves. *Scientific Reports*, 10(1), 12 2020. ISSN 20452322. doi: 10.1038/s41598-020-61136-6.

L. Mentaschi, M. Vousdoukas, E. Voukouvalas, L. Sartini, L. Feyen, G. Besio, and L. Alfieri. The transformed-stationary approach: A generic and simplified methodology for non-stationary extreme value analysis. *Hydrology and Earth System Sciences*, 20(9):3527–3547, 9 2016. ISSN 16077938. doi: 10.5194/hess-20-3527-2016.

M. Miche. Mouvements ondulatoires de la mer en prodondeur constante ou décrousante. *Annales de Ponts et Chaussées*, 1944.

S. Muis, M. Verlaan, H. C. Winsemius, J. C. Aerts, and P. J. Ward. A global reanalysis of storm surges and extreme sea levels. *Nature Communications*, 7, 6 2016. ISSN 20411723. doi: 10.1038/ncomms11969.

N. J. Murray, S. R. Phinn, R. S. Clemens, C. M. Roelfsema, and R. A. Fuller. Continental scale mapping of tidal flats across east Asia using the landsat archive. *Remote Sensing*, 4(11):3417–3426, 11 2012. ISSN 20724292. doi: 10.3390/rs4113417.

S. Narayan, T. Suzuki, M. J. Stive, H. J. Verhagen, W. Ursem, and R. Ranasinghe. ON THE EFFECTIVENESS OF MANGROVES IN ATTENUATING CYCLONE - INDUCED WAVES. *Coastal Engineering Proceedings*, 1(32), 2011. ISSN 0589-087X. doi: 10.9753/icce.v32.waves.50.

National Oceanic and Atmospheric Administration. Historical Hurricane Tracks, 2019.

R. J. Nicholls, W. A. Birkemeier, and G. h. Lee. Evaluation of depth of closure using data from Duck, NC, USA. *Marine Geology*, 148(3-4), 1998. ISSN 00253227. doi: 10.1016/S0025-3227(98)00011-5.

T. D. of Environment and G. o. B. Natural Resources. Black Mangrove (Avicennia germinans), 10 2021.

OpenStreetMap contributors. Data Derived from OpenStreetMap for Download, 12 2021.

L. K. Phan, J. S. Van Thiel De Vries, and M. J. Stive. Coastal mangrove squeeze in the Mekong Delta. *Journal of Coastal Research*, 31(2):233–243, 3 2015. ISSN 15515036. doi: 10.2112/JCOASTRES-D-14-00049.1.

T. Pullen, N. Allsop, T. Bruce, A. Kortenhaus, H. Schüttrumpf, and J. Van der Meer. EurOtop Manual on wave overtopping of sea defences and related structures An overtopping manual largely based on European research, but for worldwide application Second Edition 2018. Technical report, 2018. URL www.overtopping-manual.com.

S. Quartel, A. Kroon, P. G. Augustinus, P. Van Santen, and N. H. Tri. Wave attenuation in coastal mangroves in the Red River Delta, Vietnam. *Journal of Asian Earth Sciences*, 29(4):576–584, 2 2007. ISSN 13679120. doi: 10.1016/j.jseaes.2006.05.008.

E. Ragno, A. AghaKouchak, L. Cheng, and M. Sadegh. A generalized framework for process-informed nonstationary extreme value analysis. *Advances in Water Resources*, 130:270–282, 8 2019. ISSN 03091708. doi: 10.1016/j.advwatres.2019.06.007.

R. A. Reis, A. A. Pires-Silva, C. J. Fortes, and T. Suzuki. Experiences with SWASH on modelling wave propagation over vegetation: Comparisons with lab and field data. *Journal of Integrated Coastal Zone Management*, 20(2):145–150, 6 2020. ISSN 16468872. doi: 10.5894/RGCI-N303.

C. D. Rozas Rojas. Assessing the impact of climate change on longshore sediment transport along the central Dutch coast using statistical downscaling. Technical report, 2017. URL http://repository.tudelft.nl/.

J. D. Salas and J. Obeysekera. Revisiting the Concepts of Return Period and Risk for Nonstationary Hydrologic Extreme Events. *Journal of Hydrologic Engineering*, 19(3), 2014. ISSN 1084-0699. doi: 10.1061/(asce)he.1943-5584.0000820.

G. J. Schiereck. *Introduction to Bed, Bank and Shore Protection*. 2017. doi: 10.1201/9781315274935.

SDV - MIT Data to AI Lab. Copulas, 2018.

A. Shadmehri Toosi, S. Doulabian, E. Ghasemi Tousi, G. H. Calbimonte, and S. Alaghmand. Large-scale flood hazard assessment under climate change: A case study. *Ecological Engineering*, 147, 3 2020. ISSN 09258574. doi: 10.1016/j.ecoleng.2020.105765.

P. R. Shanas and V. S. Kumar. Trends in surface wind speed and significant wave height as revealed by ERA-Interim wind wave hindcast in the Central Bay of Bengal. *International Journal of Climatology*, 35(9), 2015. ISSN 10970088. doi: 10.1002/joc.4164.

M. Simard, T. Fatoyinbo, C. Smetanka, V. H. Rivera-Monroy, E. Castaneda, N. Thomas, L. Fatpyinbo, E. Castaneda-Moya, T. Van, E. Feliciano, D. Lagomasino, S. Lee, C. Trettin, A. Shapiro, and M. Mwita. Global Mangrove Distribution, Aboveground Biomass, and Canopy Height Get Data Citation About Us Get Data Submit Data Tools Resources Help 1. Dataset Overview Project: Carbon Monitoring System. 2019. doi: 10.3334/ORNLDAAC/1665. URL https://doi.org/10.3334/ORNLDAAC/1665.

T. J. Smith, G. H. Anderson, K. Balentine, G. Tiling, G. A. Ward, and K. R. Whelan. Cumulative impacts of hurricanes on Florida mangrove ecosystems: Sediment deposition, storm surges and vegetation. *Wetlands*, 29(1):24–34, 3 2009. ISSN 02775212. doi: 10.1672/08-40.1.

S. Solari, M. Egüen, M. J. Polo, and M. A. Losada. Peaks Over Threshold (POT): A methodology for automatic threshold estimation using goodness of fit p-value. *Water Resources Research*, 53(4):2833–2849, 4 2017. ISSN 19447973. doi: 10.1002/2016WR019426.

M. Spalding, A. McIvor, F. Tonneijck, S. Tol, and P. van Eijk. Mangroves for coastal defence Guidelines for coastal managers & policy makers Suggested Citation. Technical report, 2014. URL www.nature.org.

O. Stabrin. Verschillende wortelstelsels van mangrove, 5 2018.

H. F. Stockdon, R. A. Holman, P. A. Howd, and A. H. Sallenger. Empirical parameterization of setup, swash, and runup. *Coastal Engineering*, 53(7):573–588, 5 2006. ISSN 0378-3839. doi: 10.1016/J.COASTALENG.2005.12.005.

B. Sumer and J. Fredsøe. BOOK REVIEW HYDRODYNAMICS AROUND CYLINDRICAL STRUCTURES, World Scientific, Singapore. *Journal of Fluids and Structures*, 12(2), 1998. ISSN 08899746. doi: 10.1006/jfls.1997.0117.

A. E. Sutton-Grier, K. Wowk, and H. Bamford. Future of our coasts: The potential for natural and hybrid infrastructure to enhance the resilience of our coastal communities, economies and ecosystems, 8 2015. ISSN 18736416.

T. Suzuki, M. Zijlema, B. Burger, M. C. Meijer, and S. Narayan. Wave dissipation by vegetation with layer schematization in SWAN. *Coastal Engineering*, 59(1):64–71, 1 2012. ISSN 03783839. doi: 10.1016/j.coastaleng.2011.07.006.

T. Suzuki, C. Altomare, W. Veale, T. Verwaest, K. Trouw, P. Troch, and M. Zijlema. Efficient and robust wave overtopping estimation for impermeable coastal structures in shallow foreshores using SWASH. *Coastal Engineering*, 122:108–123, 4 2017. ISSN 03783839. doi: 10.1016/j.coastaleng.2017.01.009.

T. Suzuki, Z. Hu, K. Kumada, L. K. Phan, and M. Zijlema. Non-hydrostatic modeling of drag, inertia and porous effects in wave propagation over dense vegetation fields. *Coastal Engineering*, 149:49–64, 7 2019. ISSN 0378-3839. doi: 10.1016/J.COASTALENG.2019.03.011.

S. Tas. Coastal protection in the Mekong Delta Wave load and overtopping of sea dikes as function of their location in the cross-section, for different foreshore geometries. Technical report, 2016. URL http://repository.tudelft.nl/.

The SWASH team. SWASH, 10 2020.

U.S. Geological Survey. NASA Earth Observatory images created by Jesse Allen, using data provided by Chandra Giri, 11 2010.

J. P. Van Den Bos and H. J. Verhagen. Breakwater design Lecture notes CIE5308. Technical report, 2018.

J. Van der Meer, N. Allsop, T. Bruce, J. De Rouck, A. Kortenhaus, T. Pullen, H. Schüttrumpf, P. Troch, and B. Zanuttigh. EurOtop - Manual on wave overtopping of sea defences and related structures - Second Edition 2018. Technical report, 2018. URL www.overtopping-manual.com.

R. van Hespen, Z. Hu, Y. Peng, B. W. Borsje, M. Kleinhans, T. Ysebaert, and T. J. Bouma. Analysis of coastal storm damage resistance in successional mangrove species. *Limnology and Oceanography*, 66(8):3221–3236, 8 2021. ISSN 19395590. doi: 10.1002/lno.11875.

B. K. Van Wesenbeeck, G. Wolters, J. A. A. Antolínez, S. Kalloe, B. Hofland, W. De Boer, C. Çete, and T. J. Bouma. Woods versus waves: Wave attenuation through non-uniform forests under extreme conditions. Technical report, 2021.

V. T. M. Van Zelst. Global flood hazard reduction by foreshore vegetation MSc. thesis. Technical report, 2018. URL http://resolver.tudelft.nl/uuid:524dcd46-f697-4e85-ae6a-18a1eb4db710.

V. T. M. van Zelst, J. T. Dijkstra, B. K. van Wesenbeeck, D. Eilander, E. P. Morris, H. C. Winsemius, P. J. Ward, and M. B. de Vries. Cutting the costs of coastal protection by integrating vegetation in flood defences. *Nature Communications*, 12(1):6533, 12 2021. ISSN 2041-1723. doi: 10.1038/s41467-021-26887-4. URL https://www.nature.com/articles/s41467-021-26887-4.

H. J. Verhagen and T. T. Loi. The use of mangroves in coastal protection. Technical report, 2012.

M. Verlaan, S. De Kleermaeker, and L. Buckman. GLOSSIS: Global storm surge forecasting and information system. In *Australian Coasts and Ports 2015 Conference*, 2015.

P. Vo-Luong and S. Massel. Energy dissipation in non-uniform mangrove forests of arbitrary depth. *Journal of Marine Systems*, 74(1-2):603–622, 11 2008. ISSN 09247963. doi: 10.1016/j.jmarsys.2008.05.004.

M. I. Vousdoukas, L. Mentaschi, E. Voukouvalas, M. Verlaan, S. Jevrejeva, L. P. Jackson, and L. Feyen. Global probabilistic projections of extreme sea levels show intensification of coastal flood hazard. *Nature Communications*, 9(1), 12 2018. ISSN 20411723. doi: 10.1038/s41467-018-04692-w.

J. Wilkins. Mangrove Roots, 7 2008.

T. Wilms, F. Van Der Goot, F. Tonneijck, F. Nurhabni, and L. Sembiring. Building with Nature Approach. }Building with Nature to restore eroding tropical muddy coasts. Technical report, Dordrecht, 2020.

J. C. Winterwerp, W. G. Borst, and M. B. De Vries. Pilot study on the erosion and rehabilitation of a mangrove mud coast. *Journal of Coastal Research*, 21(2):223–230, 3 2005. ISSN 07490208. doi: 10.2112/03-832A.1.

H. Yanagisawa, S. Koshimura, K. Goto, T. Miyagi, F. Imamura, A. Ruangrassamee, and C. Tanavud. The reduction effects of mangrove forest on a tsunami based on field surveys at Pakarang Cape, Thailand and numerical analysis. *Estuarine, Coastal and Shelf Science*, 81(1):27–37, 1 2009. ISSN 02727714. doi: 10.1016/j.ecss.2008.10.001.

A

Data collection and parameter definition

A.1. Coastal mangrove locations

Coastal mangrove locations

The coastline locations of the study of Van Zelst (2018) are used as data source to identify the coastlines where vegetation is present. This data is based on shore normal transects obtained from the Aqueduct project. The Aqueduct project is a project of the American World Resources Institute, Deltares, VU University of Amsterdam, Utrecht University and the Netherlands Environmental Assessment Agency. This study is based on estimating shore line locations based on the Open Street Map. On this coastline, shore normal transects are determined and each of these transects is extended 4 km into sea and 4 km into landward direction. The distance along the shoreline between the different transects is approximately 1 km (Van Zelst, 2018). With global vegetation maps, the presence of vegetation was determined. The data of Van Zelst (2018) contained salt marsh coastlines beside the mangrove coastlines. For that reason a few filter steps are applied to end up with a dataset towards the scope of this research. The filtering steps are:

- *The locations are located between the latitudes 60° S and 66 ° N*
- *The location is identified as a location where mangrove is present*
- *The locations are located at the coastline*
- *The foreshore is based on the results of the FAST project*

The foreshore parameters should be determined within the FAST project. These are based on combining a global tide model and satellite imaginary of different tidal moments resulting to define the parameters with. The result of this data filtering is shown in figure A.1, resulting in 27440 locations with mangrove and foreshore characteristics.

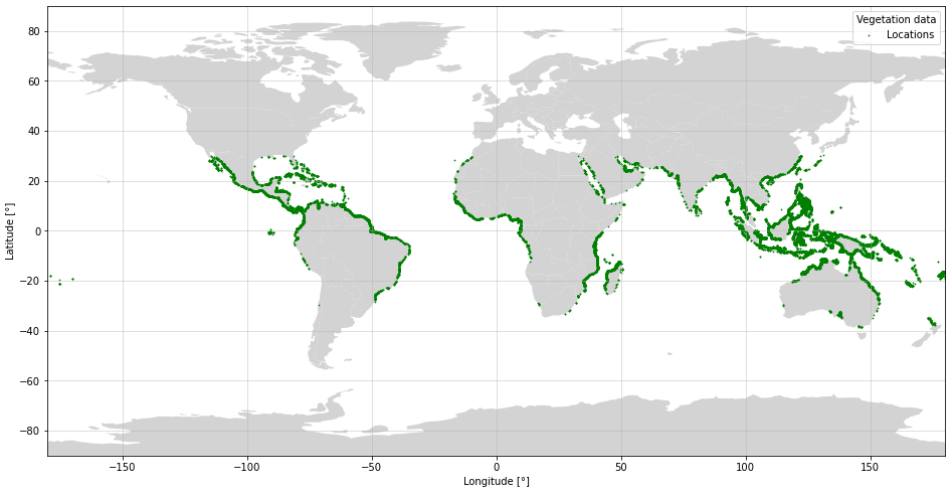

Figure A.1: *27440 locations along the coastline, identified as locations where mangrove is present, based on the study of Van Zelst (2018)*

Transect orientation

In the database of the study of Van Zelst (2018), the orientation of the transects is not included. To obtain these transects and to use these in further data collection steps, QGis 3.18 is used. With the use of the OSM coastline shape file OpenStreetMap contributors (2021), the nearest location of these points on the coastline is determined, trying to mimic the approach used in the Aqueduct project.

This resulted in two points per location, the original and its nearest neighbor on the coastline. The orientation between these points is used to define a transect with. This transects has been given a length of 0.04 degrees in off- and onshore direction, following the methodology of the Aquaduct project. However, the results from the nearest point on the coastline showed that 1361 points of the 27440 had a larger distance from the coastline than 0.01°, which is approximately $1000m$ were found. This means that approximately 5.0% of the data has a orientation based on a shoreline that is more than $1000m$ away. The reason for this is visualized in figure A.2a. Due to the choice of shoreline some points are located land inward, for example in estuaries.

While zonal statistics will be performed to obtain the vegetation parameters the transects are converted from a line to a polygon with a thickness of 0.001°, which is approximately $110m$. This width is based on the width of the vegetation raster of the study of Simard et al. (2019), which has a 30 x 30 meter grid. The result of this process is visualized in figure A.2a.

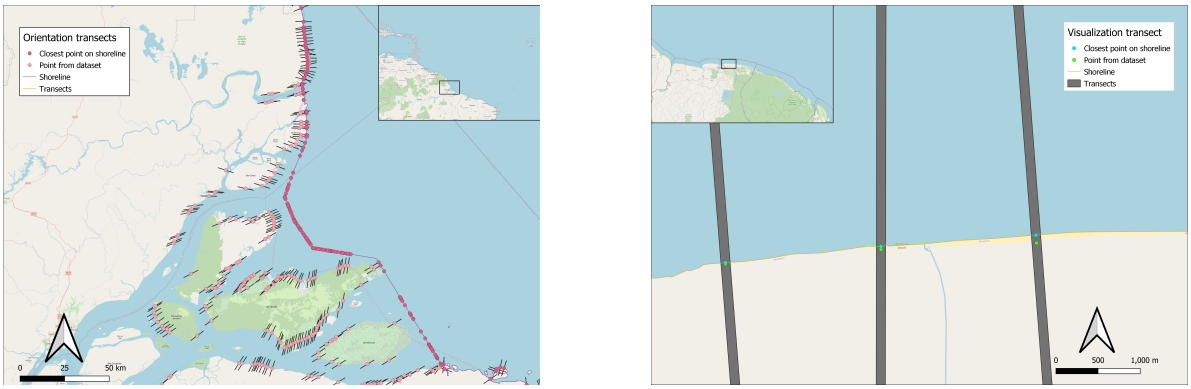

(a) *Transect orientation in Brazil, South America*

(b) *Transect determination in Suriname, South America*

Figure A.2: *Transect orientation process*

A.2. Environmental data sources

EMCWF - ERA5

ERA5 data is a product of the European Centre for Medium-Range Weather Forecasts, ECMWF, and describes atmospheric, land, and oceanic climate variables in a 30km global grid (ECMWF, 2021). The product of EMCWF, ERA5, contains 259920 grid cells, placed on a grid with a resolution of 0.5° x 0.5°. With the use of the KD-tree method, the closest neighbor of the original locations in the grid of ERA5 is identified. Eventually, 2200 points of the ERA5 database cover the spread of the mangrove locations.

In the paper of Shanas and Kumar (2015), by applying ERA-I data extreme events occurring from tropical cyclones are underestimated. That study found an underestimation of the significant wave height of 33% by comparing the ERA-I data with buoy data. This is due to the large grid size, 0.75° x 0.75° of the ERA-I data. The new data product of the EMCWF, ERA5, has a resolution of 30 km x 30 km. It is expected that this underestimation of the ERA5 data will be similar or smaller, and for that reason, the data is used without correction.

Historical sea level rise

In the global tide and surge model the average water level increased for the used 4708 measuring stations in this study with 7.1 cm between 1987 and 2018. In figure A.3 the average water level in the GTSM (Muis et al., 2016) is displayed where the color indicates the calculated average water level of the year 1987. In figure A.4, the average water level of the year 2018 are displayed on the same color bar as the previous figure.

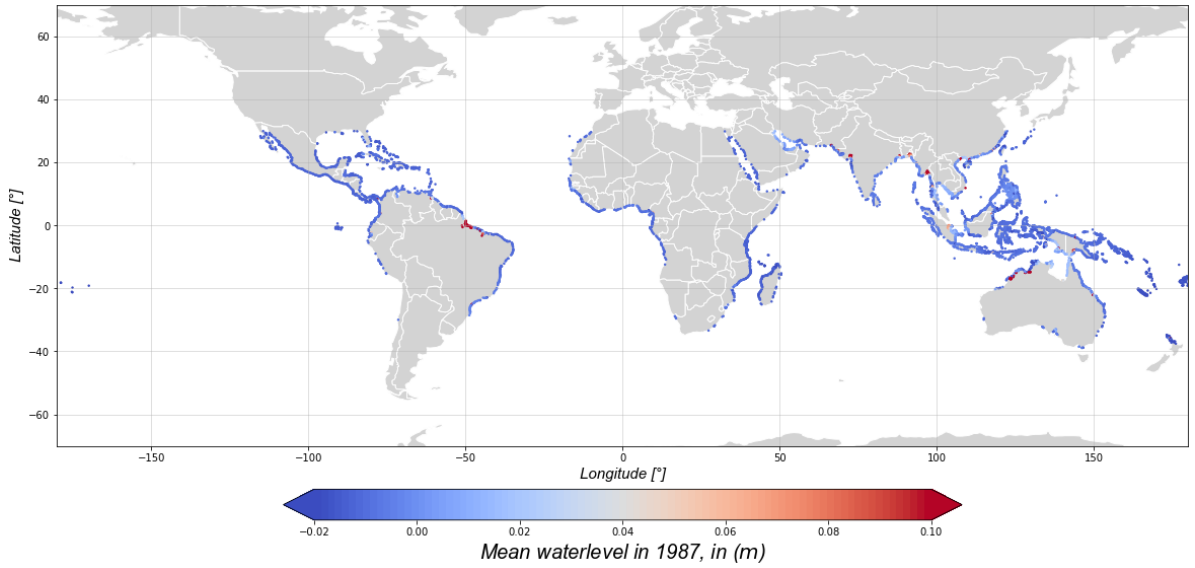

Figure A.3: *Mean waterlevel observed in the Muis et al. (2016) in the year 1987.*

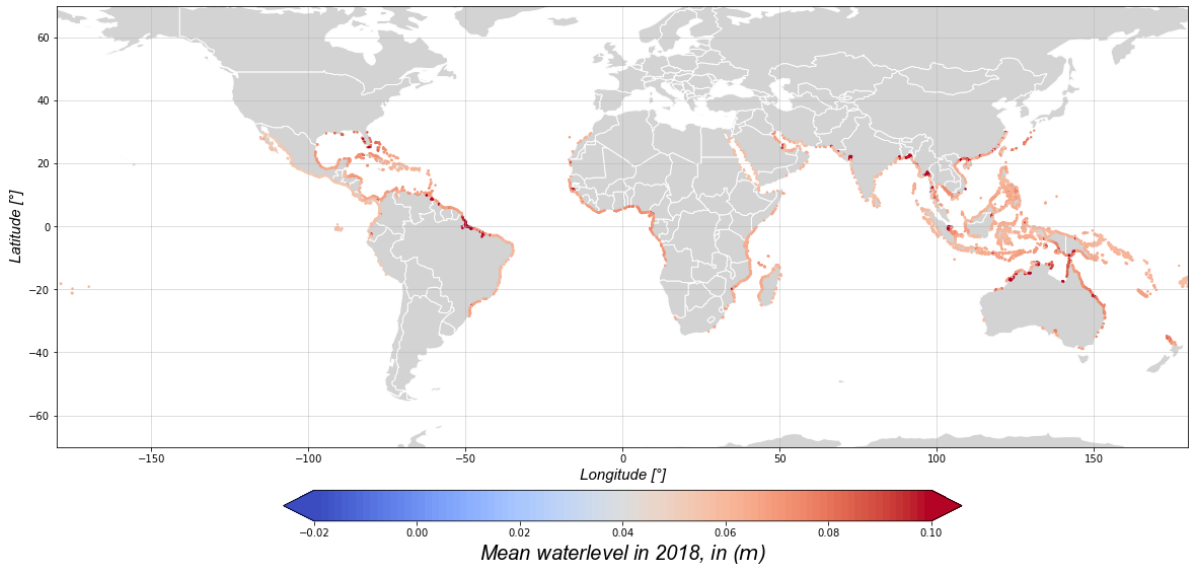

Figure A.4: *Mean waterlevel observed in the Muis et al. (2016) in the year 2018.*

An moderate increase of the water level between the period of 1987 and 2018 is observed. The maximum increase observed in these 32 years is 10.0 cm, the minimum increase observed is 0.4 cm. This moderate increase in the water level resulted in the conclusion that the sea level rise will be left out of the scope of this master thesis study.

Unique combinations

The GTSM model is defined on a finer grid closer towards shirt with respect to the ERA5 model. This results that the location of the eventual applied GTSM model and ERA5 model, are not equal. For the visualization of the performed analysis, figure A.5 is used. In this figure, the GTSM location and ERA5 location representing the mangrove locations at the southern coastline of Cuba is visualized. With the green dot, a mangrove location is defined, of which the hydrodynamic conditions are defined by these two locations.

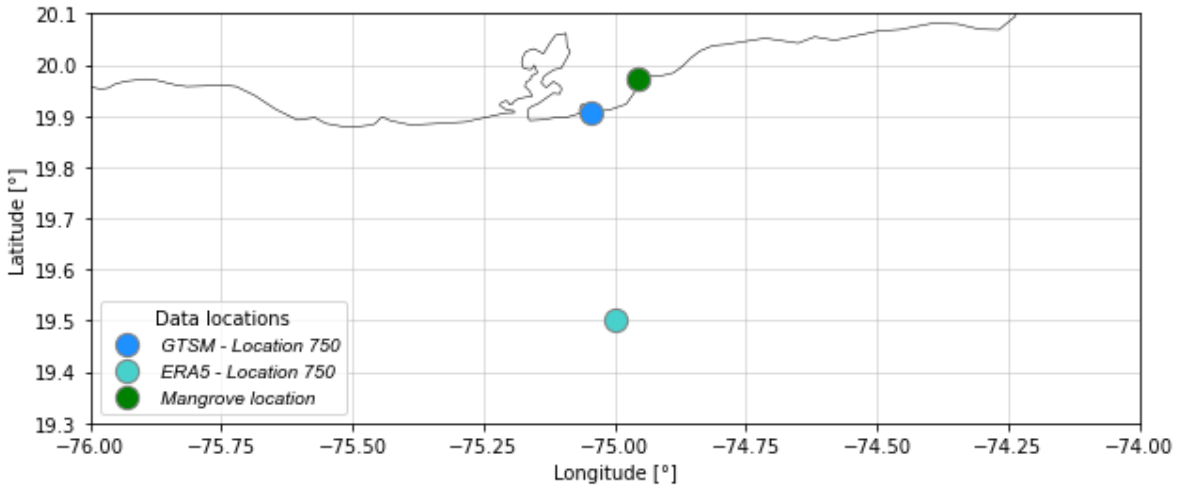

Figure A.5: *The GTSM and ERA5 location of environmental location 750 and the mangrove location represented by this environmental locations.*

A.3. Natural protection data sources and parameter definition

Nearshore data

The nearshore slopes are defined between the depth of closure and the coastline. The depth of closure is the depth of which there is no significant change in bottom elevation, determined by equation A.1 (Nicholls et al., 1998). In this equation $H_{e,t}$ and $T_{e,t}$ are respectively the significant wave height and wave period that are exceeded for only 12 hours per year. The slope is determined on a transect $4000m$ landward until $4000m$ seaward, from the point located on the OSM coastline. Then the slope is calculated from the most offshore point which is smaller than the depth of closure until the point of the mean sea level of the coastline. At some locations the depth of closure was not reached within the transects, at these locations the most offshore point is taken as starting point to calculate the nearshore slope.

$$d_c = 2.28 H_{e,t} - 68.5 \left(\frac{H_{e,t}^2}{g T_{e,t}^2} \right) \tag{A.1}$$

Foreshore data

The foreshore parameters in the study of Van Zelst (2018) are determined using the global inter tidal elevation map (Murray et al., 2012). That map shows the elevation of the tidal flats, by using data from NASA/USGS Landsat EO data and ESA/Copernicus Sentinel 2 EO data for the period of 1997-2017 and combining it with the global tide model FES2012 (Carrère et al., 2012). The resulting height of the starting point of the foreshore is with respect to the mean sea level, MSL.

The vegetation parameters of the 27440 locations with mangrove vegetation are the width and starting point of vegetation with respect to the mean sea level. With the use of the Global mangroves map (Giri et al., 2011), Globcover (ESA and UCLouvain, 2010) and the Vegetation presence map from the FAST project, the locations, and widths of these vegetation belts are determined. The FAST project is a consortium of Deltares, NIOZ, the University of Cambridge, GEOECOMAR, and the University of Cadiz, which was focused on foreshore assessment using space technology.

Vegetation data

In the study of Simard et al. (2019), the characteristics of the mangrove forests around the globe are derived from SRTM DEM data of February 2000 and lidar heights from ICESat/GLAS Spaceborne Lidar Mission collected globally between 2003 and 2009. The locations of the mangrove environments are based on the work of Giri et al. (2011). To calibrate the data in the work of Simard et al. (2019), the height of the trees was measured on-site in 331 selected plots ranging from 26°S to 25°N in a 15-year period after the SRTM data was obtained, which is 2000.

Parameters collected during the study of Simard et al. (2019), are estimates for the mangrove above ground biomass, AGB, maximum canopy height, HGB, and the basal area-weighted height, HBA. Where the HBA is based on the height of individual tree heights which are weighted in proportion to their basal area. These parameters are given on a 30-meter resolution grid. The Openstreet map shoreline is used as coastline file, to determine the orientation of the local mangrove location with. This process is explained in appendix A. Due to the limited accuracy of this addition, this will only be used to collect the average of the maximum canopy basal weighted heights.

With the use of *Zonal Statistics* of *QGis 3.18*, the average of the maximum canopy basal weighted heights is determined. In figure 3.3, the average basal area weighted height of the defined mangrove locations is visualized. For 20333 (74.1%) of the transects. These parameters are not found for all locations explained further in appendix A. For the locations without mangrove heights of the nearest neighbor are used, determined with the KD-tree method.

Vegetation parameters

With the use of a literature study, the vegetation parameters for 14 trees were defined. These are listed in table A.1. The first 7 trees represent Black mangrove with their large extending root system of pneumatophores. The second 7 trees represent Red mangrove with a prop root system. The assumptions and literature sources of these parameters are explained in further detail in the methodology.

	Roots			*Stem*			*Canopy*			*Height*
	$N(r/m^2)$	$b(cm)$	$h(m)$	$N(r/m^2)$	$b(cm)$	$h(m)$	$N(r/m^2)$	$b(cm)$	$h(m)$	h_{tot}
Tree 1	1	0	0	1	0	0	30	3.5	1.37	1.37
Tree 2	45	0.5	0.15	1	7	1.75	33	3.5	3.1	5
Tree 3	82.5	0.75	0.275	1	19	3.5	36	3.5	6.25	10
Tree 4	120	1.0	0.40	1	32	5.25	40	2.7	9.35	15
Tree 5	160	2.0	0.53	1	47	7.00	43	1.9	12.5	20
Tree 6	180	3.0	0.66	1	64	10.5	46	1.6	13.3	25
Tree 7	240	4.0	0.80	1	86	14.0	50	1.3	15.2	30
Tree 1	1	0	0	1	0	0	30	3.5	1.37	1.37
Tree 2	15	1	0.15	1	5	2	33	3.5	2.9	5
Tree 3	25	1.5	0.275	1	13	4	36	3.5	5.7	10
Tree 4	35	2.0	0.40	1	20	6	40	2.9	8.6	15
Tree 5	47	2.3	0.53	1	28	8	43	2.0	11.5	20
Tree 6	58	2.6	0.66	1	38	10	46	1.5	14.3	25
Tree 7	70	3.0	0.80	1	50	12	50	1.2	17.2	30

Table A.1: *Vegetation parameters of the three different layers, namely roots, stem and canopy, of a representative Black and Red mangrove tree, selected for 7 different heights.*

B

Extreme value analysis

B.1. Stationary vs. Non-stationary

ERA5 and GTSM provide hourly estimates of the hydrodynamic statistics for the period of 32 years, from 1987-01-01 until 2018-12-31. In global assessments of mangrove environments, the extreme events are based on a stationary assumption (Menéndez et al., 2020; van Zelst et al., 2021).

The concept of stationarity and non-stationarity of extreme events is an important theoretical aspect of this study. For that reason, further insight into the impact of a stationary approach is introduced to emphasize the importance of the non-stationary analysis. This is done by analyzing the results of a stationary approach at one of the 5809 environmental locations. Figures B.1a and B.1c show the time-series of the Proxy given over the period of the past 32 years for locations 500 and 1000. Identified with the horizontal line which implies a stationary assumption, the 97.5% quantile is identified. On the vertical axis, the flood level defined by the Proxy is given for the moment in time displayed on the horizontal axis. The plot already implies that the impact of the extreme event is increasing over time. This results in a transformation of the Generalized Pareto distribution, increasing the probability of design conditions.

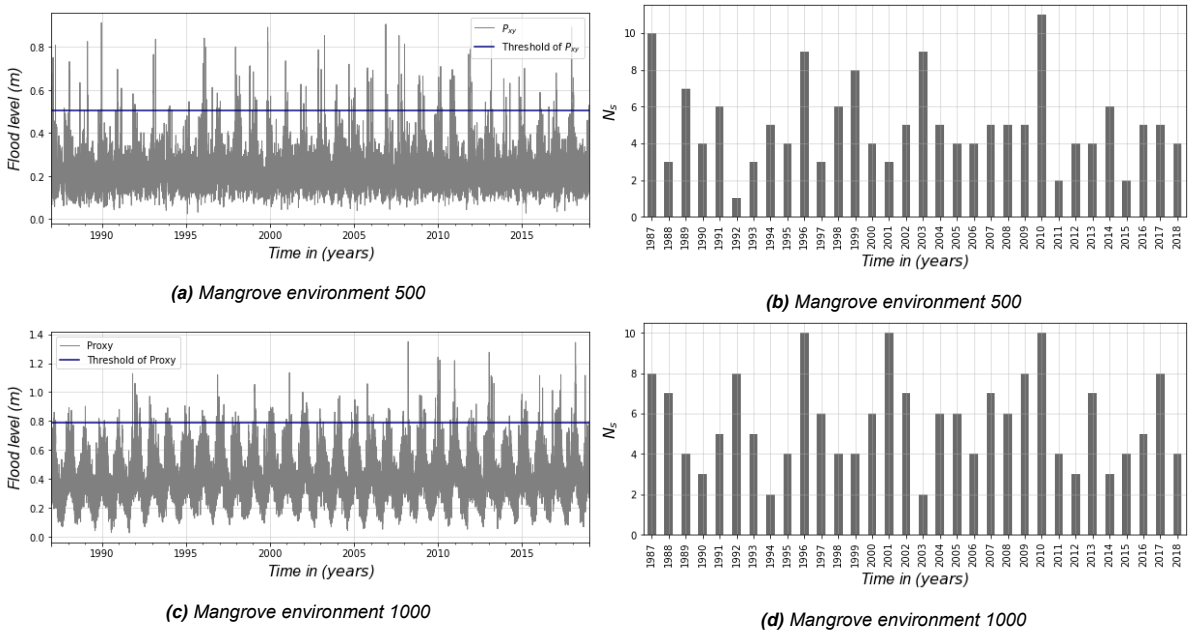

(a) *Mangrove environment 500*

(b) *Mangrove environment 500*

(c) *Mangrove environment 1000*

(d) *Mangrove environment 1000*

Figure B.1: *For two mangrove environments the analysis with a stationary assumption is visualized. The left figures show the time series of the Proxy with a 97.5% quantile as threshold, to define the extreme events with. In the right figure the N_s over the years is given for the examined time-series.*

The number of extreme events per year, N_S, for this stationary approach, are plotted in figure B.1b and B.1d. The vertical axis indicates the N_s identified and the horizontal axis the year. The distribution of N_s should follow a Poisson distribution, to make sure that the probability of occurrence of an extreme event stays stationary over time. This figure implies that this is not the case and that the probability increase over time.

When the stationary assumption would be applied to this time series the distribution of extreme events will be mainly calibrated on the last part of the time series, while these years contain more extreme events. However, this would underestimate the probability for design extreme events based on two reasons.

The first reason is that the observed non-stationarity of extreme events can be translated towards a shift in the distribution of extreme events. When the stationary assumption is applied on the Generalized Pareto distribution of the extreme events, the change of occurrence of the design event is equal over time $p_0 = p_t$. However, when the assumption is applied that the distribution is shifting over time, the conclusion can be made that $p_0 \neq p_t$ and even $p_0 < p_t$. The figures of the study of Salas and Obeysekera (2014), figure B.2a and B.2b, explain the implication of the non-stationarity of the distribution of extreme events.

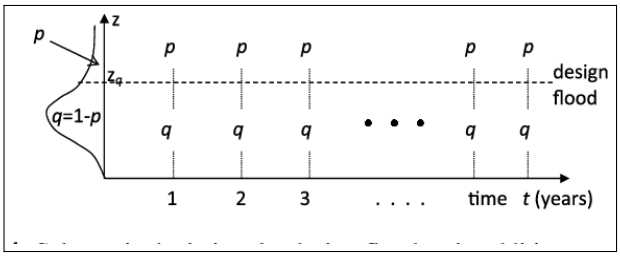

(a) *Stationary by Salas and Obeysekera (2014)*

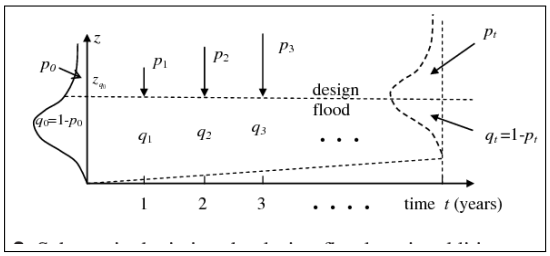

(b) *Non-stationary by Salas and Obeysekera (2014)*

Figure B.2: *Visualization of the underestimation of assuming a stationary time-series on a non-stationary extreme climate, translated towards the probability of a design flood.*

When the mean N_s is increasing over time, the probability of an extreme event above a critical level occurring, is increasing. This process is visualized in figure B.3, where the assumed Poisson distribution is transforming towards a more skewed distribution, with an increased probability of higher N_s values occurring.

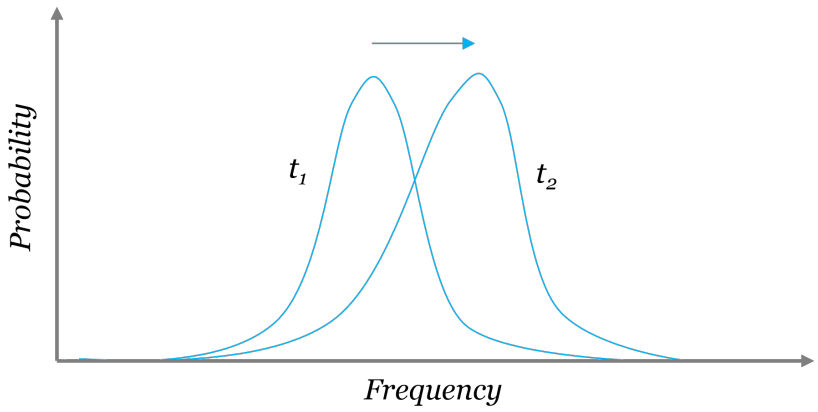

Figure B.3: *Shift in the Poisson distribution N_s over time, when the average N_s is increasing over time.*

B.2. Time window selection multivariate analysis

Resulting from the limited amount of data, the time window of 6 years would be to sensitive to outliers. This was not the case when these equations were applied on the Proxy, while the complete time series was considered in that step. For that reason, a time window of 18 years is applied for this transformation, resulting from an iterative process. This iterative process is visualized in figure B.4, where the vertical axis shows the values of the parameter H_s in the original scale for the time period of the analysis from 1987 until 2018 can be observed. The value of the parameter during a compound event is indicated with a blue dot in the figures. Based on these original values, the $T_{0y}(t)$ and $S_{0y}(t)$ is calculated resulting in the orange line and the grey area. Applying a linear assumption, a line is fitted through the time-dependent $T_{0y(t)}$ and $S_{0y}(t)$, resulting in a $Trend_{T_{0y}}$ and $Trend_{S_{0y}(t)}$ with a $T_{0y,t=0}$ and $S_{0y,t=0}$ at the first of January 1987. The different time windows are 6, 12 and 18 years, in respectively figure B.4a, B.4b and B.4c.

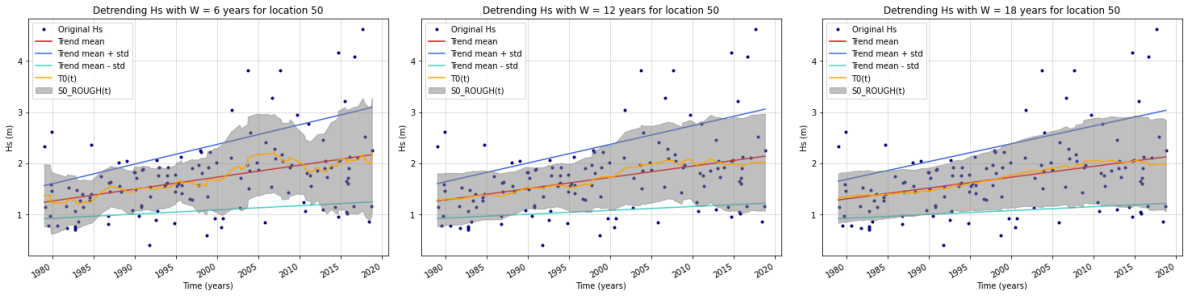

(a) *Calculation of* $S_{0y}(t)|_{\text{ROUGH}}$ ***(b)*** *Calculation of* $S_{0y}(t)|_{\text{ROUGH}}$ ***(c)*** *Calculation of* $S_{0y}(t)|_{\text{ROUGH}}$

Figure B.4: *Selecting time window for detrending univariates*

One can observe in figure B.4 that the sensitivity to outliers decreases with an increase of the time window. While a linear time-dependency of $T_{0y}(t)$ and $S_{0y}(t)$ defines the time-series of the stationary univariate and the distribution fitted on these, this sensitivity should be prevented. For that reason, a time window of 18 years is applied in the analysis.

B.3. Tropical cyclones

The implementation of the wind direction does not solve the complexity of the wind patterns in tropical cyclones. To elaborate further on this point, the results of neglecting the direction of the wind are discussed for location 750. Location 750 is located at the Southern edge of Cuba, a region known to be annually exposed to hurricanes. In figure B.5 the data extraction points of location 750 are plotted. The GTSM model of Muis et al. (2016) was used for the time-series of S for the model and the ERA5 model ECMWF (2021) the time-series of H_s and T_m.

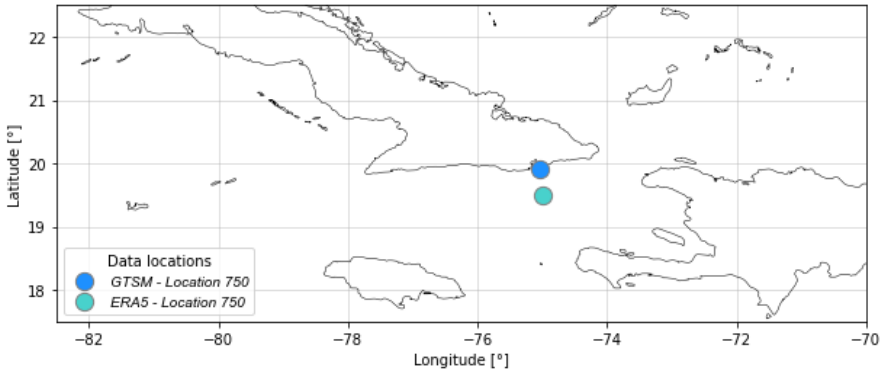

Figure B.5: *Data extraction point to construct the hydrodynamic climate of location 750 at the Southern coastline of Cuba*

At this location 186 extreme events are identified based on the proxy of Stockdon et al. (2006), resulting in an average N_s of 5.2 extreme events per year. With the use of the methodology explained, this will result in a total of 186 observed combinations over the past 32 years for the parameters H_s, T_m, and S. The parameters found at these locations are visualized in figure B.6.

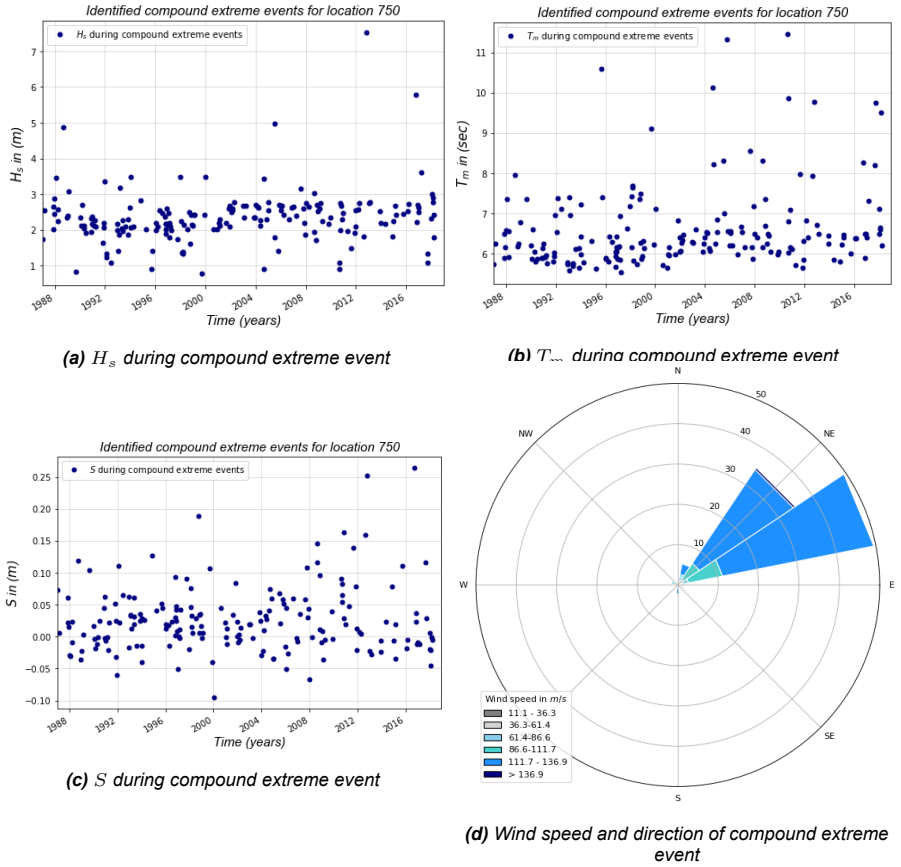

(a) H_s *during compound extreme event*

(b) T_m *during compound extreme event*

(c) S *during compound extreme event*

(d) *Wind speed and direction of compound extreme event*

Figure B.6: *Information of the identified compound extreme events for location 750 at the southern coastline of Cuba.*

Figure B.6a, B.6b and B.6c display respectively the observed H_s, T_m and S during the compound extreme events identified for the environmental location. Figure B.6d visualizes the corresponding wave directions identified after the extreme value analysis is performed. The color indicates the wind speed observed in m/s and the size of the slice indicates the number of observations, ranging from 0 till 49, for every direction. The wind rose indicates from which direction the wind came, thus a wind from the Northeast is blowing towards the Southwest. The wind rose shows a mainly directed wind during the extreme compound event from the North-Northeast till East-Northeast.

The most extreme wave observed at the ERA5 location was on the 24Th of October 2012, with a H_s of 7.53 meter and a S of only 0.25 meter. The wind at this moment was from the North-Northeast. With the use of the historical hurricane path data of National Oceanic and Atmospheric Administration (2019), a hurricane attacking the coastline of Cuba was identified, called Sandy. The track of the hurricane is plotted in figure B.7, which is moving from the south towards the coastline of Cuba. Therefore it may be expected that waves generated by this storm will attack the coastline. This small insight in a specific location indicates that further analysis has to be performed in a successive study to make sure that only the onshore-directed events are taken into account.

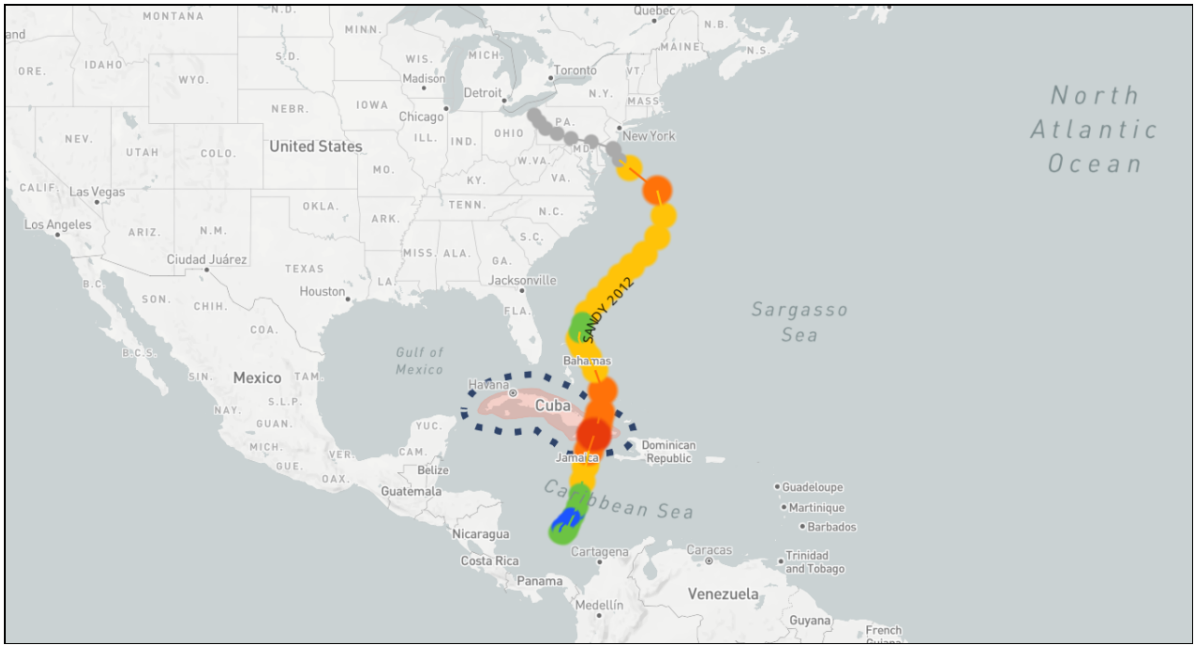

Figure B.7: *Historical hurricane track of hurricane Sandy starting at 21st of October until the 31st of October 2012 (National Oceanic and Atmospheric Administration, 2019)*

B.4. Interim results

Statistical test

At 56.9 % of the 5809 environmental locations, the desired Generalized Pareto distribution for the multi-variable Proxy was met within the requirements set. at the other 43.1 % the statistical test was not met within the limits of N_s. The spatial distribution of the performances of the statistical test is visualized in figure B.8, where a blue location identifies an environmental location where the statistical test was met. At the locations with a yellow point, the statistical test was not met and the N_s requirement was limited. The large number of locations where the statistical test was not met could be explained for three reasons, the first one is that the requirements for the classification of an extreme event in this study are two strict and a large number of extreme events is not meeting the requirements. Another reasoning is based on figure B.8, areas are known for large extreme due to the tropical cyclones are showing a better performance than more moderate climates. This could mean that the global analysis should be performed with a definition and N_s for the extreme environment, meeting the local climate. The third reasoning could be that N_s is to strictly and that the lower limit of 2.5 is not applicable for less extreme climates. Figure B.9 shows the distribution of N_s of the in total 5809 mangrove environments. The approach with choosing the largest quantile, while still meeting the requirement of the minimal number of storms per year, explains the distribution shown in figure B.10. Most locations can be found just above the N_s value of 2.5.

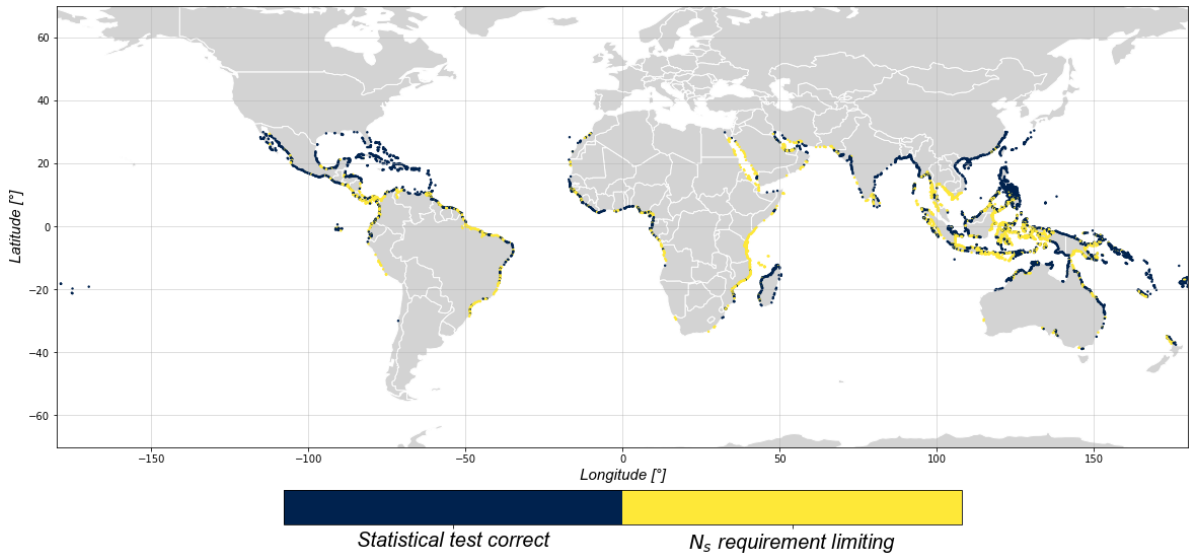

Figure B.8: *Spatial distribution of the performances of the statistical test with the stated requirements for the classification of an extreme event.*

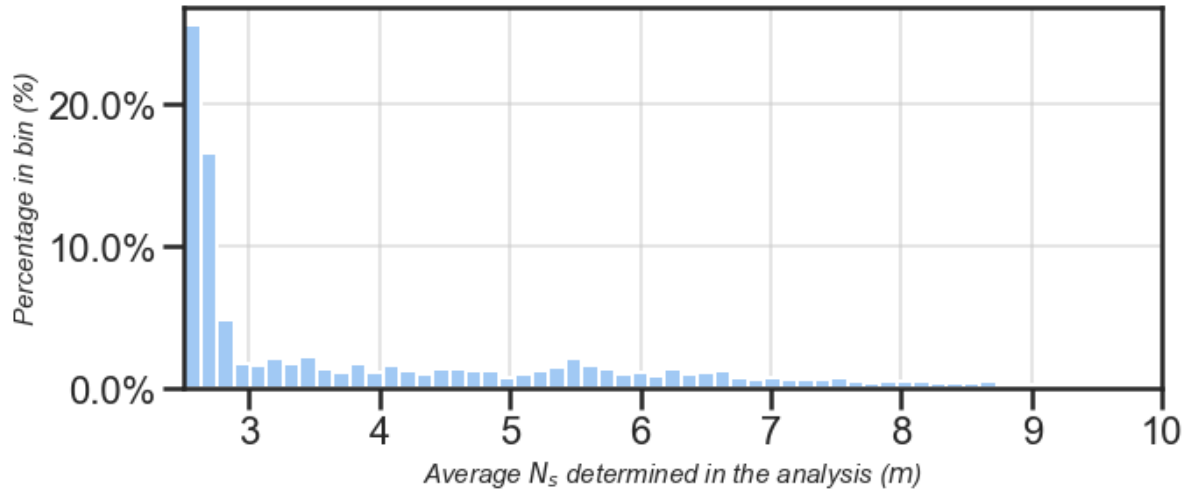

Figure B.9: *Disbribution of the found N_s of the different environments*

The maximum quantile of the data set used as threshold was 0.992, which is below the maximum quantile of 0.999 until which the algorithm was allowed to search. The distribution of the used quantiles for the extreme value analysis is shown in figure B.11, where the density in the upper tail can be explained with the approach of the minimal extreme events. The fact that the maximum quantile is not reached could indicate that the minimal duration of the extreme events is to large for this specific multivariate extreme event.

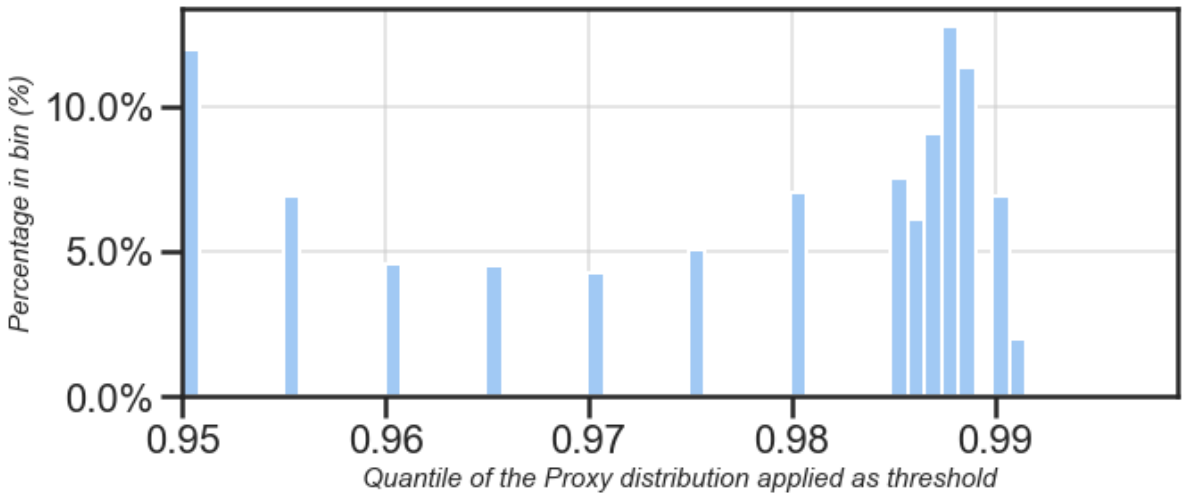

Figure B.10: *Disbribution of the found q_t of the different environments*

The spatial distribution of the quantile selected for the multivariate extreme value analysis is visualized in figure B.11. The color indicates which quantile is selected indicated in the color bar beneath. The yellow colors indicate the locations where the a higher quantile was needed to meet the requirements. The dark color indicate the opposite and a lower quantile of the data was sufficient.

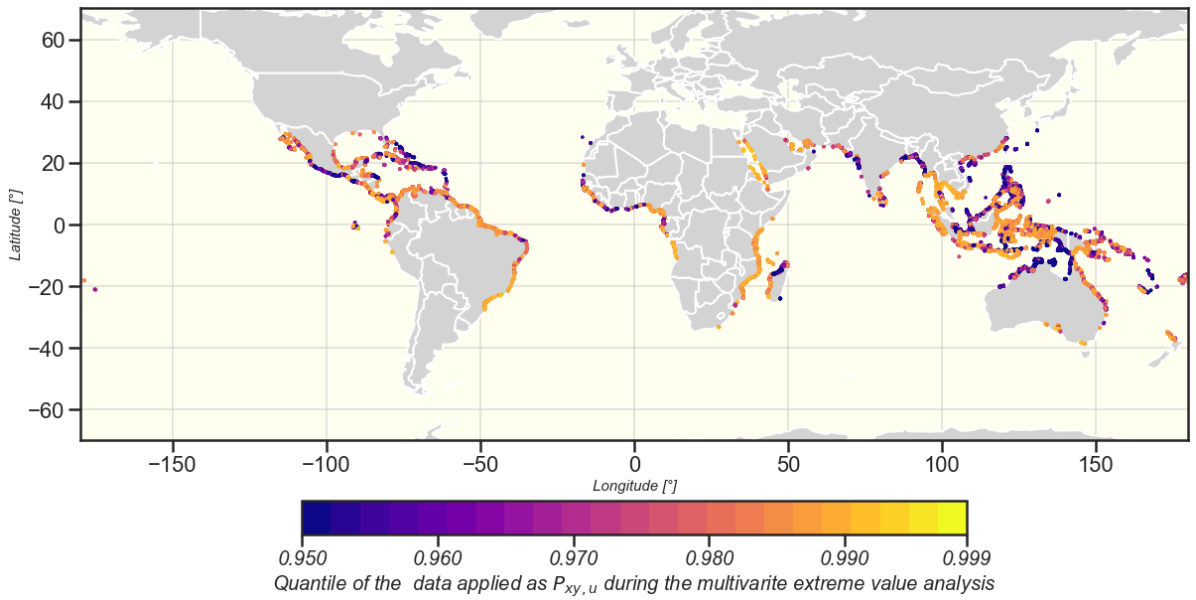

Figure B.11: *Quantile used for extreme value analysis*

Performed non-stationary extreme value analysis

This process of the multivariate extreme value analysis is visualized with the use of four of the mangrove environments in Central America. These environments are located at the coastlines of Mexico, Honduras, Cuba, and Suriname, visualized in figure B.12. The process of identifying the multivariate extreme events with the time-dependent threshold $p_{xy,u}$, is visualized for the four locations in figure B.13. The time-dependent threshold makes

sure that the extremes of the whole data series are used to calculate a time-dependent Generalized Pareto distribution. To indicate the non-stationarity of these extreme events, the mean of μ and σ are determined per location, and while the shape parameter ϵ is constant, this can be stored directly. The calculation of the trend of μ, called T_μ is defined based on a linear assumption, resulting in the black line in figure B.13.

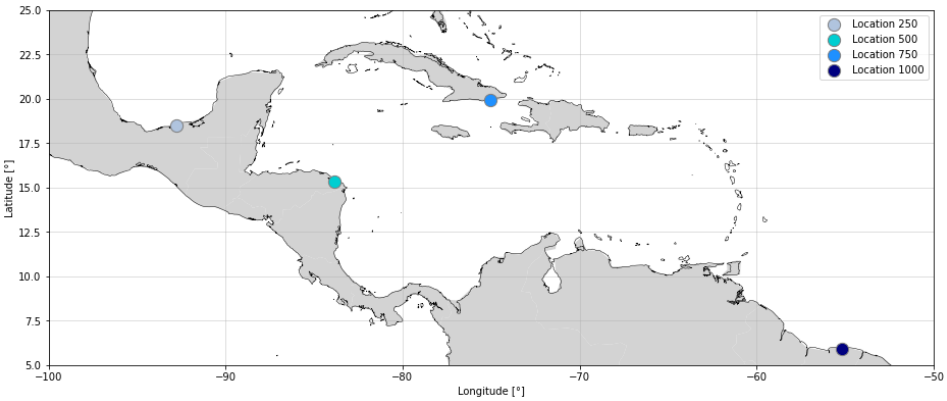

Figure B.12: *The locations of the four environments to visualize the non-stationary extreme value analysis on the Proxy in detail*

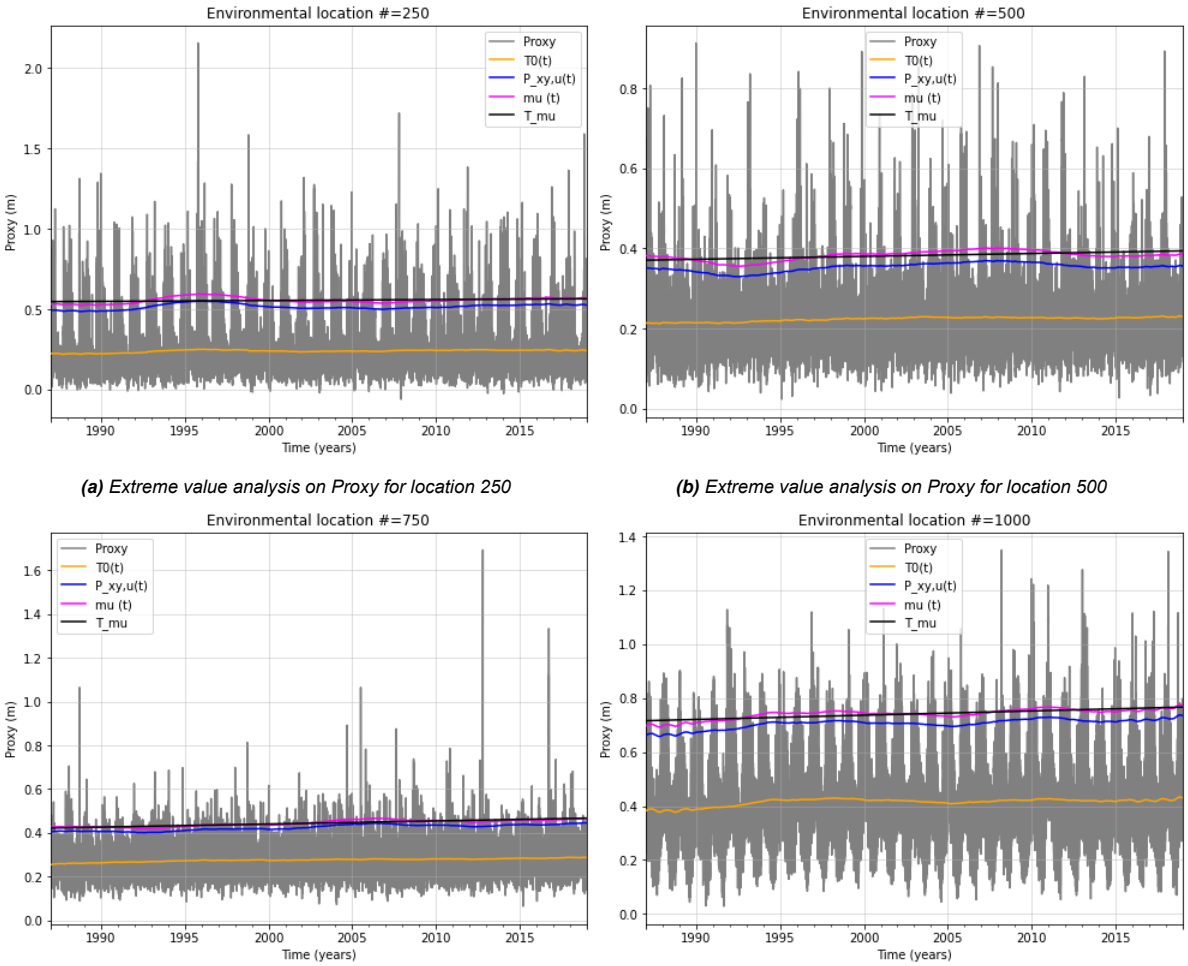

(a) *Extreme value analysis on Proxy for location 250*

(b) *Extreme value analysis on Proxy for location 500*

(c) *Extreme value analysis on Proxy for location 750*

(d) *Extreme value analysis on Proxy for location 1000*

Figure B.13: *Visualization of the applied methodology for the non-stationary POT on the Proxy.*

Observed extreme parameter values

The figures show the spatial distribution of the maximum value of the different parameters leading towards the multivariate extreme event are displayed. Figures B.14, B.15 and B.16 show respectively the distribution of the maximum H_s, T_m and S observed during an multivariate extreme event.

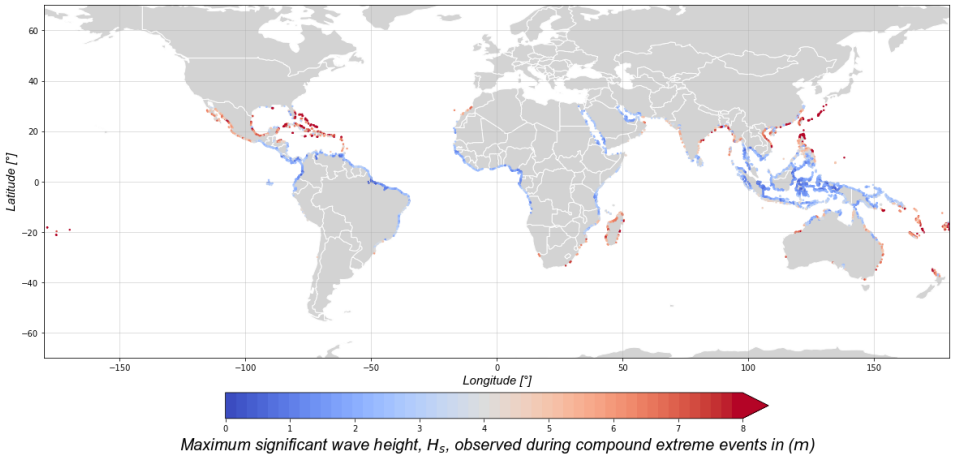

Figure B.14: *Maximum significant wave height during multivariate extreme event in the past 32 years*

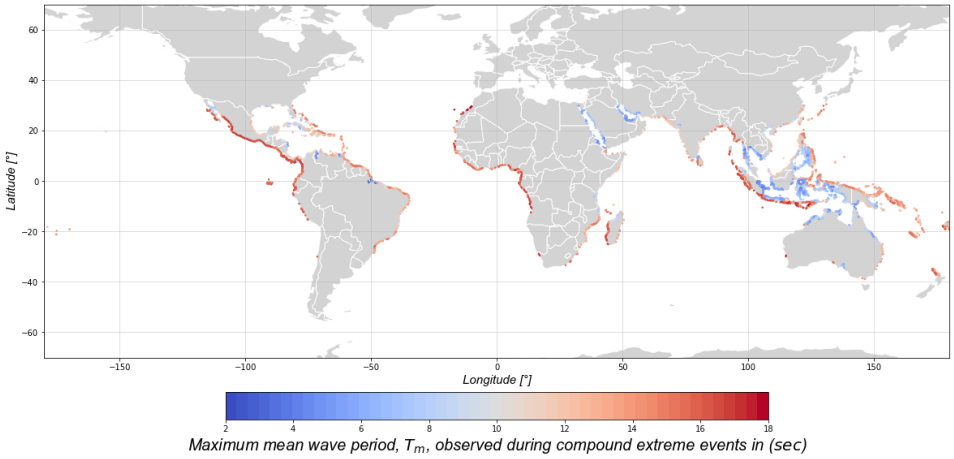

Figure B.15: *Maximum mean wave period during multivariate extreme event in the past 32 years*

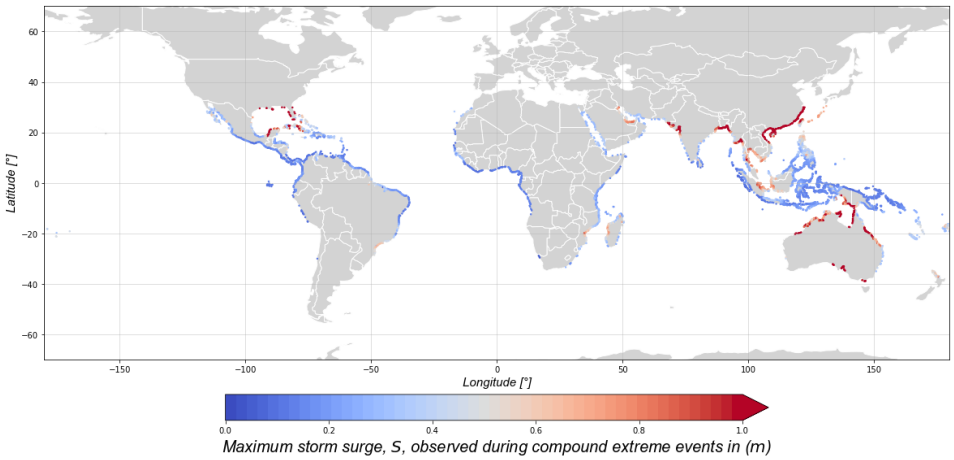

Figure B.16: *Maximum storm surge during multivariate extreme event in the past 32 years*

Trends in the 3-dimensions of the multivariate event

During the non-stationary multivariate extreme value analysis the conclusion could be made that the univariates during the non-stationary extreme events are not stationary. The average increase of the extreme events, defined with $T_{T_{0_{y,t}}}$ is for the three parameters 0.06 m, 0.16 s and 0.7 cm for respectively the H_s, T_m and S during these multivariate extreme events.

The spatial distribution of these trends are visualized in figures B.17, B.18 and B.19. Where the colorbar indicates if the observed trend is positive or negative. Red implies a positive trend of the mean of specific parameter during the multivariate extreme events and blue indicates a decrease.

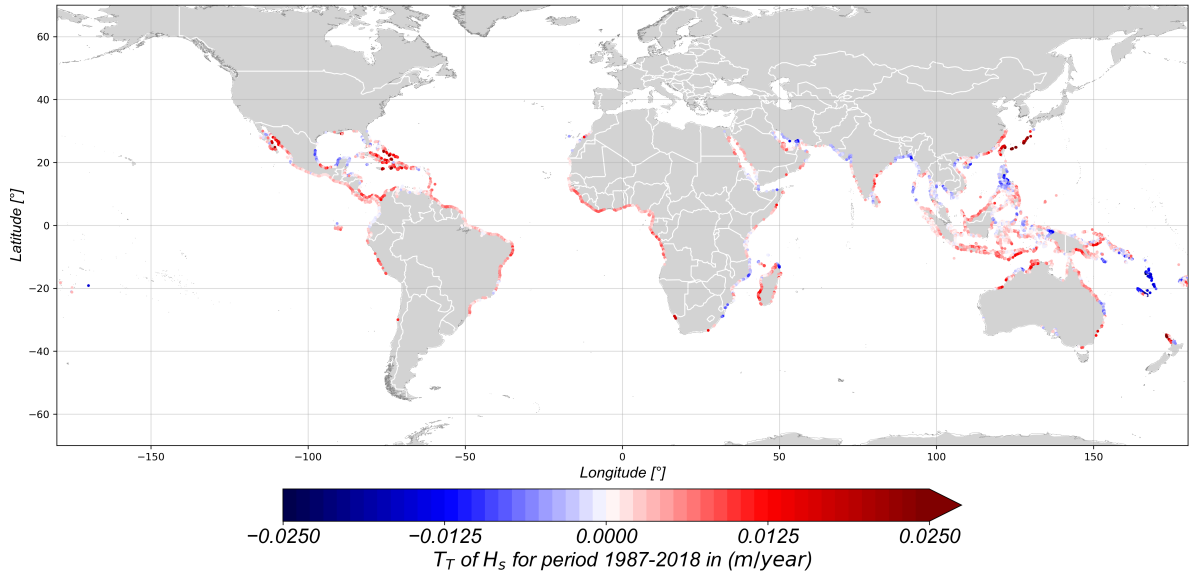

Figure B.17: *Spatial distribution of the average H_s during the specified extreme event in the period 1987 till 2018. Red indicates an increase in the specific environment and blue indicates a decrease.*

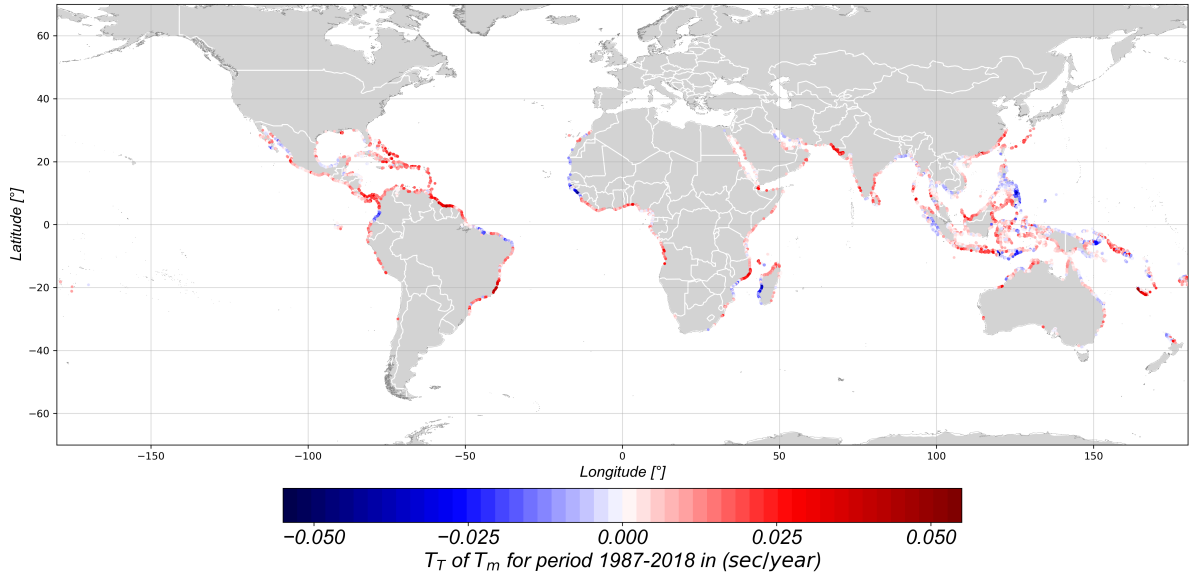

Figure B.18: *Spatial distribution of the average T_m during the specified extreme event in the period 1987 till 2018. Red indicates an increase in the specific environment and blue indicates a decrease.*

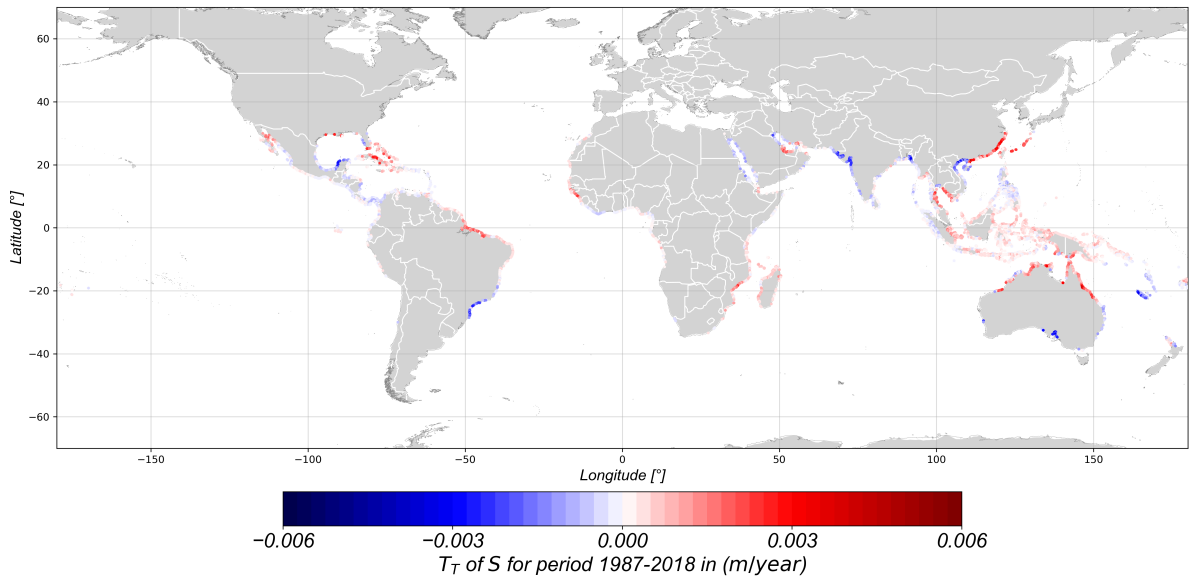

Figure B.19: *Spatial distribution of the average S during the specified extreme event in the period 1987 till 2018. Red indicates an increase in the specific environment and blue indicates a decrease.*

C

Statistical upscalling

C.1. Fitting stationary univariates

To represent the region of interest of the different univariates, the choice was made to find a statistical distribution that is close towards the empirical distribution. With the use of 12 locations selected with a step size of 500 within the 5809 environmental locations, the goodness of fit is examined. The environmental locations selected are visualized in figure C.1. Location 3500 is located at almost the same location as 4000, due to this, the location is not visible in the figure.

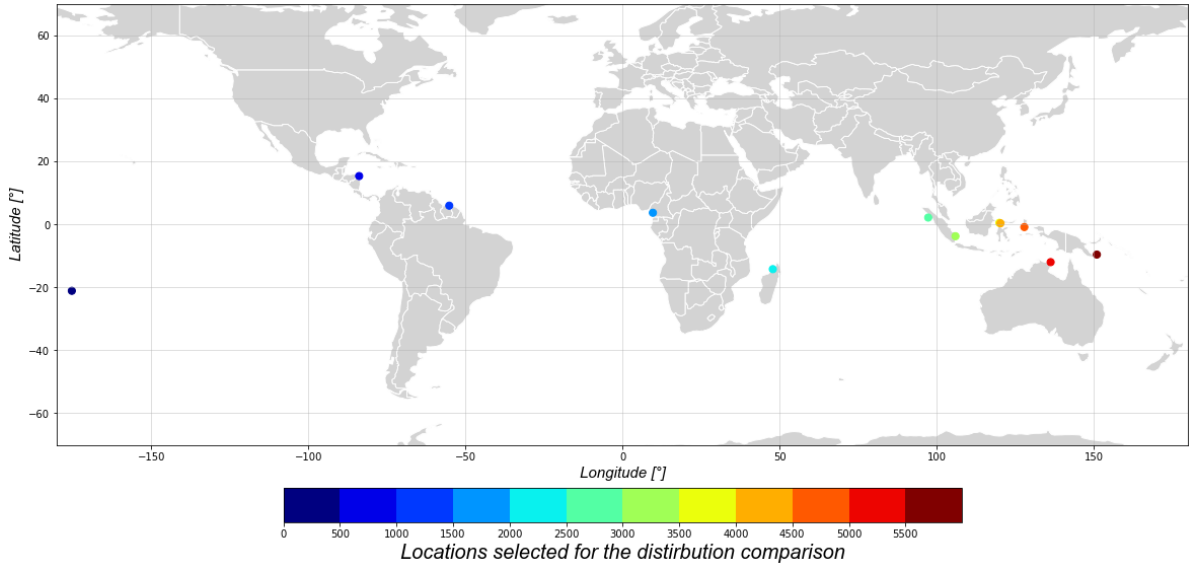

Figure C.1: *The spatial distribution of the 12 selected locations to test the different fittings for the stationary H_s^*, T_m^* and S^**

After a first selection, four different statistical distributions are selected to test the fitting for. These distributions are listed below:

- A Log-Normal distribution
- An Exponentially modified Normal distribution
- A Weibull distribution
- A Generalized Pareto distribution

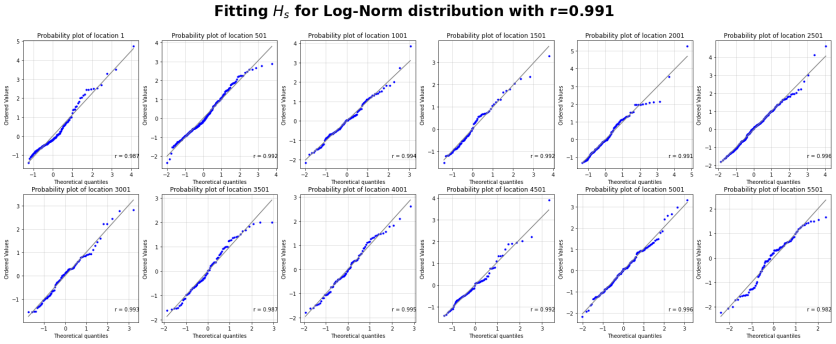

(a) *Log-Normal distribution*

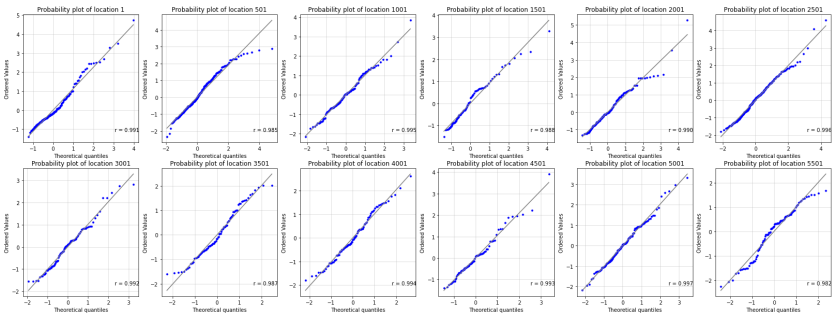

(b) *Exponentially modified Normal distribution*

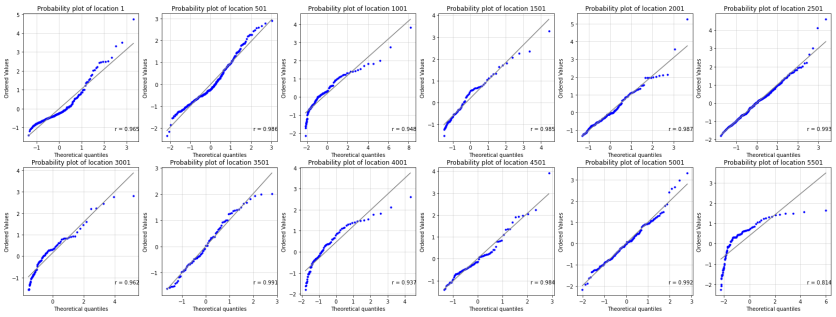

(c) *Weibull distribution*

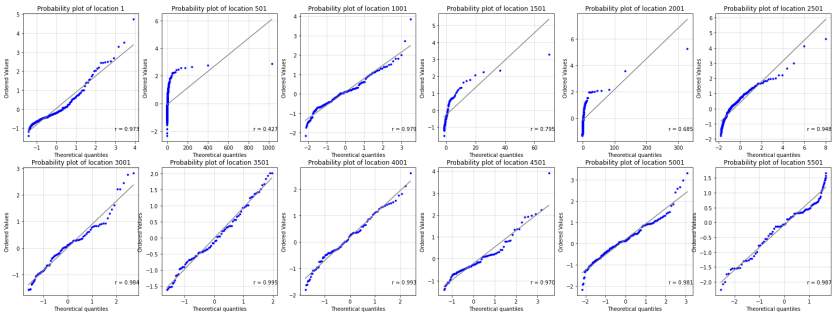

(d) *Generalized Pareto distribution*

Figure C.2: *Tested distributions for H_s^* visualized in QQ-plots*

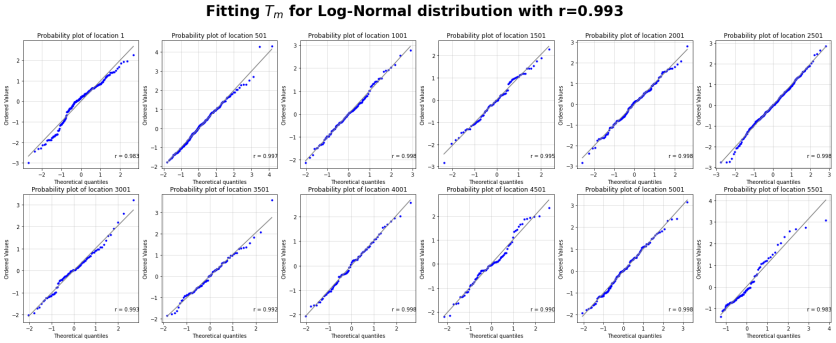

(a) *Log-Normal distribution*

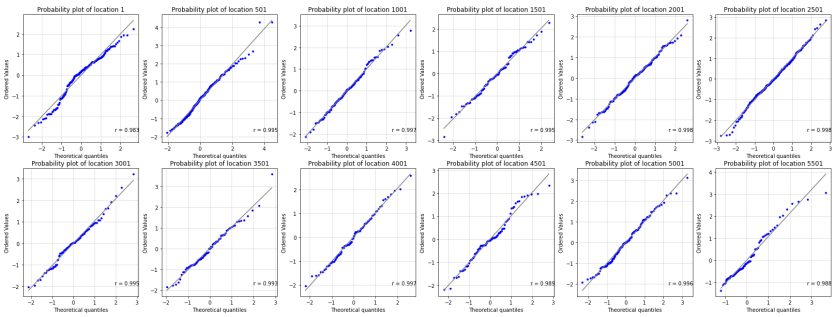

(b) *Exponentially modified Normal distribution*

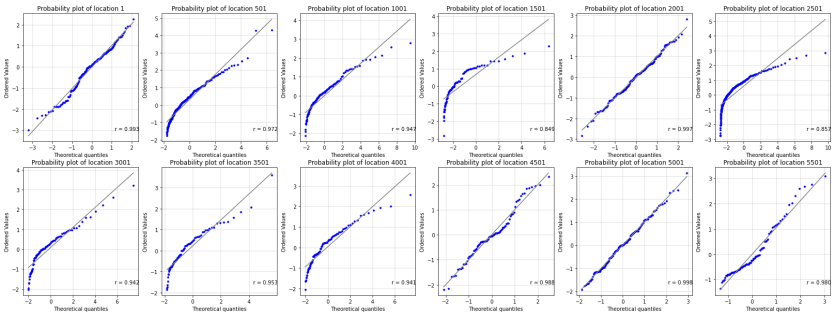

(c) *Weibull distribution*

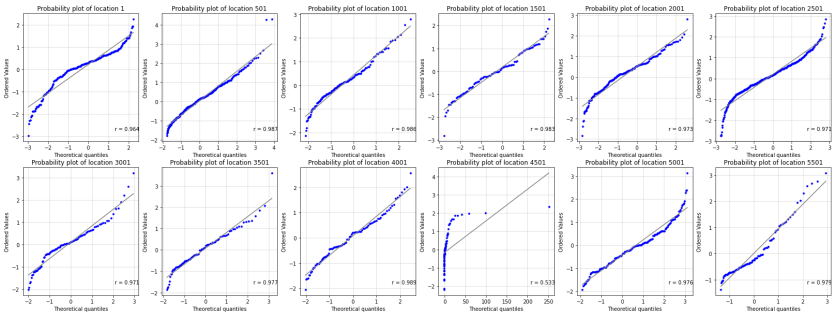

(d) *Generalized Pareto distribution*

Figure C.3: *Tested distributions for T_m^* visualized in QQ-plots*

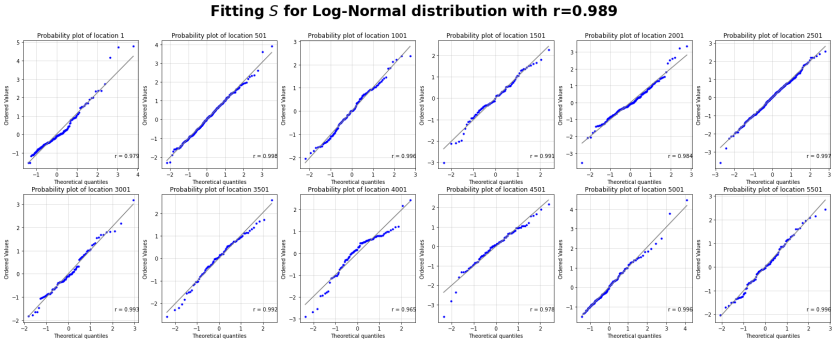

(a) *Log-Normal distribution*

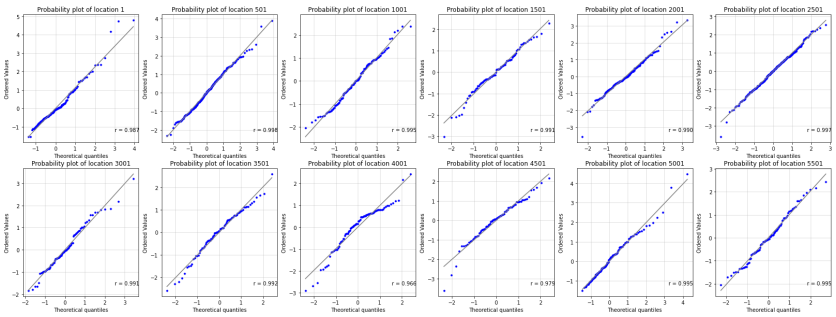

(b) *Exponentially modified Normal distribution*

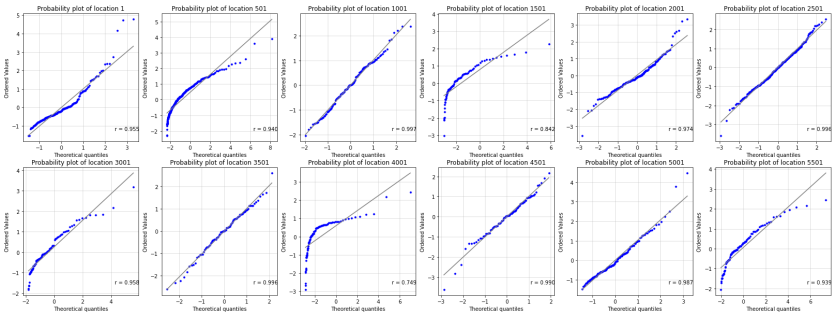

(c) *Weibull distribution*

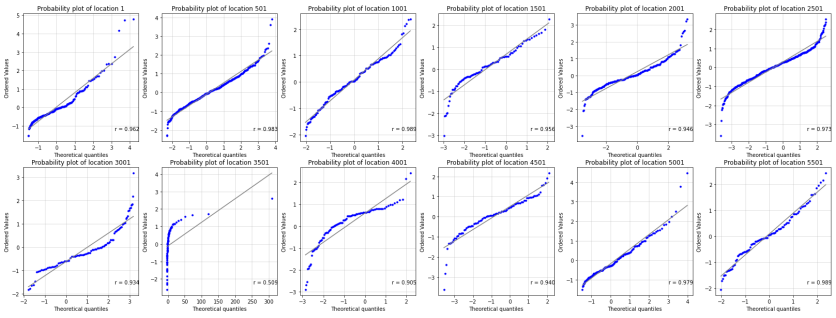

(d) *Generalized Pareto distribution*

Figure C.4: *Tested distributions for S^* visualized in QQ-plots*

C.2. Representative mangrove locations

For the visualization of the statistically upscalling method applied to the 6-dimensional data set, figure C.5 is produced. The steps and locations of the Maximum dissimilarity points and cluster centroids are visualized with respectively grey and magenta. The original data set is identified with light grey. The six parameters are respectively from left to right, $widht_{ns}$, $width_{fs}$, h_{fs}, $z_{0,veg}$, h_{veg} and HAT.

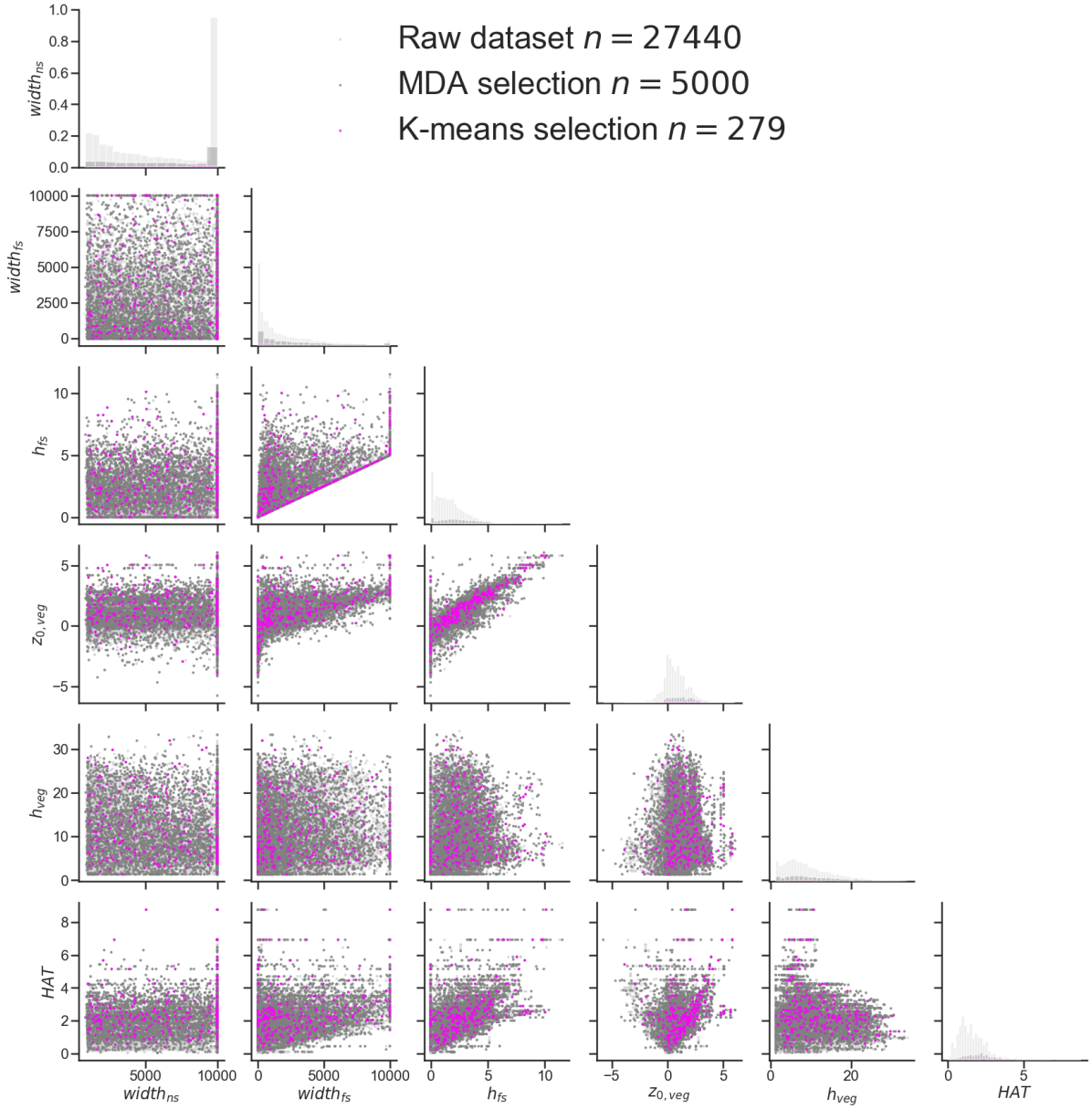

Figure C.5: *Visualization of the statistically upscaling steps applied to the 6-dimensional mangrove locations data set*

C.3. Distribution over the representative mangrove environments

Figure C.6 displays the number of environmental locations assigned to a particular cluster. The different colors indicate the clusters, related to the colors of figure 4.11. The number of environmental locations assigned to a cluster range between 8 and 500, which are respectively cluster 43 and 47. When the maximum dissimilarity function was not applied, the minimum of the k-means algorithm would be optimized more towards cluster 47. This would decrease the level of representation of the environmental locations of cluster 1.

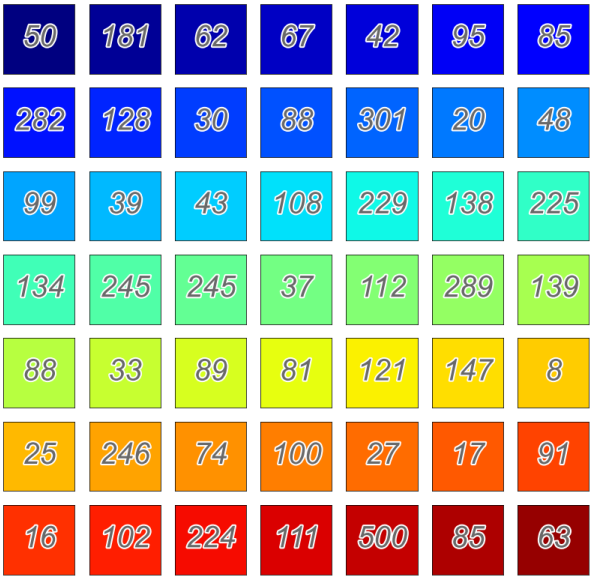

Figure C.6: *Number of the 5809 environmental locations designated to particular cluster for the 31-dimensional non-stationary mangrove climates.*

These different environmental clusters were used to calculate the 1/40 year design condition based on the sampled multivariate extreme events. For the global assessment, these design conditions for the years 1987 and 2018 are subject to the different mangrove locations. The distribution of the original 27440 location over the 49 representative mangrove environments is shown in figure C.7. The first row indicates respectively as in figure C.6 the representative mangrove environment 1 until 7. This procedure continues till the last row where the representative mangrove environments 43 to 49 are visualized. The number in the boxes of the different representative mangrove environments indicate the number of locations of the original 27440 location belonging to the specific representative mangrove environment.

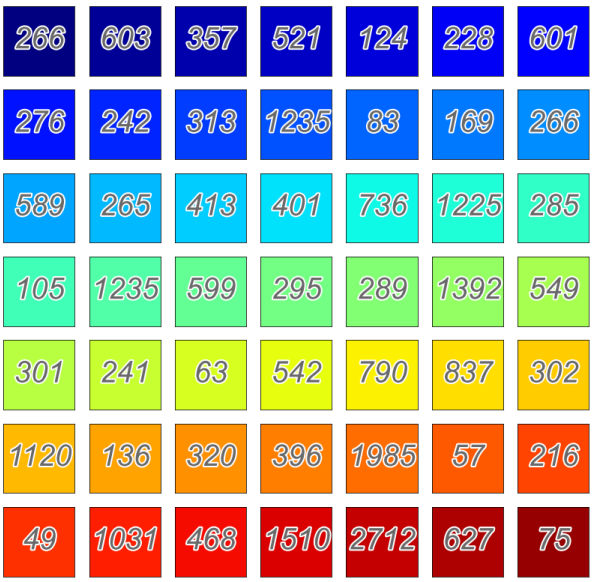

Figure C.7: *Number of the 27440 mangrove locations designated to the 49 different representative mangrove environments.*

In figure C.8 the distribution of the possible combinations is sorted per cluster. The different representative mangrove environments are indicated in the same order as the previous figures. The reduction in computational demand becomes clear by comparing figure C.7 with C.8. Where for example cluster 47 first demanded 2712 SWASH computations for every design condition, it only needs 215 SWASH computations when the representative mangrove locations are introduced.

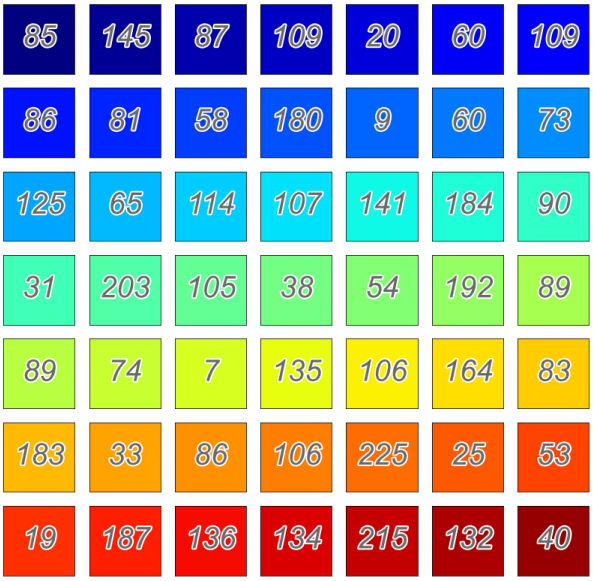

Figure C.8: *Number of the 289 representative mangrove locations designated to the 49 different representative mangrove environments.*

D

Hydrodynamic model

D.1. Evanescent modes

With the use of test runs on a test domain the reduction in the significant wave height H_s was identified. The domain on which the test runs were applied is shown in figure D.1. The red lines in the figure indicate the measuring location of the domain where the output is generated. For a set of input conditions the output at 25 meter is collected and processed to indicate the drop in significant wave height by SWASH. These runs were in contrast to the other runs performed with a computational space-discretization of 5 meter instead of 1 meter, to reduce the computational demand.

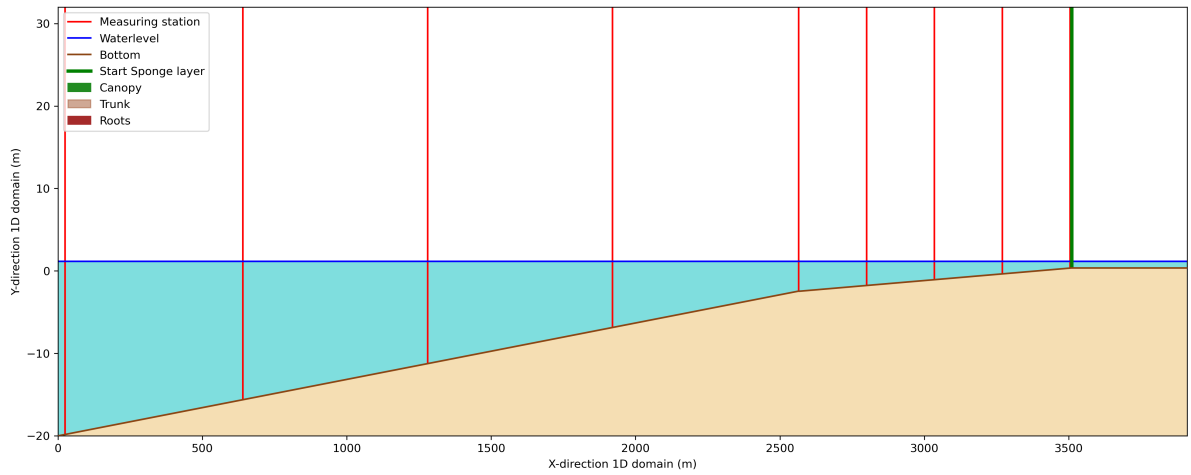

Figure D.1: *Measuring locations*

The significant wave height calculated with the time-series of the waterlevel at x=25 meter. Figure D.2 shows the under estimation in terms of H_S for the different test runs. The left plot within the figure shows the significant wave height against the mean wave period. The right figure shows the significant wave height against the storm surge. The color of the points within these scatter plots indicates the drop in wave height observed after 5 grid cells, equal to 25 meter. These decreases were up to almost 10% of the input. Resulting that when this would be ignored, the computations were simulated with less extreme events than the extreme value analysis indicated.

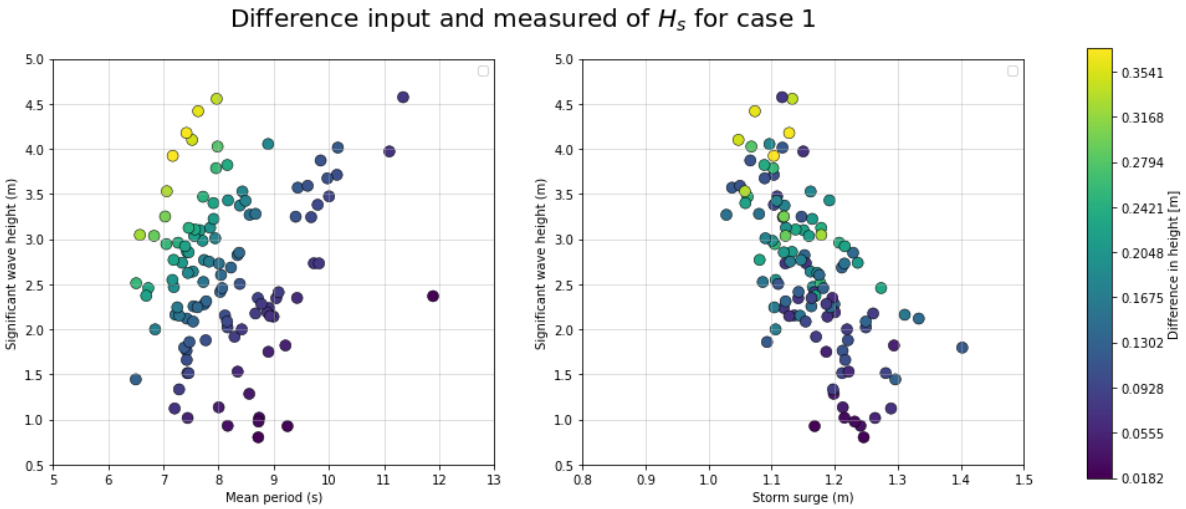

Figure D.2: *In the left panel the H_s is visualized against the T_m. The right panel the H_s is plotted against the T_m. The colorbar indicates the underestimation of the H_s in meter.*

The assumption that this drop is larger for waves with a larger wave steepness was introduced based on the results of figure D.2. By calculating the wave steepness of the different waves using equation 3.16, the relation between the drop in wave height and the steepness is indicated to validate this assumption. With a Spearman's rank correlation for the test case above 0.95, meaning a strong correlation between the wave steepness and the drop in significant wave height, this assumption is determined as useful. Therefore a linear relation between the wave steepness and the significant wave height was assumed to result in the method of figure D.3. In this figure the observed drops in wave height are plotted at the locations of the significant wave height and mean wave period that were the initial input. The isolines in the figure indicate the drop in wave height based on the wave steepness and a linear relation between the wave steepness and the drop. The results are indicating an approach to prevent the iterative process.

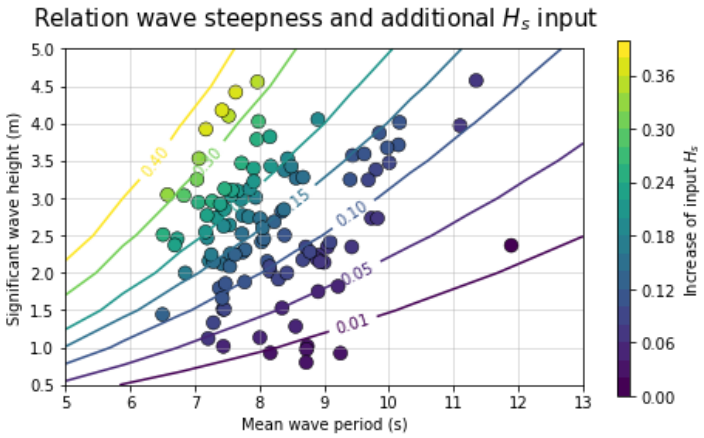

Figure D.3: *Observed drop in significant wave height and the applied relation between the wave steepness and the increase of the significant wave height at the boundary of the domain.*

Eventually the input of the test runs of figure D.2 are corrected for the wave height drop with the use of the found relation of figure D.5, resulting in a maximum drop of only 7 centimeters in stead of the initial 36 centimeters. This due to the fact that the second run is also containing evanescent modes. This approach will be applied on all input combinations.

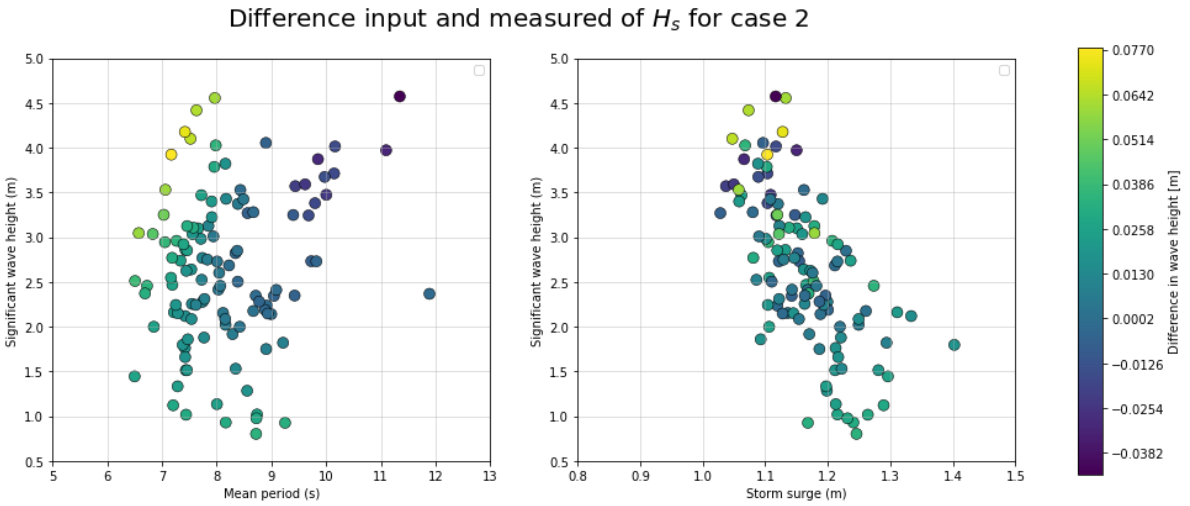

Figure D.4: *figures/08.Hydrodynamic*$_Model/Input/Dif.png$

Figure D.5: *In the left panel the H_s is visualized against the T_m. The right panel the H_s is plotted against the T_m. The color bar indicates the underestimation of the H_s in meter.*

This calibration has been performed in a computational domain with a space-discretization step of 5 meter, in the eventual runs a space-discretization of 1 meter is applied. A smaller step in space, results in a smaller wave dissipation in the numerical model. For that reason, another validation step is performed to check if the found relation still holds described in the chapter itself.

D.2. Coastal safety of the magnrove tree

With the 7 representative trees for Black and Red mangroves the functionality of the mangrove tree as a coastal protection element is investigated. In figure D.6, the results of the SWASH computations for 42 runs are visualized. For every tree height and tree type, three runs with different water levels are performed. These different water levels are listed on the vertical axis of the figure. On the horizontal axis, the required width of vegetation needed is plotted to meet the safety requirement. The safety requirement is that the dike may only be heightened 2 meters above the water level to make sure that no run-up will overtop the dike. The bathymetry used in this analysis has a nearshore width of 1960 meters and a foreshore width of 590 meters, with the nearshore starting at a depth of -20 meters and the eventual horizontal plane at 0.18 meter. The water levels on the lower axis are relative to the horizontal plane of the vegetation. At all the runs a storm event with a significant wave height, H_s, of 4 meters and a mean wave period , T_m, of 10 seconds is applied.

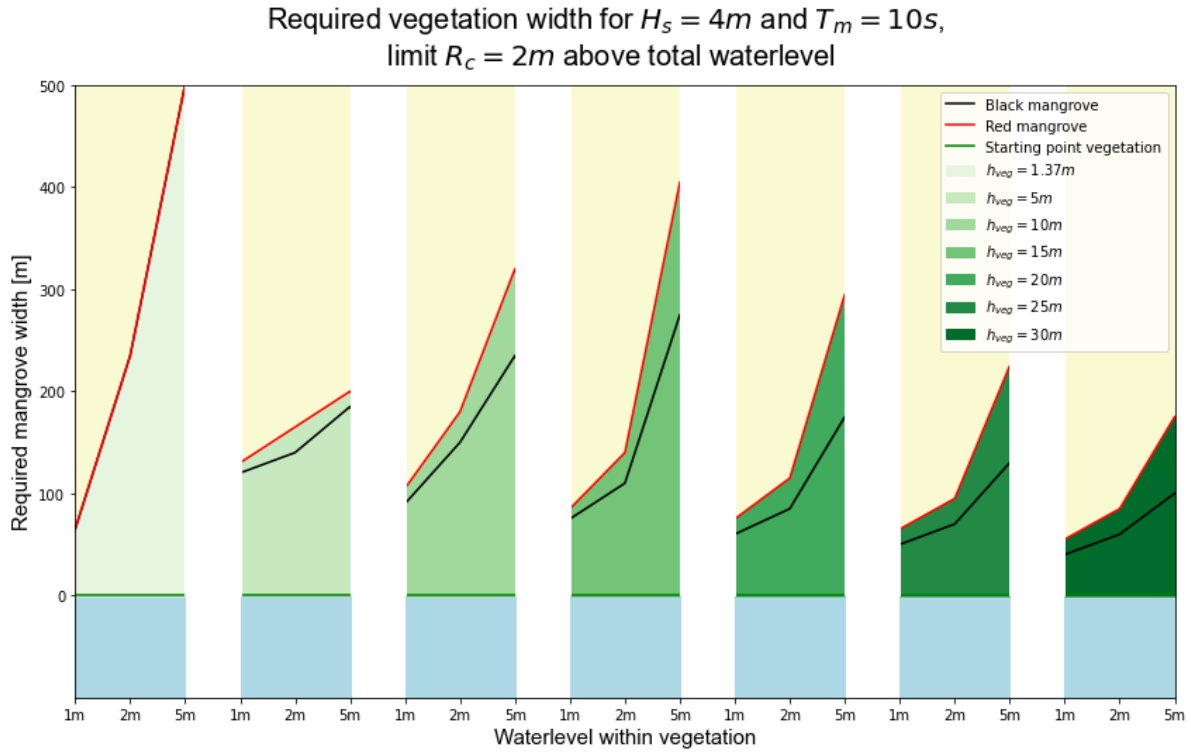

Figure D.6: *Comparison in coastal protection between Black and Red mangrove type of trees expressed in required mangrove width for different water levels within the vegetation.*

One can analyze several processes from these results. The first one to mention is the influence of the water level, higher water levels result in all the seven trees an increase in vegetation width needed to attenuate the required amount of wave energy. While higher water levels mean that more wave energy will reach the vegetation and thus more vegetation is needed to attenuate wave energy. This reduction in reduced energy dissipation on the nearshore and foreshore, due to an increase in water level can be concluded for all the trees of this analysis.

The in-homogeneity between the wave attenuation capacity of the different trees can be explained with several steps. The first tree of the analysis, with a height of 1.37 m is representing a pioneering species, following van Zelst et al. (2021), only be created from one layer. The other six trees are represented by three layers, one for the roots, another for the stems, and the last layer for the canopy of the tree. The assumption made by defining the parameters of these trees is that the biomass of the different layers is increasing when the height of the tree is increasing.

The increase in biomass following the increase in height of the tree, explains the decrease of vegetation width needed for the 1 and 2 m water level in the mangrove forest. Modeled with an increase in the parameters $N_{v,i}$, $b_{v,i}$ and $h_{v,i}$, the wave attenuation capacity of the different layers is increasing, as a result of a more dense root system and thicker stems. One can observe this process by the decreasing vegetation width needed between trees two and seven.

However, with an increase in the height of the tree, h_{veg}, the height of the stems is increasing. This means that the canopy is growing out of the water level and that waves are attacking more and more the rather open region around the stems as visualized in figure 2.3 (Spalding et al., 2014). This layer with a sparse density is less effective in attenuating the waves, explaining the increase in vegetation width needed for the 5-meter water level between the first and the third tree. From the fourth tree on, the needed vegetation width is decreasing again, due to the fact that the canopy has completely grown out of the water and the increase in biomass is taking over the efficiency of wave attenuation. The increase in vegetation width needed for the 1 and 2meter water level runs between trees 1 and 2 follows this explanation.

D.3. Identifying most extreme event

To make the study feasible within the time frame of this master thesis a simplification based on the coastal safety assessment is applied to select the most extreme events. By implementing three different transects and subject the same set of test runs the difference between the transects is observed. In figure D.7 three different transects are visualized, differing in width and slope. In the three figures on the right the required crest height of the dike is plotted for different combinations of an extreme event. Due to the same spatial distribution of the required crest height of the dikes, the conclusion is made that one transect can be used to select the most extreme event. It is furthermore observed that the most extreme events are in the region with the largest wave height and wave period.

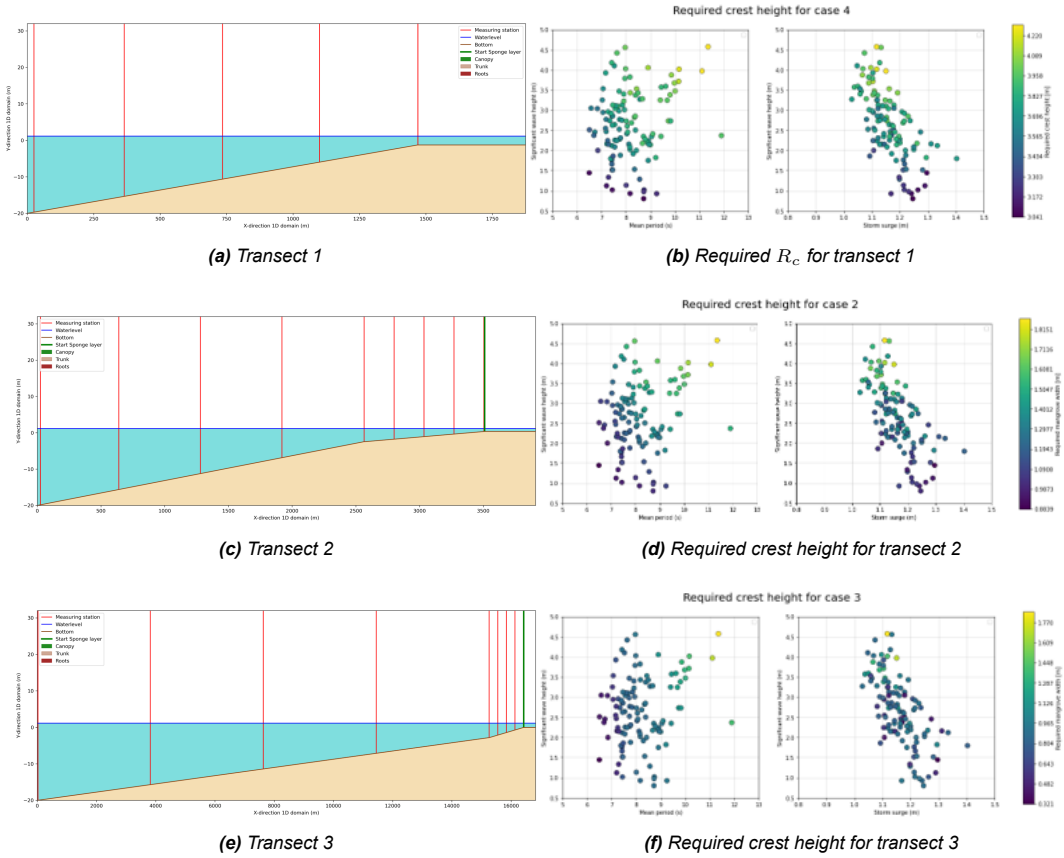

(a) *Transect 1*

(b) *Required R_c for transect 1*

(c) *Transect 2*

(d) *Required crest height for transect 2*

(e) *Transect 3*

(f) *Required crest height for transect 3*

Figure D.7: *Influence of bathymetry on the selection of the defining the design condition.*

D.4. Identifying required mangrove width

Figure D.8a and D.8b show two test cases which are used to visualize the optimization process applied at the different SWASH runs. In the first figure a numerical domain without vegetation has been introduced. The second figure is the same numerical domain with the addition of a vegetation grid. The length of the vegetation plane is extended to 2000 meter in the test case to give a further insight in the way the results are found in this analysis.

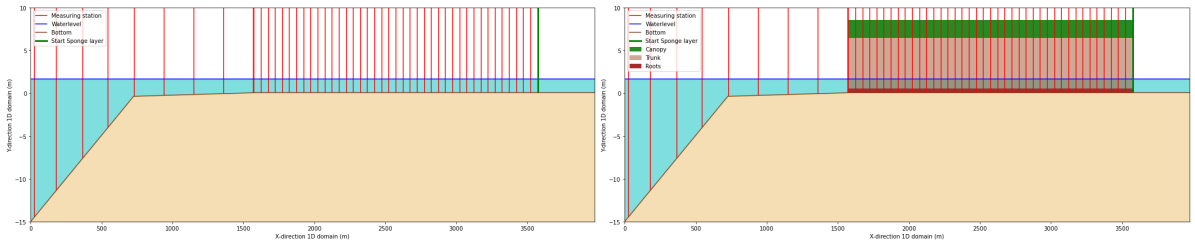

(a) *Numerical domain without vegetation* ***(b)*** *Numerical domain with vegetation*

Figure D.8: *Computational domains used to visualize the optimization problem for defining the impact on the coastal protection offered by mangroves.*

The results of the two SWASH runs, is translated in the coastal safety assessment performed in this master thesis for the different combinations of representative mangrove environments and locations. In the test case a requirement of a maximum R_c of 0.5 m is introduced. Figure D.9 shows with the light blue line the evolution of the required R_c along the x-axis of the numerical domain. The first measuring location with an R_c below the requirement is indicated as as the location with sufficient wave attention for the placement of the dike. The dark blue line in the figure indicates the evolution of R_c

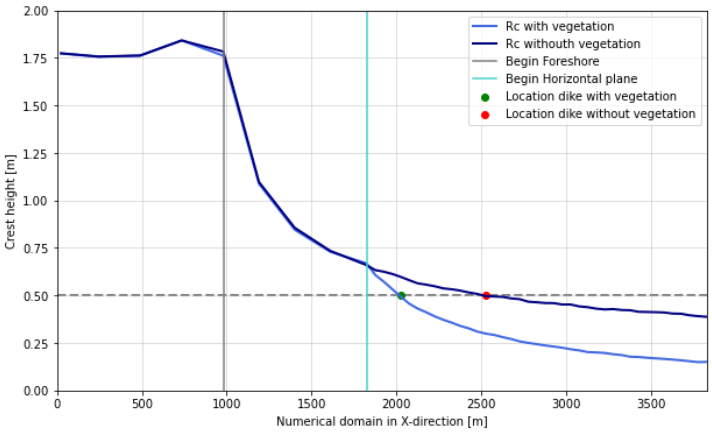

Figure D.9: *Optimization process to define the location of the dike by visualizing the processed output of the SWASH model for the two test cases.*

The impact of the wave attenuation capacity of mangrove can be observed by comparing the light blue and dark blue line in figure D.9, representing respectively the propagation with and without mangrove vegetation. Resulting from the coastal vegetation of mangrove, less width of the horizontal plane is needed to dissipate enough energy for the requirement of R_c.

D.5. Space discretization

During the study, locations were detected with a large energy concentration in the lowest bin of the spectrum. One of the domains where this process occurred is visualized in figure D.10. In this figure the bathymetry of the domain is indicated with the yellow line, having a total length of 19020 meters, with a starting point at the horizontal location -20 meters. The last part of the domain is the sponge layer, with a width of 1000 meters. The blue line indicates the water level, located at 5 meters. The red lines indicate the locations where the output of SWASH is generated. This output is generated at the beginning of the hydrodynamic model (x=25 meter) and at every five meter in the vegetation belt.

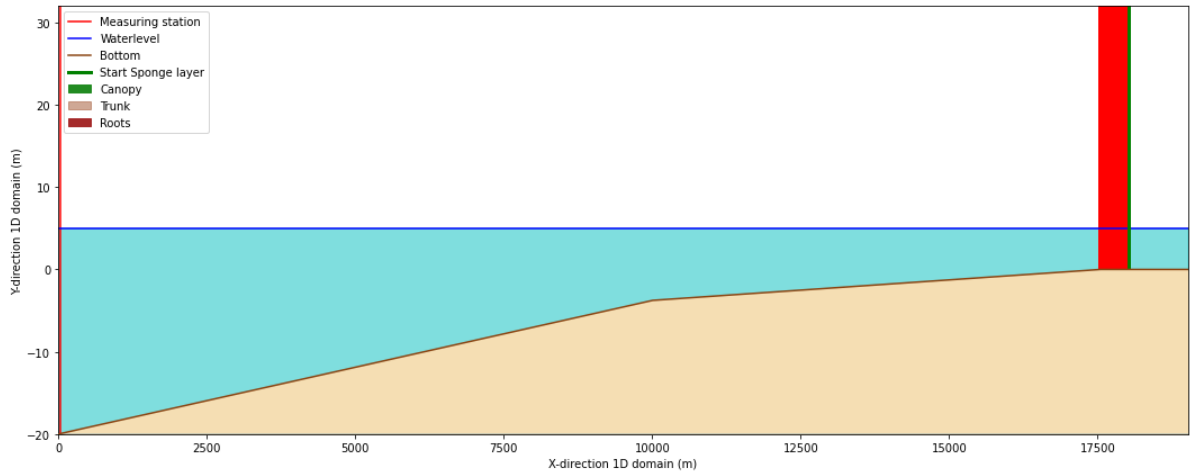

Figure D.10: *The bathymetery applied for the test runs to identified*

At this location, the observation was made that a large part of the energy is transferred towards the lowest bin, which will be visualized further in this chapter. The cause of this problem is examined by changing the horizontal space-discretization from the original 5 meters to 2.5 and 1 meter. It was examined if this could be the origin of the extreme concentration of energy in long-period waves, with a frequency smaller than 0.07 Hz.

The time-discretization step applied is 0.5 seconds and the different space-discretization steps applied are 5, 2.5, and 1 meter. The forcing conditions of the system are the JONSWAP spectrum (Hasselmann et al., 1973), with a H_s of 5 meters and a T_m of 10.3 seconds. The resulting time series, including the spin up-time are visualized in figure D.11, D.12 and D.13. The grey line indicates the time series of the water level at location x = 25 meters. The light blue line indicates the time series of the water level that can be observed at the beginning of the horizontal vegetation plot and the orange line is the time series of the water level at the end of the vegetation plane.

One can observe based on the difference between figure D.11 and D.13 that a decrease of the space-discretization increases the short-period wave signal. Furthermore, an increase in wave height can be observed.

The decrease of the space-discretization step in the results seems to have a positive influence on the results of the model. A possible reason for this could be that due to the larger space step, a continuity error occurs in the SWASH model. While the space-discretization of 1 meter results in a reduced energy transfer to the long-period waves, the choice is made to apply the 1-meter space discretization during the runs.

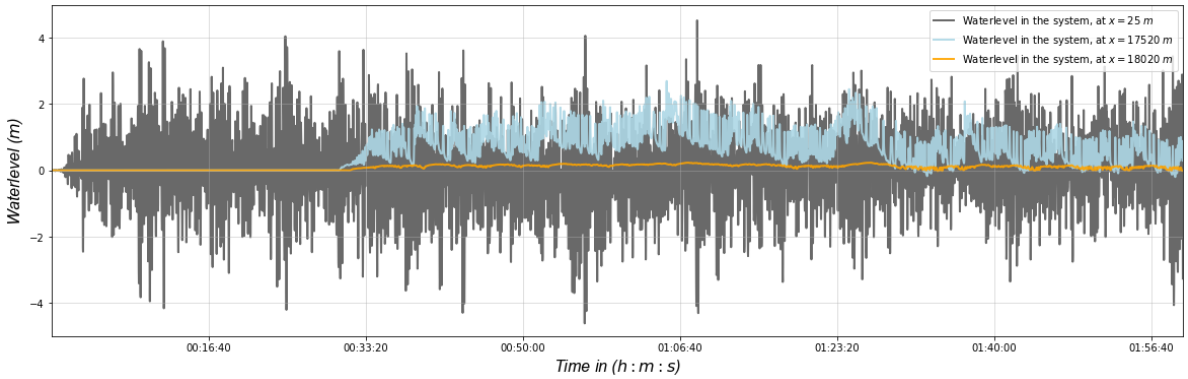

Figure D.11: *Resulting time-series from the SWASH run with a space-discretization step of 5 meter*

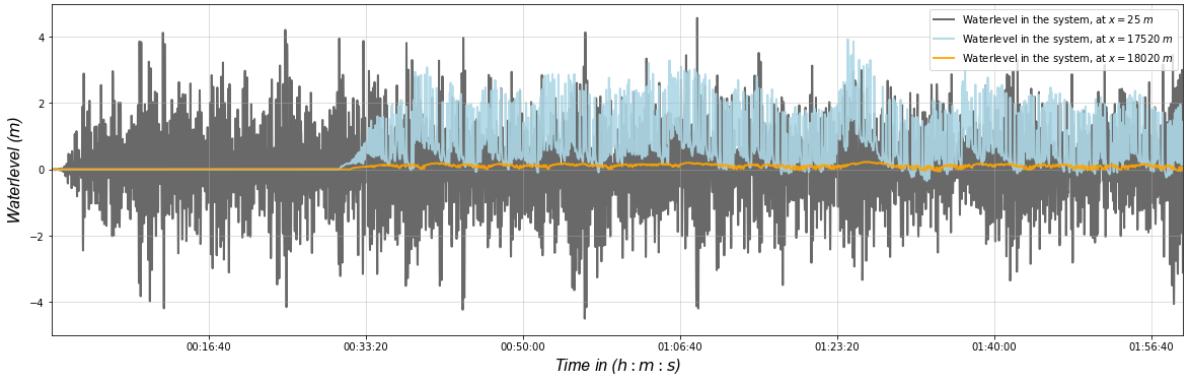

Figure D.12: *Resulting time-series from the SWASH run with a space-discretization step of 2.5 meter*

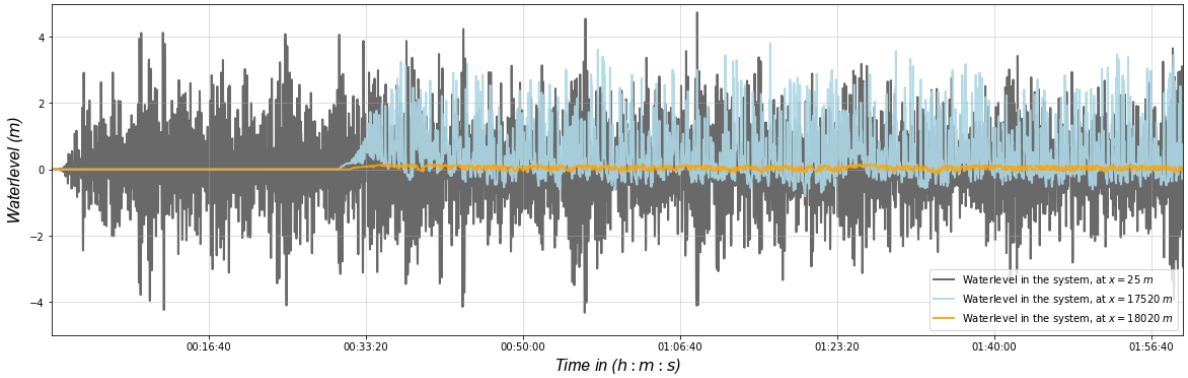

Figure D.13: *Resulting time-series from the SWASH run with a space-discretization step of 1 meter*

Using a frequency analysis the evolution of the wave-signal is transformed towards a spectral density plot. The results of this transformation of the data set is visualized in figure D.14,D.15 and D.16.

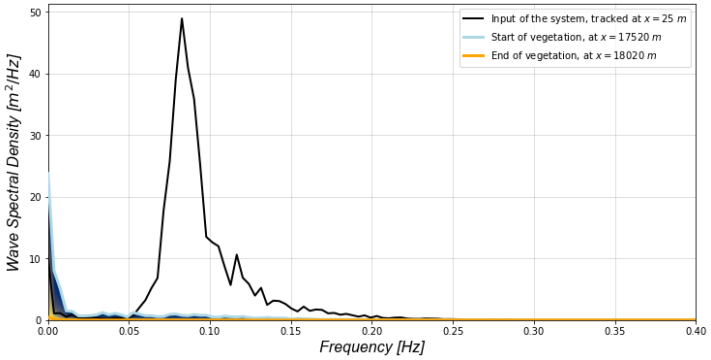

Figure D.14: *Resulting spectral density plot from the SWASH run with a space-discretization step of 5 meter*

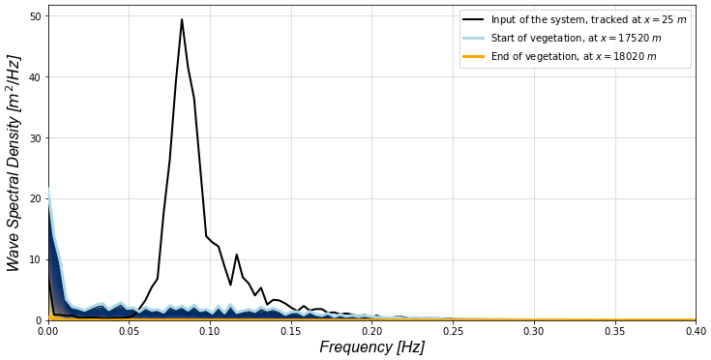

Figure D.15: *Resulting spectral density plot from the SWASH run with a space-discretization step of 2.5 meter*

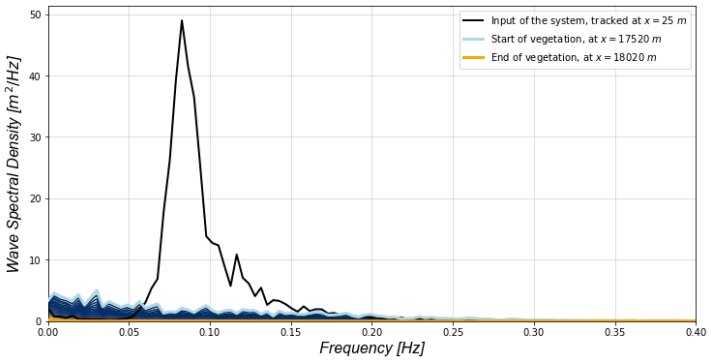

Figure D.16: *Resulting spectral density plot from the SWASH run with a space-discretization step of 1 meter*

D.6. Output at long shallow foreshores

As mentioned in the discussion the applied grid size resulting from the available computational capacities resulted in a reduced accuracy of solving waves in shallow water. The cases discussed are listed in table D.1, with which the increase in water depth and the width of the foreshore differs over the different representative mangrove locations. These four cases are selected to validate the hypothesis that the obtained time-series of the water level is depending on the water depth and the length of the shallow part expressed in the width of the foreshore.

Representative mangrove location	w_{ns}	w_{fs}	WTL
68	10000 m	4656 m	3.3 m
134	10000 m	0 m	4.0 m
150	10000 m	8246 m	0.5 m
154	10000 m	1795 m	0.5 m

Table D.1: *Domain parameters of 4 representative mangrove locations present in representative mangrove environment 19, during the 1987 event with H_s of 4.3 m and T_m of 11.5 sec*

In figure D.17, the spectral density analysis is visualized for the result of SWASH for the 4 input cases. The observation can be made that in the two cases with a water depth of 3.3 and 4 m energy is still present in the waves above 0.05 Hz. At the locations with a water depth of only 0.5 meter, the energy in the waves above 0.05 Hz is fully dissipated and only energy in the long-period waves can be observed.

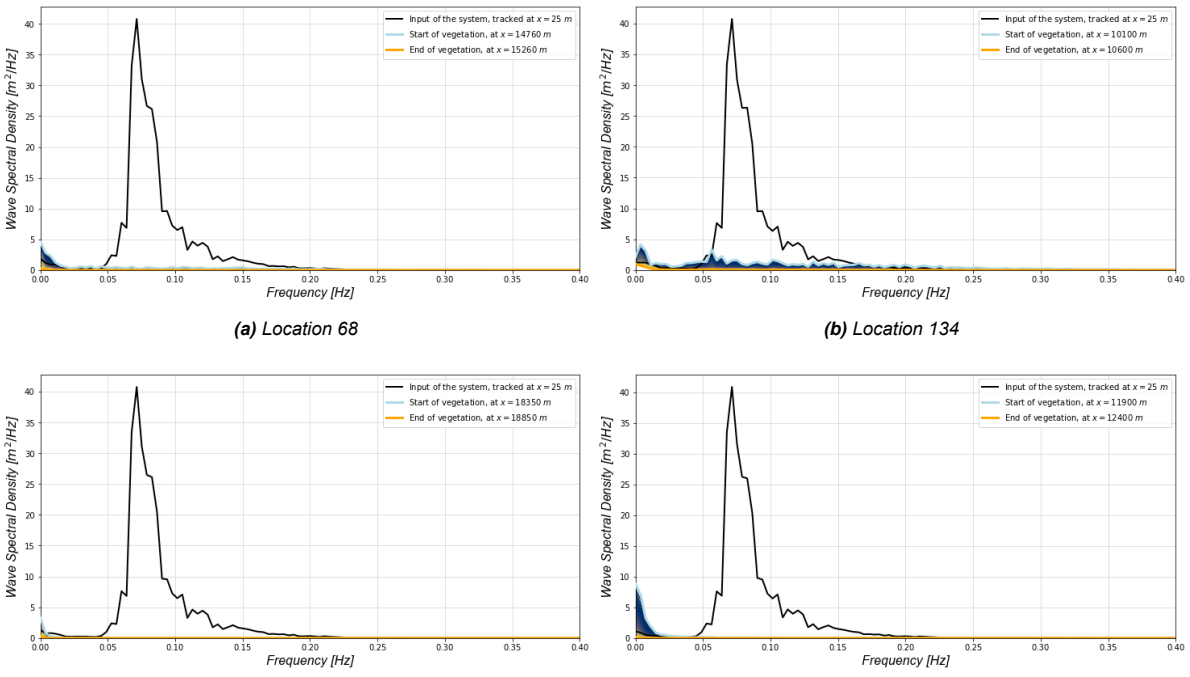

(a) *Location 68*

(b) *Location 134*

(c) *Location 150*

(d) *Location 152*

Figure D.17: *Spectral density analysis for four representative mangrove location with H_s of 4.3 m and T_m of 11.5 sec.*

If this observation is compared with the time series leading towards these results of the spectral density analysis, the observation can be made that the system is indeed visualizing more short waves at cases 68 and 134, as visualized in figure D.18 and D.19. At the locations with the water depth of only 0.5 meter, skewed long waves can be observed, as shown in figure D.20 and D.21. The expectation is that this is a result of the bottom friction and the phase-resolving approach.

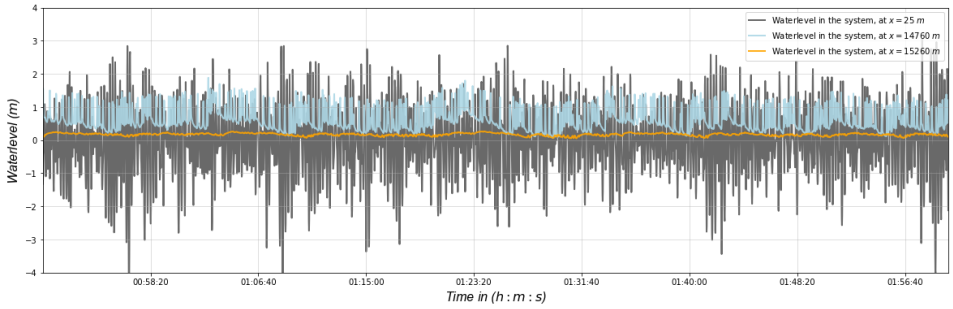

Figure D.18: *Time series of SWASH output of representative mangrove location 68 with H_s of 4.3 m and T_m of 11.5 sec.*

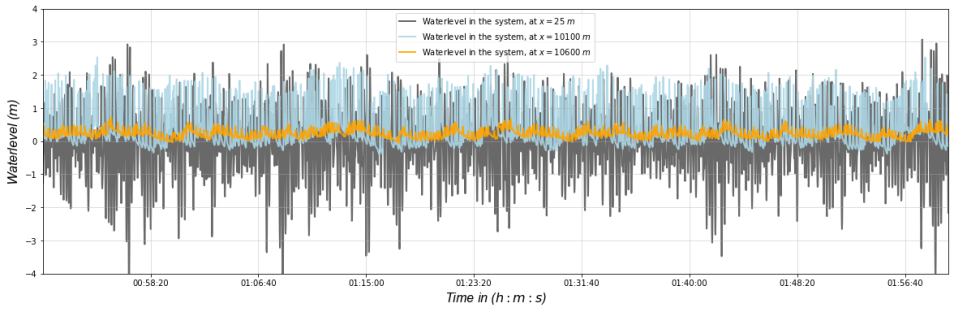

Figure D.19: *Time series of SWASH output of representative mangrove location 134 with H_s of 4.3 m and T_m of 11.5 sec.*

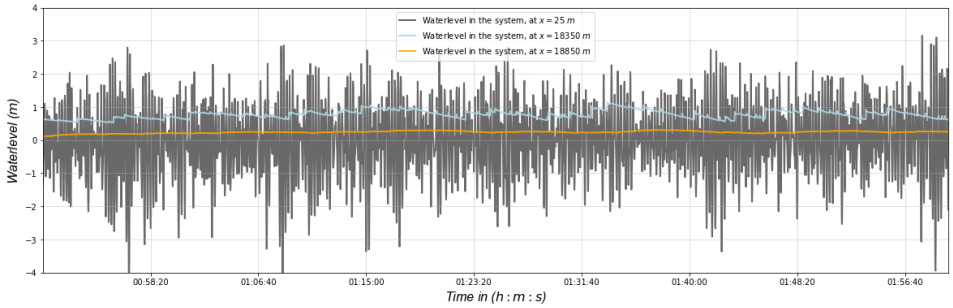

Figure D.20: *Time series of SWASH output of representative mangrove location 150 with H_s of 4.3 m and T_m of 11.5 sec.*

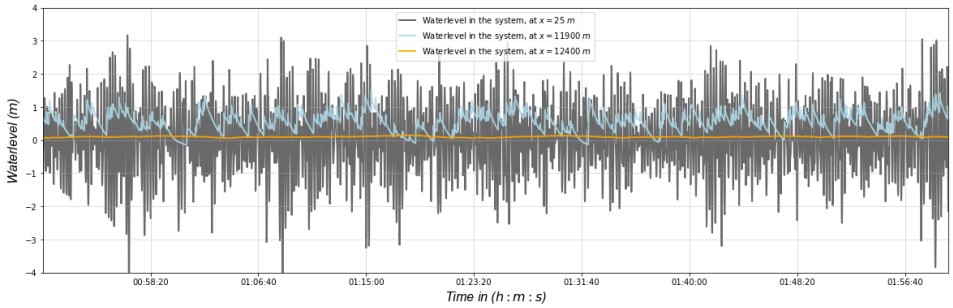

Figure D.21: *Time series of SWASH output of representative mangrove location 152 with H_s of 4.3 m and T_m of 11.5 sec.*

D.7. Wave attenuation mangrove vegetation

The second discussion point for the results of the hydrodynamic model creates further insight into the relative use of the results of this study. In figure D.22 the significant wave height H_S is given along the 500 meter vegetation belt for the four test cases of appendix D.6.

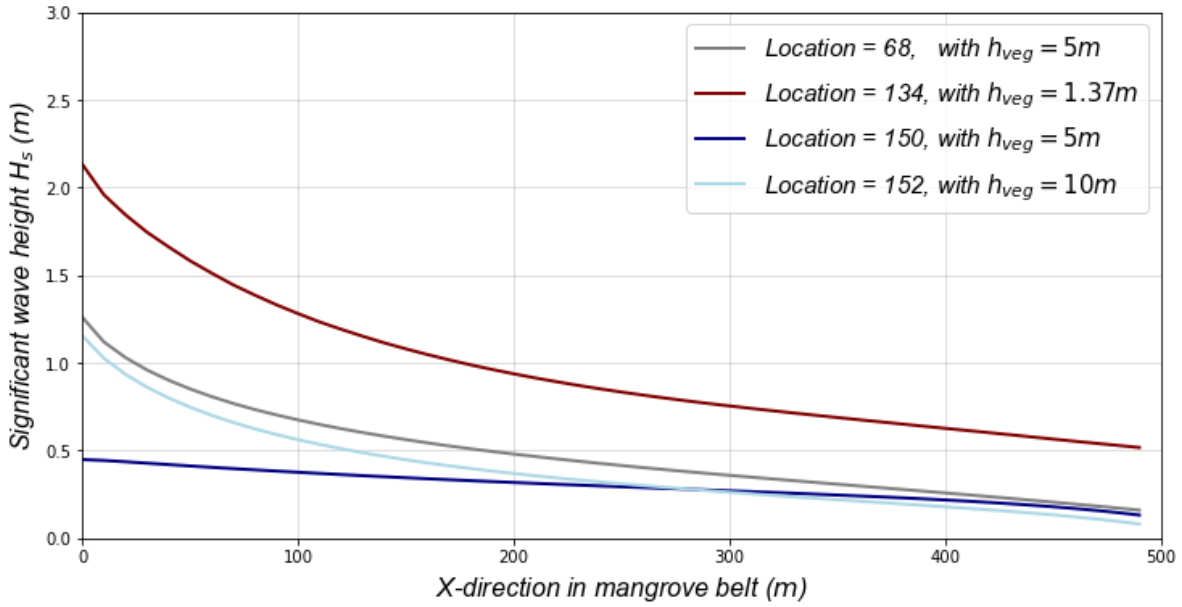

Figure D.22: *Decrease in significant wave height H_s within the mangrove belt.*

In literature, it is stated that the significant wave height decreases with 0.14% to 1.1% per meter vegetation (Mcivor et al., 2012). Based on the different wave heights of the four test cases the mean percentage decrease of H_S can be calculated, with the results given in table D.2. This means that the wave attenuation capacity of the trees is within the described range.

Representative mangrove location	$\Delta \bar{H}_S$	h_{veg}	WTL
68	0.39 %/m	5 m	3.3 m
134	0.27 %/m	1.37 m	4.0 m
150	0.25 %/m	5 m	0.5 m
152	0.51 %/m	10 m	0.5 m

Table D.2: *Average decreases in H_s for 4 representative mangrove locations present in representative mangrove environment 19, during the 1987 event with H_s of 4.3 m and T_m of 11.5 sec*

Measured in several studies, the wave attenuation capacity of mangrove forest depends on the water level (Quartel et al., 2007; Brinkman, 2006). This result is also observed in the model of this study when the results of representative mangrove locations 68 and 150 are compared. This emphasizes the importance of defining extreme events for mangrove environments by implementing the water level in the multivariate extreme event.

E

Coastal safety assessment

E.1. Most extreme multivariate extreme event

The methodology applied resulted in the 1/40 year design condition for 1987 and 2018. These design conditions are multivariate extreme events. One can observe the spatial distribution of T_m during these 1/40 year design conditions in figure E.1 and E.2.

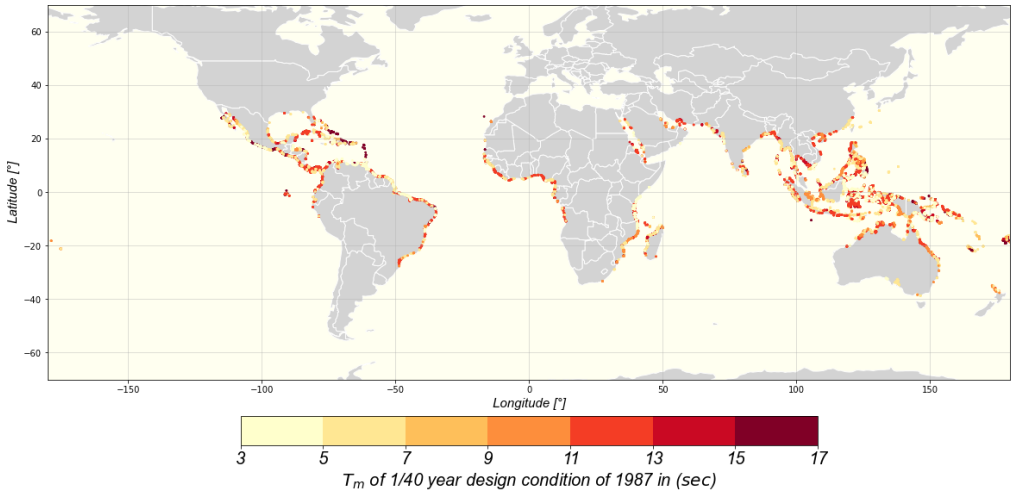

Figure E.1: *Spatial distribution of H_s for the 1/40 year design condition for the year 1987.*

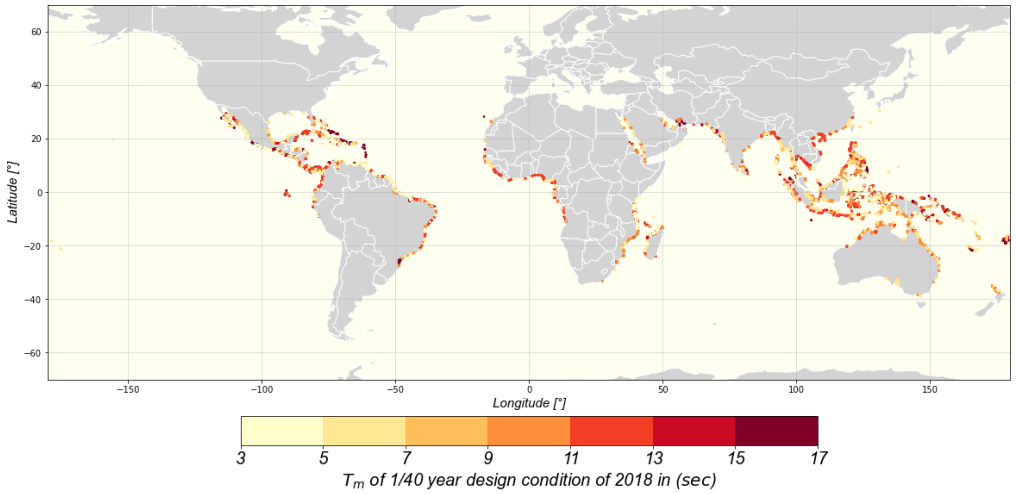

Figure E.2: *Spatial distribution of H_s for the 1/40 year design condition for the year 2018.*

The spatial distribution of S during this multivariate extreme event is given in figures E.3 and E.4. These values represent the S during the 1/40 year design conditions.

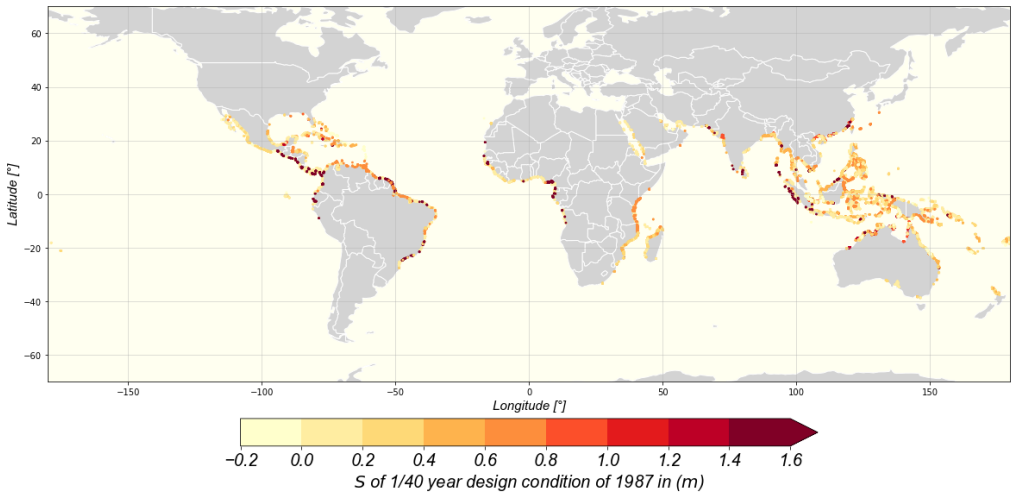

Figure E.3: *Spatial distribution of H_s for the 1/40 year design condition for the year 1987.*

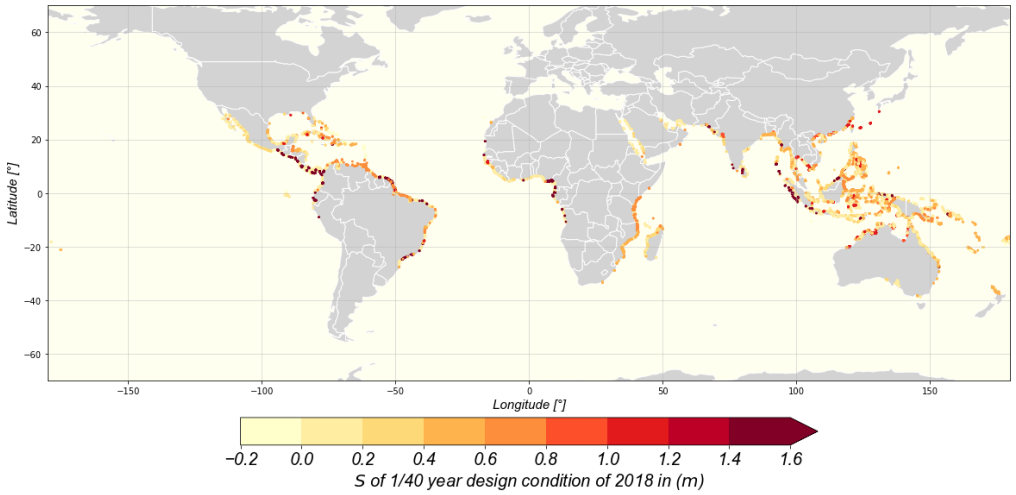

Figure E.4: *Spatial distribution of H_s for the 1/40 year design condition for the year 2018.*